Doctoral theses at NTNU, 2013:286

Jan Fredrik Helgaker

Modeling Transient Flow in Long Distance Offshore Natural Gas Pipelines

Doctoral Thesis

Jan Fredrik Helgaker

ISBN 978-82-471-4702-3 (printed version)
ISBN 978-82-471-4703-0 (electronic version)
ISSN 1503-8181

NTNU – Trondheim
Norwegian University of Science and Technology

NTNU
Norwegian University of Science and Technology
Thesis for the degree of Philosophiae Doctor
Faculty of Engineering Science & Technology
Department of Energy and Process Engineering

Doctoral theses at NTNU, 2013:286

NTNU – Trondheim
Norwegian University of Science and Technology

NTNU

Jan Fredrik Helgaker

Modeling Transient Flow in Long Distance Offshore Natural Gas Pipelines

Thesis for the degree of Philosophiae Doctor

Trondheim, November 2013

Norwegian University of Science and Technology
Faculty of Engineering Science & Technology
Department of Energy and Process Engineering

NTNU – Trondheim
Norwegian University of
Science and Technology

NTNU
Norwegian University of Science and Technology

Thesis for the degree of Philosophiae Doctor

Faculty of Engineering Science & Technology
Department of Energy and Process Engineering

ISBN 978-82-471-4702-3 (printed version)
ISBN 978-82-471-4703-0 (electronic version)
ISSN 1503-8181

Doctoral theses at NTNU, 2013:286

Printed by Skipnes Kommunikasjon as

Abstract

The objective of this thesis is to improve flow modeling through offshore natural gas pipelines. Gassco is a state owned Norwegian company responsible for the operation of 7800 km offshore natural gas pipelines located in the North Sea. The pipelines have a diameter of 1 m and can be up to 1000 km in length. Measurements of the state of the gas, such as pressure, mass flow, temperature and composition are available only at the inlet and outlet. To know the state of the gas between these two points one has to rely on computer models. Gassco uses commercial tools to model the flow of gas through their pipelines. These have previously given inaccurate results, especially during transient conditions.

The flow of natural gas through long distance offshore pipelines is modeled by numerically solving the governing equations for one-dimensional compressible viscous heat conducting flow. An implicit finite difference scheme is used to solve the governing equations. Both spatial and temporal discretization errors are computed. The implemented flow model is validated by running simulations on one of Gassco's offshore pipelines. Modeled results show good agreement with measured values, however some discrepancies are present, especially in the modeled outlet gas temperature. These discrepancies are determined to be caused by physical approximation errors, and not because of numerical errors or model simplifications.

The sensitivity of the selection of the equation of state for high pressure natural gas pipelines is investigated by comparing the SRK, Peng-Robinson, BWRS, GERG 88 and GERG 2004 equations of state. Gassco currently uses a BWRS equation of state which is especially tuned for hydrocarbons. In a typical offshore natural gas pipeline, the difference in computed inlet pressure between using the tuned BWRS and the GERG 2004 equation of state was determined to be approximately 0.1 MPa (1 bar). Although GERG 2004 is believed to be the most accurate equation of state, it is computationally demanding compared to BWRS, resulting in BWRS being the preferred choice. Although there is a difference in computed inlet pressure between GERG 2004 and BWRS, this difference is relatively constant during both steady state and transient conditions. By tuning the equivalent sand grain roughness, the computed inlet pressure using both GERG 2004 and BWRS can be matched in order to compensate for differences in the equation of state.

The heat exchange between the gas and the surrounding environment is modeled using two different approaches. The steady external heat transfer model currently used by Gassco is compared to an unsteady external heat transfer model which

includes heat accumulation in the ground. It is shown by example that the steady heat transfer model over predicts the amplitude of temperature changes in the flow compared to the unsteady heat transfer model. The unsteady heat transfer model also improves the modeled inlet pressure and outlet mass flow during transient conditions. Although the modeled temperature is improved using the unsteady heat transfer model, there is still a discrepancy between modeled and measured outlet gas temperature. The most important parameters which can account for this deviation are the ambient sea bottom temperature, soil thermal conductivity and pipe burial length.

Preface

This thesis is submitted in partial fulfillment of the requirements for the degree of Doctor of Philosophy (PhD) at the Norwegian University of Science and Technology (NTNU). The work has been performed in the period September 2010 - August 2013.

The research has been carried out at the Faculty of Engineering Science and Technology, Department of Energy and Process Engineering (EPT) in the Fluids engineering group. Professor Tor Ytrehus (EPT) has been the main supervisor, while Professor Bernhard Müller (EPT) and senior scientist Stein Tore Johansen (SINTEF Materials and Chemistry) have been the co-supervisors.

The research has been funded by the Norwegian gas operating company Gassco AS, which is located outside Haugesund. The main objective of this thesis is to improve flow modeling through offshore natural gas pipelines.

Jan Fredrik Helgaker
Trondheim, August 2013

Acknowledgments

As my PhD thesis is nearing the end it is time to acknowledge and thank those who have made it possible for me to finish this work.

First I want to thank my supervisor Professor Tor Ytrehus for giving me this opportunity and for all the time he has devoted to me during these three years. His office door has always been open whenever I had questions, and I am very grateful to him for letting me pursue my own ideas, while at the same time keeping me on track in order to finalize the thesis. I would also like to thank my co-supervisors, Professor Bernhard Müller and senior scientist Stein Tore Johansen from SINTEF Materials and Chemistry. Bernhard's solid knowledge in computational fluid dynamics and Stein Tore's experience with pipe flow modeling was of great value to the project.

Although I have been a PhD student at the Department of Energy and Process Engineering at NTNU, I have officially been employed at the Polytec Research Institute in Haugesund. I would like to thank Gunnar Birkeland for giving me this opportunity and for letting me have an office at NTNU in Trondheim. Whenever I have visited Haugesund I have always been well looked after by other Polytec employees, something I am very grateful for. I would especially like to acknowledge Sigmund Mongstad Hope for leading the research project my PhD was a part of, and always giving me assistance and help when I needed it. A special thanks also goes to Tony Oosterkamp for all the cooperative work and discussions we had together, which were very useful in my work.

This project focuses on flow modeling through offshore natural gas pipelines, and has been funded by Gassco AS. I am very grateful for their support and for allowing me to participate at international conferences. I would especially like to thank Leif Idar Langelandsvik, Willy Postvoll and Ben Velde for giving me feedback on my work.

My workplace has been at the Department of Energy and Process Engineering at the Norwegian University of Science and Technology. I would never have completed this thesis had it not been for all the excellent colleagues I have had during these past three years. I would like to thank all the permanent staff at EPT for

supporting me, especially my colleagues at Strømingsteknisk Lars Sætran, Per-Åge Krogstad, Iver Brevik, Reidar Kristoffersen, Helge Andersson, Arnt Egil Kolstad, Eugen Uthaug, Ingrid Wiggen and Debbie Koreman. A big thanks goes to all my fellow PhD colleagues Simen, Kristian Etienne, Vagesh, Karl Yngve, Halvor, Christopher, Joris, Claudio, Michael, Ignat, Pål Egil, Asif, Fabio, Eze, Luca and Tania. Life at the office would have been dull without you. Among my fellow PhD colleagues I would especially like to acknowledge Halvor Lund and Claudio Walker for all the valuable discussions we had, and for all the cross country skiing and orientering we did together.

In January 2013 I spent a short two week stay at Warsaw University of Technology, Faculty of Environmental Engineering, Heating and Gas Systems Department. I would like to thank Professor Andrzej Osiadacz and Dr. Maciej Chaczykowski for giving me this opportunity and for the fruitful discussions we had.

I am very grateful for the support from family and friends during these past years. I would like to thank my parents Barbara and Trygve and brother Aleksander, and especially my partner Christine for her love and support, and for patiently waiting for me during this last year. I'm coming home now.

The completion of this PhD marks the end of an eight year stay in Trondheim and at NTNU. I have only fond memories from this time period, and would like to thank everybody who has contributed to it. I will miss all my colleagues and friends in Trondheim, Tuesday orientering, Bymarka, long summer evenings and riding my road bike into the sunset at Byneset. When the sun shines, Trondheim is one of the most beautiful places I have ever been.

Jan Fredrik Helgaker
Trondheim, August 2013

Contents

Publications

[a] J.F. Helgaker. An implicit method for 1D unsteady flow in a high pressure transmission pipeline. In Proceedings of *First ECCOMAS Young Investigators Conference 2012*, Aveiro, 2012.

[b] J.F. Helgaker and T. Ytrehus. Coupling between Continuity/Momentum and Energy Equation in 1D Gas Flow. Energy Procedia, Vol. **26** (2012), pages 82-89, In Proceedings of *2nd Trondheim Gas Technology Conference*, Trondheim, 2011.

[c] T. Ytrehus and J.F. Helgaker. Energy Dissipation Effect in the One-Dimensional Limit of the Energy Equation in Turbulent Compressible Flow. Journal of Fluids Engineering - Transactions of The ASME, Vol. **135** (6), (2013).

[d] J.F. Helgaker, A. Oosterkamp and T. Ytrehus. Transmission of Natural Gas through Offshore Pipelines - Effect of unsteady heat transfer model. In B. Skallerud and H. Andersson, editors, *MekIT'13: Seventh national conference on Computational Mechanics*, pages 113-131, Akademika Publishing, 2013.

[e] J.F. Helgaker, B. Müller and T. Ytrehus. Transient Flow in Natural Gas Pipelines using Implicit Finite Difference Schemes. Submitted to Journal of Fluids Engineering, June 2013.

[f] J.F. Helgaker, A. Oosterkamp, L.I. Langelandsvik and T. Ytrehus. Validation of 1D Flow Model for High Pressure Offshore Natural Gas Pipelines. Submitted to Journal of Natural Gas Science and Engineering, June 2013.

I am the sole author of article [a]. As the first author of articles [b], [d], [e] and [f] I carried out the work and performed the computations with ideas and feedback from supervisors T. Ytrehus and B. Müller. In article [c] the general expression for the correction factor was developed by T. Ytrehus, while all implementations and computations were done by myself. In article [d] A. Oosterkamp did the 2D heat transfer computations. In article [f] the analysis and discussions on the heat transfer model were done together with A. Oosterkamp, while the analysis and discussions on the friction factor were done together with L.I. Langelandsvik.

Nomenclature

A pipe cross section [m^2]

A_h area through which heat transfer occurs [m^2]

c speed of sound [m/s]

c_p heat capacity at constant pressure [J/(kg·K)]

c_v heat capacity at constant volume [J/(kg·K)]

D pipe diameter [m]

dr draught factor

f friction factor

g gravitational constant [m/s^2]

h film heat transfer coefficient [$W/(m^2 \cdot K)$]

k heat transfer coefficient [W/(m·K)]

$\dot{m}$ mass flow rate [kg/s]

Nu Nusselt number

Pr Prandtl number

p pressure [Pa]

p_c critical pressure [Pa]

Q heat flow [W]

R gas constant [J/(kg·K)]

Re Reynolds number

r pipe radius [m]

T temperature [K]

T_a ambient temperature [K]

T_c critical temperature [K]

t time [s]

U total heat transfer coefficient [W/(m^2·K)]

u gas velocity [m/s]

w accentric factor

x spatial coordinate [m]

Z compressibility factor

α reduced Helmholtz free energy

δ reduced density

ϵ equivalent sand grain roughness [m]

θ pipe inclination angle

λ thermal conductivity [W/(m·K)]

μ viscosity [kg/(m·s)]

ρ density [kg/m^3]

τ reduced temperature

Δt temporal discretization length [s]

Δx spatial discretization length [m]

Substances

CH_4	methane
C_2H_6	ethane
C_3H_8	propane
nC_4H_{10}	n-butane
iC_4H_{10}	isobutane
nC_5H_{12}	n-pentane
iC_5H_{12}	isopentane
N_2	nitrogen
CO_2	carbon dioxide

Chapter 1

Introduction

1.1 Background and motivation

Natural gas is an important primary energy source accounting for almost one forth of the worlds primary energy consumption [1]. It is a multi-component gas mixture with methane being the primary constituent; other components typically being ethane, propane, butane, nitrogen, carbon dioxide and other heavier hydrocarbons. Natural gas can be used for heating, cooking, electric power generation and in several other energy demanding processes. Although it is a fossil fuel, it produces considerably less carbon dioxide per joule delivered compared to other fossil fuels such as oil and coal. For oil the CO_2 emissions are approximately 50% more compared to natural gas, while for coal it is 100% [2]. Because of its longer estimated future availability compared to crude oil, natural gas will play an important role as a primary energy source in the coming years [3].

The world production of natural gas in 2010 was 3178 billion cubic meters, 3.3% of which was produced by Norway [1]. Norwegian natural gas which is extracted from the continental shelf in the North Sea is first transported to processing terminals offshore and on the mainland where unwanted components are removed. It is then fed into long export pipelines and transported to continental Europe and the UK. The Norwegian pipeline infrastructure is operated by the state owned company Gassco. An overview of the offshore pipeline network is shown in Figure 1.1.

The network consists of 7800 km offshore pipelines which have a diameter of approximately 1 m. The longest pipeline is Langeled with a length of 1166 km, which was until the opening of the Nord Stream pipeline from Russia to Germany in November 2011, the longest offshore pipeline in the world.

In Gassco's case, the transport pipelines in Figure 1.1 are operated by a single compressor station at the inlet. Measurements of the state of the gas, such as pressure, mass flow, temperature and composition are available only at the inlet and outlet. To know the state of the gas between these two points one has to rely on mathematical models. These models have several important applications

Figure 1.1: Overview of the pipeline network operated by Gassco. Figure courtesy of Gassco.

which include designing, monitoring and operating the pipelines. They also play an integral part in software based leak detection systems. It is therefore crucial that these models are as accurate as possible, but at the same time fast and efficient as they are used in real time applications.

Accurate models for transmission of natural gas through long distance pipelines are also of great importance when determining the pipeline hydraulic capacity. When a pipeline is built, the capacity is determined by using available inlet and outlet pressure as boundary conditions for the model, together with other available flow parameters. High accuracy in pipeline transport capacity calculations is important to ensure optimal utilization of the pipeline network. The calculated transport capacity has to be close to, but not larger than the true capacity, as failure to deliver the forecasted capacity can result in penalties and a poor reputation as a gas operator [4].

Gassco uses commercial tools to model the flow of gas through their pipe network. In recent years they have had an active research program to improve flow modeling in their offshore natural gas pipelines. In the PhD thesis by Langelandsvik in 2008 [5] an increased knowledge about frictional pressure drop at large flow rates resulting from analysis of pipeline operational data led to increased capacity estimations of $0.2 - 1\%$ in several of Gassco's pipelines. Other important contributions have been; improved heat transfer modeling and predicting the correct heat transfer coefficient [6], improved pipeline capacity by using real time sea bottom temperature data [7] and improved viscosity correlations [8] - [9]. However, most of the research up to now has considered steady state conditions only, with little emphasis on transient flow. During large transients, Gassco has observed significant deviations between modeled and measured pressure. In Figure 1.2 the modeled inlet pressure from one of Gassco's offshore pipelines is shown, which was computed using their commercial tools. During the transient there is a considerable difference between modeled and measured inlet pressure. At the end of the simulation the difference is almost 5 bar (0.5 MPa). Also, considerable differences between measured and modeled outlet temperature have been observed. These observed discrepancies led to the initiation of a research program to improve flow modeling during transient conditions in long distance offshore natural gas pipelines, which this PhD thesis is a part of.

Transmission of natural gas through high pressure pipelines is modeled by solving the governing equations for one-dimensional compressible viscous heat conducting flow. The governing equations form a system of hyperbolic partial differential equations which have to be solved numerically. A good overview of different numerical methods for one-dimensional compressible flow can be found in base literature articles, for instance by Thorley and Tiley [10]. Numerical methods include the method of characteristics, finite difference, finite volume and finite element methods. Several articles on numerical techniques for one-dimensional compressible flow were published during the 80s and 90s; see for instance the work by Issa and Spalding [11], Wylie et al. [12], Poloni et al. [13], Kiuchi [14] and Osiadacz [15]. Research articles in recent years have been more focused on modeling of physical processes in gas pipelines rather than numerical methods used to model the flow through

Figure 1.2: Modeled inlet pressure (in bar) from one of Gassco's offshore pipelines, computed using their commercial tool. During the transient there is a considerable difference between modeled and measured inlet pressure.

them. These include the work by Abbaspour and Chapman [16] and Osiadacz and Chaczykowski [17] who both consider the non-isothermal pipe flow model. Recent articles published by Chaczykowski consider both the sensitivity of the gas pipeline flow model to the selection of the equation of state [18] and the effect of a pipeline thermal model, which accounts for heat accumulation in the ground [19]. Although both of these articles consider a very detailed flow model, the inlet pressure of the pipeline was only 8.4 MPa. In Gassco's long distance export pipelines the inlet pressure can be up to 20 MPa, well above that which is typically considered in the literature. To the authors knowledge, few research articles other than those published by Gassco have considered pipelines operating under such high pressures.

1.2 Objective of thesis

The objective of this PhD thesis is to study transient flow in long distance offshore natural gas pipelines and determine whether the discrepancies between modeled and measured values in Gassco's pipelines are due to numerical errors or physical modeling approximation errors. In order to do this a method for modeling transient one-dimensional compressible viscous heat conducting flow will be developed. This method will then be applied to Gassco's offshore pipelines and numerical results will be compared to measured values. The main objectives of this thesis are:

- Implement a numerical method which can be used to solve the governing equations for unsteady one-dimensional compressible viscous heat conducting flow.
- Determine if possible what numerical errors are present in the solution and verify the developed method with other results in the literature.

- Validate the implemented method by running simulations on Gassco's offshore pipelines under transient conditions and compare results to measured values.
- Investigate the effect of the equation of state for pipelines operating at high pressures ($18 - 20$ MPa).
- Investigate the effect of an unsteady heat transfer model and determine what effect including heat accumulation in the ground has on the modeled flow results.

Gassco currently uses commercial tools to model the flow through their pipe network. It is desirable that the results of this work could be used to give recommendations for possible improvements of the current software used by Gassco.

1.3 Research method

This thesis focuses on mathematical modeling of one-dimensional compressible viscous heat conducting flow and is purely a computational study. Unless stated otherwise, all the results in this thesis have been computed by the author. Computed flow results will be compared to measured values from offshore pipelines which have been collected from SCADA systems. Uncertainties in these measurements will be commented on.

1.4 Outline of thesis

This thesis is organized as follows. In Chapter 2 the governing equations for one-dimensional compressible viscous heat conducting flow are presented. The procedure of how to derive the partial differential equations for pressure, mass flow and temperature is included in the Appendix. Correlations for determining the friction factor and different equations of state are included. Also, equations for calculating the heat transfer between the gas and the pipeline surroundings with and without considering heat accumulation in the ground are presented.

In Chapter 3 numerical methods are presented. In this work finite difference methods have been used to numerically solve the governing equations. Both explicit and implicit methods are considered.

Results are presented in Chapter 4. Both the hydraulic and full non-isothermal models are considered. Spatial and temporal discretization errors for pressure, mass flow and temperature are computed. The flow model is verified by comparing results with those found in the literature. Validation is performed by running simulations on one of Gassco's offshore pipelines and comparing results to measured values.

In Chapter 5 a short discussion on model simplifications is included. The most important physical processes which are incorporated into the model are discussed in detail, and the sensitivity of the different parameters is considered. The most important processes which are investigated are the determination of the friction

factor, selection of the equation of state and how to model the heat exchange between the gas and the pipeline surroundings.

Conclusions and outlook are included in Chapter 6. Summary of research articles are given in Chapter 7. The research articles are attached at the end of the thesis.

Chapter 2

1D Compressible Flow Model

2.1 Governing flow equations

The governing equations for one-dimensional compressible viscous heat conducting flow are found by averaging the three-dimensional equations for mass, momentum and energy conservation across the pipe section. The results is:

Continuity

$$\frac{\partial \rho}{\partial t} + \frac{(\rho u)}{\partial x} = 0 \tag{2.1}$$

Momentum

$$\frac{\partial(\rho u)}{\partial t} + \frac{\partial(\rho u^2 + p)}{\partial x} = -\frac{f\rho|u|u}{2D} - \rho g \sin\theta \tag{2.2}$$

Energy

$$\rho c_v \left(\frac{\partial T}{\partial t} + u\frac{\partial T}{\partial x}\right) + T\left(\frac{\partial p}{\partial T}\right)_\rho \frac{\partial u}{\partial x} = \frac{f\rho u^3}{2D} - \frac{4U}{D}(T - T_a) \tag{2.3}$$

The continuity and momentum equations are expressed on the conservative form, while the energy equation is in the non-conservative internal energy form. In the momentum equation the first term on the right hand side is the friction term where f is the friction factor, while the last term is the gravity term where $\sin\theta$ is the pipe inclination angle. In the energy equation the second term on the left hand side represents the Joule-Thomson effect, which is cooling during expansion. On the right hand side the first term is the dissipation term, which is the breakdown of mechanical energy to thermal energy. The final term represents the heat exchange between

the gas and the pipeline surroundings, where the total heat transfer coefficient U has the usual definition

$$U = \frac{Q}{A_h(T - T_a)} \tag{2.4}$$

where Q is the heat flow, T_a the ambient temperature and A_h the area through which heat transfer occurs. The density ρ can be traded for the pressure p by using a real gas equation of state

$$\frac{p}{\rho} = ZRT \tag{2.5}$$

where $Z = Z(p, T)$ is the compressibility factor. Introducing the mass flow rate $\dot{m} = \rho u A$, where A is the pipeline cross-section, the partial differential equations for pressure, mass flow and temperature can be developed into

$$\frac{\partial p}{\partial t} = \left[\frac{1}{p} - \frac{1}{Z}\left(\frac{\partial Z}{\partial p}\right)_T\right]^{-1}\left(\left[\frac{1}{T} + \frac{1}{Z}\left(\frac{\partial Z}{\partial T}\right)_p\right]\frac{\partial T}{\partial t} - \frac{ZRT}{pA}\frac{\partial \dot{m}}{\partial x}\right) \tag{2.6}$$

$$\begin{aligned}\frac{\partial \dot{m}}{\partial t} &= \frac{\dot{m}ZRT}{pA}\left(-2\frac{\partial \dot{m}}{\partial x} + \dot{m}\left[\frac{1}{p} - \frac{1}{Z}\left(\frac{\partial Z}{\partial p}\right)_T\right]\frac{\partial p}{\partial x} - \dot{m}\left[\frac{1}{T} + \frac{1}{Z}\left(\frac{\partial Z}{\partial T}\right)_p\right]\frac{\partial T}{\partial x}\right) \\ &- A\frac{\partial p}{\partial x} - \frac{fZRT\dot{m}|\dot{m}|}{2DAp} - \frac{pA}{ZRT}g\sin\theta\end{aligned} \tag{2.7}$$

$$\begin{aligned}\frac{\partial T}{\partial t} &= -\frac{\dot{m}ZRT}{pA}\frac{\partial T}{\partial x} - \frac{\dot{m}(ZRT)^2}{pAc_v}T\left[\frac{1}{T} + \frac{1}{Z}\left(\frac{\partial Z}{\partial T}\right)_\rho\right] \\ &\times \left(\frac{1}{\dot{m}}\frac{\partial \dot{m}}{\partial x} - \left[\frac{1}{p} - \frac{1}{Z}\left(\frac{\partial Z}{\partial p}\right)_T\right]\frac{\partial p}{\partial x} + \left[\frac{1}{T} + \frac{1}{Z}\left(\frac{\partial Z}{\partial T}\right)_p\right]\frac{\partial T}{\partial x}\right) \\ &+ \frac{f}{2c_vD}\left(\frac{ZRT|\dot{m}|}{pA}\right)^3 - \frac{ZRT}{pc_v}\frac{4U}{D}(T - T_a)\end{aligned} \tag{2.8}$$

The procedure of deriving the equations above is included in the Appendix. The energy equation can also be expressed in enthalpy or total energy form, opposed to the internal energy form which is used here. Chaczykowski [19] uses the internal energy form, while Abbaspour and Chapman [16] use the enthalpy form. All three representations are correct.

2.2 Friction factor

The friction factor f is a dimensionless quantity which accounts for pressure loss due to interaction between the fluid and the pipe wall. Except for laminar flow at low Reynolds numbers there is no exact formula for the friction factor in pipelines. All correlations which exist are based empirical data. Predicting the correct friction factor and its behavior for different flow regimes is of great importance when determining the hydraulic capacity of transport pipelines [5].

The Colebrook-White correlation [20] is perhaps the most widely used correlation for determining the friction factor in natural gas pipelines

$$\frac{1}{\sqrt{f}} = -2\log\left(\frac{\epsilon}{3.7D} + \frac{2.51}{Re\sqrt{f}}\right) \tag{2.9}$$

where ϵ is the equivalent sand grain roughness, D the pipeline diameter and Re the Reynolds number of the flow. The formula is a merge between the formula derived by Prandtl for completely smooth turbulent flow and that of Nikuradse for rough turbulent flow, where the Reynolds dependent term is that of the smooth flow and ϵ the rough turbulent flow. Values of the friction factor as a function of Reynolds number computed from the Colebrook-White correlation for different equivalent sand grain roughness are presented in Figure 2.1.

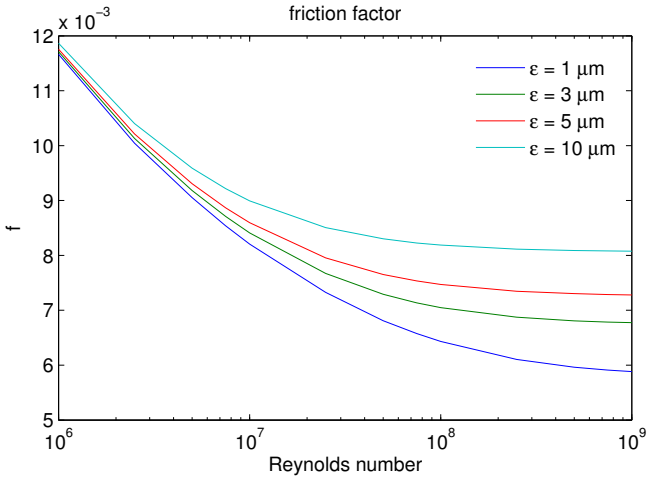

Figure 2.1: Friction factor f as a function of Reynolds number computed using the Colebrook-White correlation (Equation (2.9)) for different roughness values typical of long distance transport pipelines.

Even though the Colebrook-White correlation was developed as early as 1939, it is still widely used in the industry today. For transportation of natural gas the Reynolds number is typically of the order 10^7, meaning the friction factor lies in the transition region between smooth and fully rough turbulent flow. In the work by Langelandsvik et al. [21], based on analysis of operational data from natural gas pipelines, it is stated that the friction factor in the transition region in the Colebrook-White correlation bears significant uncertainty. Experimental results from a large scale laboratory setup by Langelandsvik et al. [22] revealed that the transition from smooth to fully rough turbulent flow is more abrupt than that suggested by Colebrook-White. A development of a friction factor correlation which can predict a more abrupt transition between smooth and fully rough turbulent flow was suggested by Langelandsvik et al. [21], but to the authors knowledge, the traditional Colebrook-White correlation is generally still the preferred choice.

An alternative to the Colebrook-White correlation was suggested by GERG in 2000 and published in the article by Gersten et al. [23]. The suggested correlation is

$$\frac{1}{\sqrt{f}} = -\frac{2}{n}\log\left[\left(\frac{\epsilon}{3.7D}\right)^n + \left(\frac{1.499}{drRe\sqrt{f}}\right)^{0.942\cdot n\cdot dr}\right] \tag{2.10}$$

where dr is the draught factor which accounts for other pressure losses such as curvature and pipe joints, and n is used to control the shape of the transition. $n = 1$ corresponds to a smooth Colebrook-White transition while $n = 10$ a more abrupt transition. There are however few published articles which consider this friction factor correlation and limited information is available as to what values of dr and n should be used. Based on experiments a value of $n = 3$ was suggested by Sletfjerding [24].

One major disadvantage of the Colebrook-White correlation is that it is an implicit relation, meaning an iterative procedure has to be used to compute the value of f. This can be computationally demanding, especially if the friction factor is calculated for each pipe section during each time step of the simulation. An alternative is to use an explicit relation for the friction factor f. One such relation is Haalands formula [25]

$$\frac{1}{\sqrt{f}} = -1.8\log\left[\left(\frac{\epsilon}{3.7D}\right)^{1.11} + \frac{6.9}{Re}\right] \tag{2.11}$$

2.3 Equation of state

State variables are related to each other through a real gas equation of state

$$\frac{p}{\rho} = ZRT \tag{2.12}$$

where $Z = Z(p, T)$ is the compressibility factor. The compressibility factor is a dimensionless quantity which depends on pressure and temperature. Under standard conditions $Z \to 1$ and Equation (2.12) reduces to the ideal gas law. The sensitivity of the pipeline gas flow model to the selection of the equation of state was investigated by Chaczykowski [18], where only small differences in flow variables were observed when using different equations of state. However, the inlet pressure of the considered pipeline was only 8.4 MPa, which is well below that of typical offshore pipelines which can be up to $18-20$ MPa. Therefore, the influence of the equation of state for high pressure pipelines will be considered. The different equations of state investigated are SRK, Peng-Robinson, BWRS, GERG 88 and GERG 2004.

2.3.1 SRK

The Soave Redlich-Kwong (SRK) equation of state was first published in 1972 [26] and is a modification of the Redlich-Kwong equation of state of 1949 [27]. It is a cubic equation of state and can be written in polynomial form as

$$Z^3 - (1-B)Z^2 + (A - B^2 - B)Z - AB = 0 \tag{2.13}$$

where

$$\begin{aligned} A &= \frac{a\alpha p}{(RT)^2} \\ B &= \frac{bp}{RT} \\ a &= 0.42747\frac{(RT_c)^2}{p_c} \\ b &= 0.08664\frac{RT_c}{p_c} \\ \alpha &= \left[1 + (0.480 + 1.574w - 0.176w^2)\left(1 - \sqrt{\frac{T}{T_c}}\right)\right]^2 \end{aligned} \tag{2.14}$$

w is the accentric factor and T_c and p_c denote critical temperature and pressure. Mixing rules for gases with multiple components can be found in the literature [26].

2.3.2 Peng-Robinson

The Peng-Robinson equation of state is structurally similar to the SRK equation of state and was published in 1976 [28]. It is however an improvement compared to SRK with respect to prediction of liquid density [29]. In polynomial form it can be written as

$$Z^3 - (1 - B)Z^2 + (A - 3B^2 - 2B)Z - (AB - B^2 - B^3) = 0 \tag{2.15}$$

where

$$\begin{aligned} A &= \frac{a\alpha p}{(RT)^2} \\ B &= \frac{bp}{RT} \\ a &= 0.45724\frac{(RT_c)^2}{p_c} \\ b &= 0.07780\frac{RT_c}{p_c} \\ \alpha &= \left[1 + (0.37464 + 1.5422w - 0.26992w^2)\left(1 - \sqrt{\frac{T}{T_c}}\right)\right]^2 \end{aligned} \tag{2.16}$$

As with SRK the reader is referred to the literature for mixing rules. Owing to their simple mathematical structure both SRK and Peng-Robinson allow for convenient compressibility factor calculations, and are therefore still used in the industry today.

2.3.3 BWRS

Benedict-Webb-Rubin-Starling (BWRS) is a virial equation of state derived from statistical mechanics. It was developed especially for the gas industry and was

published in 1973 [30]. The general form of the BWRS equation of state reads

$$\begin{aligned}\frac{p}{\rho} &= RT\left(1+\frac{1}{RT}\left[\left(B_0RT-A_0-\frac{C_0}{T^2}+\frac{D_0}{T^3}-\frac{E_0}{T^4}\right)\rho+\left(bRT-a-\frac{d}{T}\right)\rho^2\right.\right.\\ &+ \left.\left.\alpha\left(a+\frac{d}{T}\right)\rho^5+\frac{c\rho^2}{T^2}(1+\gamma\rho^2)\exp^{-\gamma\rho^2}\right]\right) \qquad (2.17)\end{aligned}$$

Equation (2.17) contains 11 coefficients which depend on critical density, critical temperature and the accentric factor. BWRS is used by Gassco today, but with coefficients which have been especially tuned for hydrocarbons and which differ from those found in the literature. For known pressure and temperature the density is determined from Equation (2.17) by using an iterative method such as Newtons method. Once the density is known the compressibility factor is determined from Equation (2.12).

2.3.4 GERG 88

The European Gas Research Group (GERG) has performed several research studies to develop formulas for determining the compressibility factor of natural gas mixtures. The GERG 88 virial equation of state [31] was developed to accurately predict the compressibility factor of natural gas mixtures for pressures up to 12 MPa in the temperature range $265-335$ K. The GERG 88 equation of state takes the form

$$\begin{aligned}Z &= 1+B_M(T)\rho_m+C_M(T)\rho_m^2\\ B_M(T) &= \sum_{i=1}^{n}\sum_{j=1}^{n}x_ix_jB_{ij}(T)\\ C_M(T) &= \sum_{i=1}^{n}\sum_{j=1}^{n}\sum_{k=1}^{n}x_ix_jx_kC_{ijk}(T) \qquad (2.18)\end{aligned}$$

where $B_M(T)$ and $C_M(T)$ are the second and third virial coefficients which depend on temperature and gas composition. x_i, x_j and x_k represent the mole fractions of the ith, jth and kth component. For compressibility factor calculations GERG 88 is claimed to have an uncertainty of less than 0.1% for pressures up to 12 MPa and temperatures in the range $265-335$ K.

2.3.5 GERG 2004

The GERG 2004 equation of state for natural gas mixtures [32] is the most recently developed equation of state. GERG 2004 allows for accurate compressibility factor calculations for pressures and temperatures up to 30 MPa and 365 K. The formula is explicit in Helmholtz free energy a with density and temperature as independent variables. Introducing the reduced density and temperature δ and τ

the compressibility factor can be determined from the relation

$$\frac{p(\delta,\tau)}{\rho RT} = 1 + \delta\alpha_\delta^r \tag{2.19}$$

where α_δ^r is the dimensionless Helmholtz free energy. For a more detailed description on how to determine α_δ^r the reader is referred to the GERG 2004 technical monograph [32]. The GERG 2004 equation of state can also be used to conveniently determine other thermodynamical quantities such as heat capacity, Joule-Thomson coefficient, internal energy, enthalpy and entropy. Of all the different equations of state presented here, GERG 2004 is the only one where it is explicitly stated that it has been verified for pressures up to 30 MPa. An expansion of GERG 2004, referred to as GERG 2008, has also recently been published [33]. The only difference between GERG 2004 and GERG 2008 is that GERG 2008 includes components which were not considered in GERG 2004, namely n-nonane, n-decane and hydrogen sulfide. These components were not considered in this work.

2.3.6 Compressibility factor

The compressibility factor for a typical North Sea natural gas mixture was calculated using all of the different equations of state presented above. The pressure range was set to $1-25$ MPa and calculations were done at 4 different temperatures (273, 283, 293 and 303 K). The gas composition (mole fraction) was set to: $CH_4 - 89.16\%$, $C_2H_6 - 7.3513\%$, $C_3H_8 - 0.5104\%$, $nC_4H_{10} - 0.0251\%$, $iC_4H_{10} - 0.0311\%$, $nC_5H_{12} - 0.0009\%$, $iC_5H_{12} - 0.0024\%$, $N_2 - 0.6980\%$, $CO_2 - 2.2208\%$.

Results for the compressibility factor are presented in Figure 2.2. Below 10 MPa the different equations of state predict similar values of the compressibility factor Z. However, for pressures above 10 MPa considerable discrepancies between the different equations of state are observed. As GERG 2004 is the only one which is claimed to be accurate for high pressures it is also considered to be the best reference. The tuned BWRS (marked as BWRS*) which Gassco currently uses predicts compressibility factors which are slightly higher than those of GERG 2004 for pressures above 10 MPa. How this effects the flow will be investigated in Chapter 5.

In Equations (2.6) - (2.8) the partial derivatives of Z with respect to pressure and temperature are required, which have been computed by taking the derivative of Z for all correlations. The partial derivative of Z with respect to temperature at constant pressure is presented in Figure 2.3, the partial derivative of Z with respect to pressure at constant temperature in Figure 2.4 and the partial derivative of Z with respect to temperature at constant density in Figure 2.5. In Figure 2.3 and Figure 2.4 the computed values agree well with each other over the entire pressure range. In Figure 2.5 some discrepancies above 15 MPa are observed. Values of the partial derivatives of Z are seldom found in the literature. The partial derivatives of Z computed from the Peng-Robinson equation of state can be found in the article by Nagy and Shirkovskiy [34].

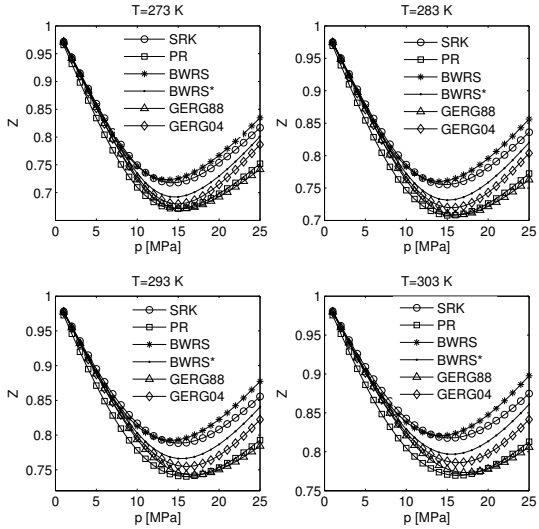

Figure 2.2: Compressibility factor Z as a function of pressure at different temperatures computed from the SRK, Peng-Robinson, BWRS, BWRS tuned (BWRS*), GERG 88 and GERG 2004 equations of state.

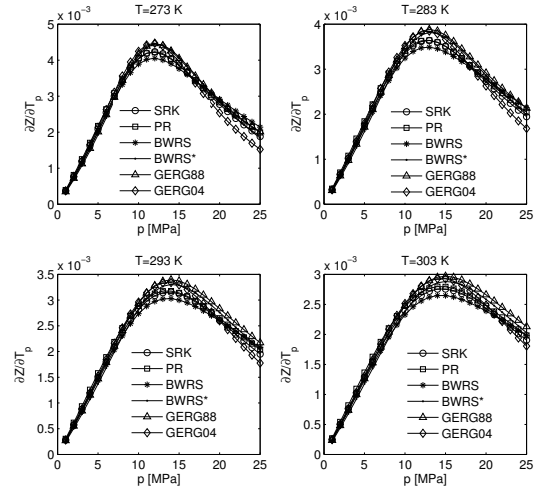

Figure 2.3: Partial derivative of Z with respect to temperature at constant pressure $(\partial Z/\partial T)_p$.

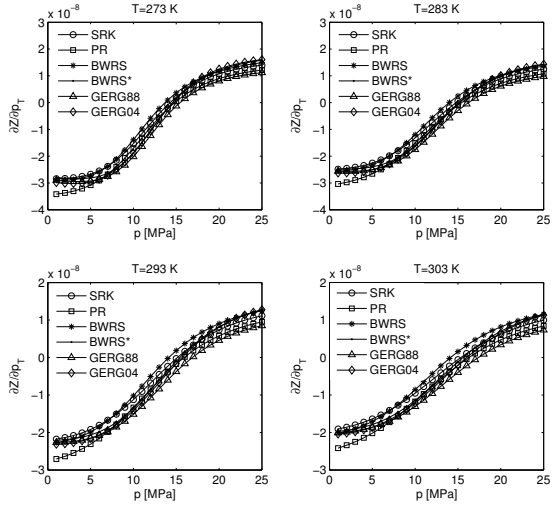

Figure 2.4: Partial derivative of Z with respect to pressure at constant temperature $(\partial Z/\partial p)_T$.

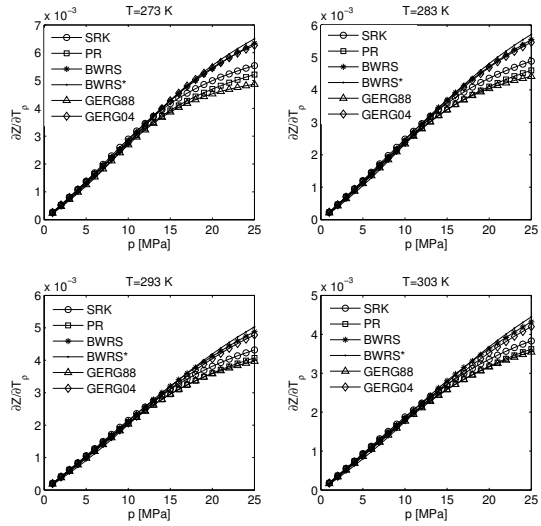

Figure 2.5: Partial derivative of Z with respect to temperature at constant density $(\partial Z/\partial T)_\rho$.

2.4 Heat transfer model

The heat exchange between the gas and the pipeline surroundings is represented by the final term in Equation (2.8). Two different approaches for modeling the heat exchange will be considered. The first case is a steady heat transfer model using a total heat transfer coefficient to predict the heat transfer between the gas and the environment. In the second case, an unsteady heat transfer model which takes into account heat accumulation in the ground is considered.

2.4.1 Steady heat transfer model

In the steady heat transfer model the heat exchange between the gas and the surroundings is modeled using a total heat transfer coefficient U. This approach is currently used by Gassco today [6]. The total heat flow between the gas and the pipeline surroundings is defined as

$$Q = UA_h(T - T_a) \tag{2.20}$$

where U is the total heat transfer coefficient, A_h the area though which heat transfer occurs, T the temperature of the gas and T_a the ambient temperature. The total heat transfer coefficient is a combined mode of three different heat transfer processes. The first process is the heat transfer between the gas and the inner wall which is modeled using an inner film heat transfer coefficient determined from the Dittus-Boelter relation [35] for turbulent flow

$$Nu = \frac{hL}{\lambda} = 0.023 \cdot Re^{0.8} \cdot Pr^n \tag{2.21}$$

where Nu, Re and Pr are the Nusselt, Reynolds and Prandtl numbers respectively. h is the film heat transfer coefficient, L the characteristic length and λ the thermal conductivity of the gas. When the gas is cooled by the ambient, $n = 0.4$, and in the reverse case $n = 0.3$.

The second process it the heat transfer through the pipe wall which is modeled as a conductive process. The thermal resistance of multilayer cylindrical wall is defined as

$$h_w = \sum_{i=1}^{n} \frac{\ln(r_{oi}/r_{ii})}{\lambda_i} \tag{2.22}$$

where λ_i is the thermal conductivity of wall layer i and r_o and r_i is the outer and inner radius respectively.

The final process is the heat transfer between the outer wall and the surrounding environment which is modeled using an outer film heat transfer coefficient. The film heat transfer coefficient depends on whether the pipeline is buried under ground or, as in the case of offshore pipelines, exposed to sea water. For a pipeline buried under ground, either a deep or shallow burial coefficient can be used, depending on the burial depth. For a pipeline which is exposed to sea water the following Nusselt number relation can be used

$$Nu = 0.26 \cdot Re^{0.6} \cdot Pr^{0.3} \tag{2.23}$$

Using an electrical circuit analogy the total heat transfer coefficient U is equal the sum of all thermal resistances. For a pipeline which is buried under ground, consisting of three different wall layers like that shown in Figure 2.6, the total heat transfer coefficient U is determined to be [36]

$$U = \left(\frac{1}{h_i} + r_1 \frac{\ln(r_2/r_1)}{\lambda_1} + r_1 \frac{\ln(r_3/r_2)}{\lambda_2} + r_1 \frac{\ln(r_4/r_3)}{\lambda_3} + \frac{r_1}{r_3 h_o} \right)^{-1} \tag{2.24}$$

where h_i and h_o are the inner and outer film heat transfer coefficients.

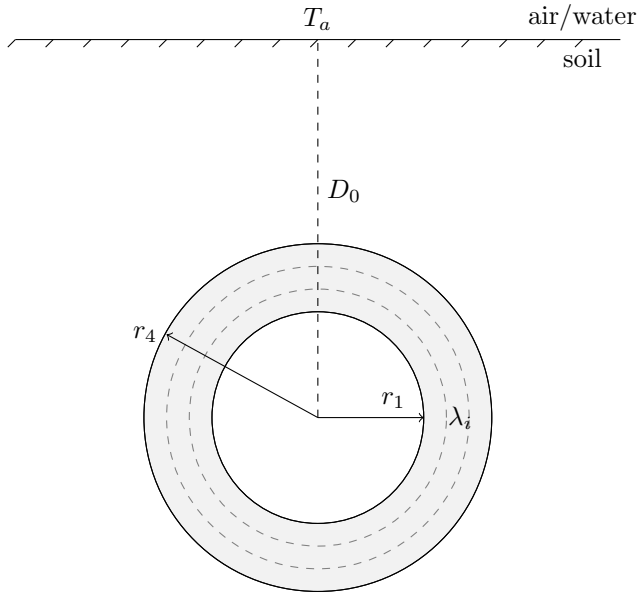

Figure 2.6: Cross section of buried pipeline consisting of three wall layers with inner radius r_1 and outer radius r_4. Each pipe layer has its specific thermal conductivity λ_i. D_0 is the burial depth from the ground to the pipe centerline and T_a the ambient temperature.

2.4.2 Unsteady heat transfer model

In the steady state heat transfer model the heat transfer is calculated using a total heat transfer coefficient U. This allows for simple calculations of the heat exchange between the gas and the surrounding environment. However, such an approach does not take into account heat accumulation in the ground surrounding the pipeline. In the work by Chaczykowski [19] the heat transfer is considered as unsteady, so that the effect of heat accumulation in the ground is taken into account. Transient heat conduction in the solid surrounding the pipeline is now modeled by solving the one-dimensional radial heat conduction equation. Assuming azimuthal symmetry,

the unsteady one-dimensional radial heat conduction equation takes the form

$$\rho c_p \frac{\partial T}{\partial t} = \frac{\lambda}{r} \frac{\partial}{\partial r} \left(r \frac{\partial T}{\partial r} \right) \tag{2.25}$$

The model is axial symmetric where each thermal layer is represented by a coaxial cylindrical shell, which is now considered as a thermal capacitor, and not a thermal resistance as in the steady heat transfer model. The setup is shown in Figure 2.7.

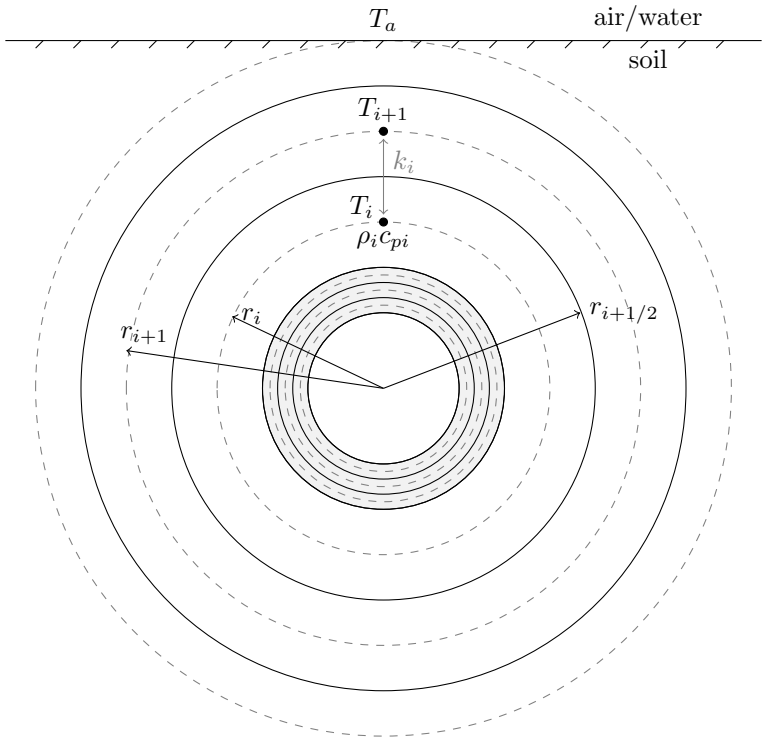

Figure 2.7: Cross-section of buried pipeline for the unsteady heat transfer model. Thermal elements are represented by coaxial cylindrical layers. Each layer is assigned a temperature T_i, density ρ_i and heat capacity c_{pi}.

In the work by Chaczykowski [19], the following equations are solved for the un-

steady external heat transfer model

$$\begin{aligned} Q &= \frac{k_0 D}{4}(T - T_1^{n+1}) \\ \rho_1 c_{p1}\frac{T_1^{n+1} - T_1^n}{\Delta t} &= \frac{k_1}{A_1}(T_2^{n+1} - T_1^{n+1}) - \frac{k_0}{A_1}(T_1^{n+1} - T) \\ \rho_i c_{pi}\frac{T_i^{n+1} - T_i^n}{\Delta t} &= \frac{k_i}{A_i}(T_{i+1}^{n+1} - T_i^{n+1}) - \frac{k_{i-1}}{A_i}(T_i^{n+1} - T_{i-1}^{n+1}) \\ \rho_N c_{pN}\frac{T_N^{n+1} - T_N^n}{\Delta t} &= \frac{k_N}{A_N}(T_a - T_N^{n+1}) - \frac{k_{N-1}}{A_N}(T_N^{n+1} - T_{N-1}^{n+1}) \end{aligned} \quad (2.26)$$

The midpoint of the cylindrical shell is located at a distance r_i from the pipe centerline, and is assigned a temperature T_i, density ρ_i and heat capacity c_{pi}. k_i is the heat transfer coefficient between elements $i-1$ and i which depends on the thermal conductivity λ_i. A_i is the area of element i ($A_i = \pi(r_{i+1/2}^2 - r_{i-1/2}^2)$). There are in total N cylindrical shells. When solving the one-dimensional flow equations (Equation (2.6)-(2.8)) at a new time level, the heat flow Q from the previous time step is used in the energy equation to model the heat exchange between the gas and the surroundings. For an updated gas temperature, the radial heat equation is solved in the domain surrounding the pipeline to update the temperature field around the pipeline and determine the new heat flow Q. Solving the radial heat equation involves finding the numerical solution to the system of equations above (Equation (2.26)). These are dicretized in an implicit way using a backward Euler method for the time integration and centered differences for the spatial derivatives.

2.5 Other properties

2.5.1 Viscosity

The viscosity of the gas in micropoise (1 micropoise = 10^{-7} kg/(m·s)) can be determined from the Lee-Gonzalez-Eakin (LGE) [37] correlation

$$\mu = K \exp(X(\rho/1000)^Y) \quad (2.27)$$

where

$$\begin{aligned} K &= \frac{(9.4 + 0.02M)(9T/5)^{1.5}}{209 + 19M + (9T/5)} \\ X &= 3.5 + \frac{986}{(9T/5)} + 0.01M \\ Y &= 2.4 - 0.2X \end{aligned} \quad (2.28)$$

where M is the molecular weight. The viscosity does not appear directly in the flow equations, but effects the pressure drop along the pipeline as the friction factor depends on the Reynolds number, which in turn depends on the viscosity. The viscosity for the natural gas mixture in Section 2.3 as a function of pressure at different temperatures is presented in Figure 2.8.

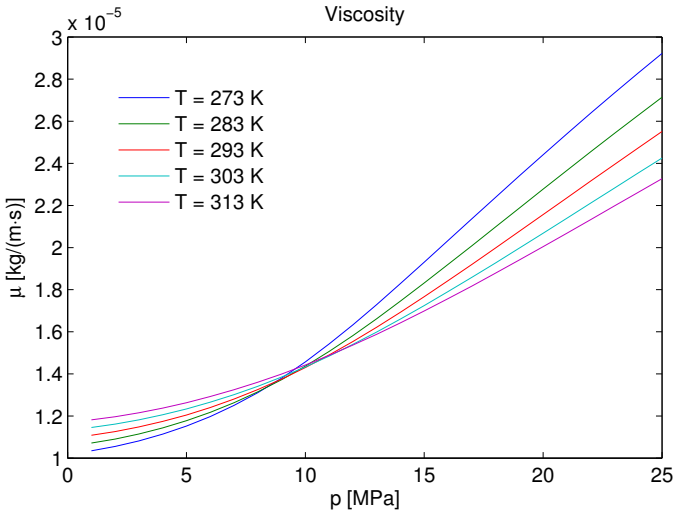

Figure 2.8: Viscosity μ for the natural gas mixture in Section 2.3 as a function of pressure at different temperatures.

2.5.2 Heat capacity

Both the heat capacity at constant volume (c_v) and at constant pressure (c_p) are needed in the flow model. The heat capacity at constant volume appears directly in the energy equation, while the heat capacity at constant pressure appears in the Prandtl number when determining the inner wall film heat transfer coefficient in the heat transfer model. The heat capacity at constant volume and pressure can be determined from the GERG 2004 equation of state [32]. Using the same gas mixture as in Section 2.3, results for c_v and c_p as a function of pressure at different temperatures are presented in Figures 2.9 and 2.10 respectively.

2.5.3 Joule-Thomson coefficient

The Joule-Thomson effect is the change in temperature upon expansion which occurs without heat transfer or work. For natural gas pipelines it is the cooling upon expansion. The Joule-Thomson coefficient is defined as

$$\mu_{JT} = \left(\frac{\partial T}{\partial p}\right)_h = \frac{R}{c_p}\frac{T^2}{p}\left(\frac{\partial Z}{\partial T}\right)_p \tag{2.29}$$

For an ideal gas $\mu_{JT} = 0$. The Joule-Thomson coefficient as a function of pressure at different temperatures is presented in Figure 2.11.

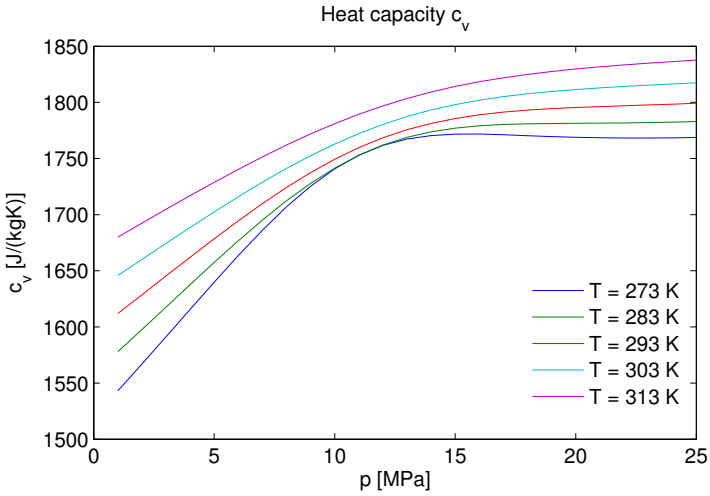

Figure 2.9: Heat capacity c_v for the natural gas mixture in Section 2.3 as a function of pressure at different temperatures.

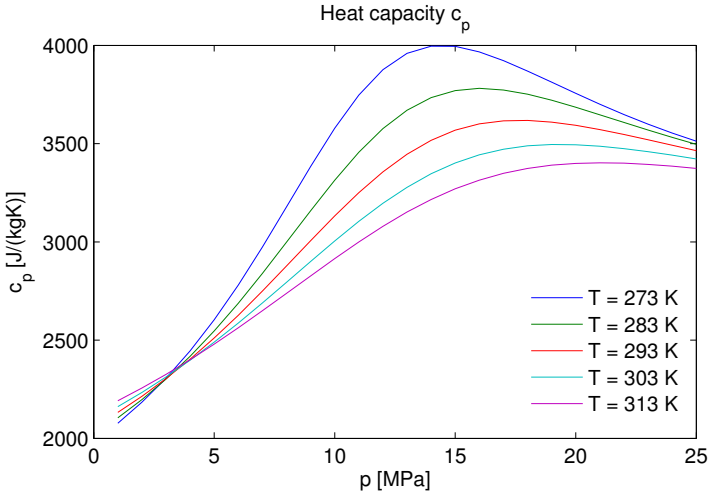

Figure 2.10: Heat capacity c_p for the natural gas mixture in Section 2.3 as a function of pressure at different temperatures.

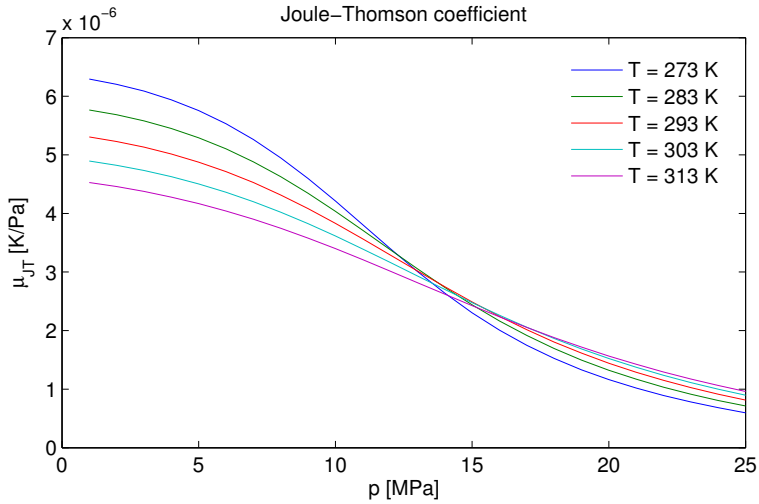

Figure 2.11: Joule-Thomson coefficient for the natural gas mixture in Section 2.3 as a function of pressure at different temperatures.

Chapter 3

Numerical Methods

The governing equations in Section 2.1 form a system of hyperbolic partial differential equations which have to be solved numerically. This chapter discusses different numerical methods which can be used to solve such a system of equations, with emphasis on finite difference methods.

An overview of different numerical techniques for one-dimensional compressible flow can be found in base literature articles, for instance by Thorely and Tiley [10]. Numerical methods include the method of characteristics, finite difference, finite volume and finite element methods. The method of characteristics was popular a few decades ago, see for instance Issa and Spalding [11] and Poloni et al. [13]. However, as will be pointed out in the following sections, the method of characteristics is slow and more difficult to implement compared to finite difference methods. Finite difference methods are commonly used to model one-dimensional compressible flow, see for instance Poloni et al. [13], Kiuchi [14], Greyvenstein [38], Abbaspour and Chapman [16], Chaczykowski [19] and Modisette [39]. It has been stated that for high pressure pipelines finite element methods are lengthy and tedious, and have therefore not been widely used [10]. A finite element method was implemented by Bisgaard et al. [40], with numerical results being compared to experimental values. Chaiko uses a finite volume approach to model transient flow in pipelines [41]. A third order Runge-Kutta discontinuous Galerkin method was successfully implemented by Gato and Henriques [42]. Osiadacz and Yedroudj [43] show that finite difference methods have considerable advantage over finite element methods with respect to computational time.

Before proceeding, a simplified flow model will be introduced. Assuming a horizontal pipeline and neglecting the convective term in the momentum equation, the continuity and momentum equations are simplified to

$$\frac{\partial \rho}{\partial t} + \frac{\partial (\rho u)}{\partial x} = 0 \tag{3.1}$$

$$\frac{\partial (\rho u)}{\partial t} + \frac{\partial p}{\partial x} = -\frac{f \rho u |u|}{2D} \tag{3.2}$$

where pressure p and density ρ are related through

$$\frac{p}{\rho} = c^2 \tag{3.3}$$

where c is defined as the constant speed of sound. Replacing the density with pressure and introducing the mass flow rate $\dot{m} = \rho u A$ (A being the pipeline cross section), Equations (3.1) - (3.2) are developed into

$$\frac{\partial p}{\partial t} + \frac{c^2}{A}\frac{\partial \dot{m}}{\partial x} = 0 \tag{3.4}$$

$$\frac{1}{A}\frac{\partial \dot{m}}{\partial t} + \frac{\partial p}{\partial x} = -\frac{f c^2 \dot{m}|\dot{m}|}{2DA^2 p} \tag{3.5}$$

This hydraulic model is the same as that of Kiuchi [14]. It assumes isothermal conditions with a constant temperature along the pipeline.

3.1 Method of characteristics

The method of characteristics (MOC) is a technique for solving hyperbolic partial differential equations. It reduces the partial differential equations into a family of ordinary differential equations, which can be solved by integrating along the characteristic curves from some initial data.

The method can be illustrated by considering the hydraulic model. Multiplying Equation (3.4) by λ and adding Equation (3.5) yields

$$\lambda\left[\frac{p_x}{\lambda} + p_t\right] + \frac{1}{A}\left[c^2\lambda\dot{m}_x + \dot{m}_t\right] + \frac{f c^2 \dot{m}|\dot{m}|}{2DA^2 p} = 0 \tag{3.6}$$

where the partial derivatives are represented by subscripts. Using the relations

$$\frac{dp}{dt} = p_x\frac{dx}{dt} + p_t \tag{3.7}$$

$$\frac{d\dot{m}}{dt} = \dot{m}_x\frac{dx}{dt} + \dot{m}_t \tag{3.8}$$

leads to the result

$$\frac{dx}{dt} = \frac{1}{\lambda} = \lambda c^2 \tag{3.9}$$

Solving the equation for λ ($\lambda = \pm 1/(c)$) and substituting back into Equation (3.9) yields

$$\frac{dx}{dt} = \pm c \tag{3.10}$$

The partial differential equations for p and $\dot{m}$ have now been reduced to two sets of ordinary differential equations (one set for each value of λ). These can be integrated along the characteristic lines. For the C^+ characteristic the equations are

$$C^+ \begin{cases} \frac{1}{c}\frac{dp}{dt} + \frac{1}{A}\frac{d\dot{m}}{dt} + \frac{f c^2 \dot{m}|\dot{m}|}{2DA^2 p} = 0 \\ \frac{dx}{dt} = c \end{cases} \tag{3.11}$$

and for the C^-

$$C^- \begin{cases} -\frac{1}{c}\frac{dp}{dt} + \frac{1}{A}\frac{d\dot{m}}{dt} + \frac{fc^2\dot{m}|\dot{m}|}{2DA^2p} = 0 \\ \frac{dx}{dt} = -c \end{cases} \tag{3.12}$$

The principle behind the MOC, illustrated in Figure 3.1, is to integrate the C^+ equation along the characteristic $dx/dt = c$ to relate the unknown values p_P and $\dot{m}_P$ to initial values p_A and $\dot{m}_A$. The same procedure is done for the C^- equation along the characteristic $dx/dt = -c$ to find a relation between p_P and $\dot{m}_P$ and initial values p_B and $\dot{m}_B$. This gives two algebraic equations for the two unknown values p_P and $\dot{m}_P$.

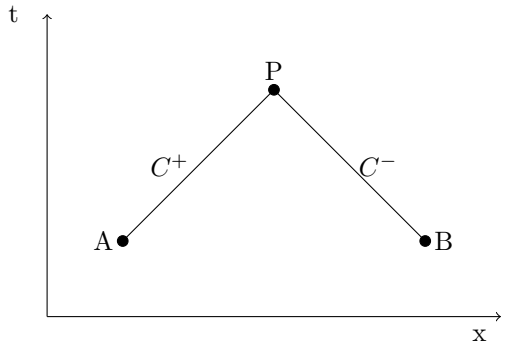

Figure 3.1: Characteristic lines in x-t diagram. Unknown values p_P and $\dot{m}_P$ are related to initial values p_A, p_B, $\dot{m}_A$ and $\dot{m}_B$ by integrating along the characteristic curves C^+ and C^-.

The governing equations can be solved by either using the natural method of characteristics or the mesh method of characteristics. The natural method is unconditionally stable and can handle discontinuities [10]. However, when calculating the updated flow conditions at point P, the space and time location in the $x-t$ diagram is the point where the characteristics from points A and B meet. This means that there is no freedom in the choice of the time step Δt, it is set by the conditions of the characteristics. For the example above the characteristic curves are $dx/dt = \pm c$. If the convective term in the momentum equation had not been neglected the characteristic curves would have been $dx/dt = u \pm c$, which is shown in the book by Wiley [44]. This adds further complications to the natural method of characteristics. Because the left and right traveling characteristics have slightly different slopes in the $x-t$ diagram they will not meet at the same grid points from the previous time level, but rather somewhere in between.

When modeling the transmission of natural gas through pipelines one would like to set the time step to a specific value based on available boundary conditions, and when calculating the flow conditions at a new time level it is desirable to have them at specified grid points. This is the basics of the mesh method, which interpolates values to a structured grid. This also allows freedom in the choice of time step Δt. The mesh method is however only conditionally stable and the time and spatial

steps are restricted by the CFL condition

$$(|u| + c)\frac{\Delta t}{\Delta x} \leq 1 \tag{3.13}$$

The mesh method of characteristics is illustrated in Figure 3.2.

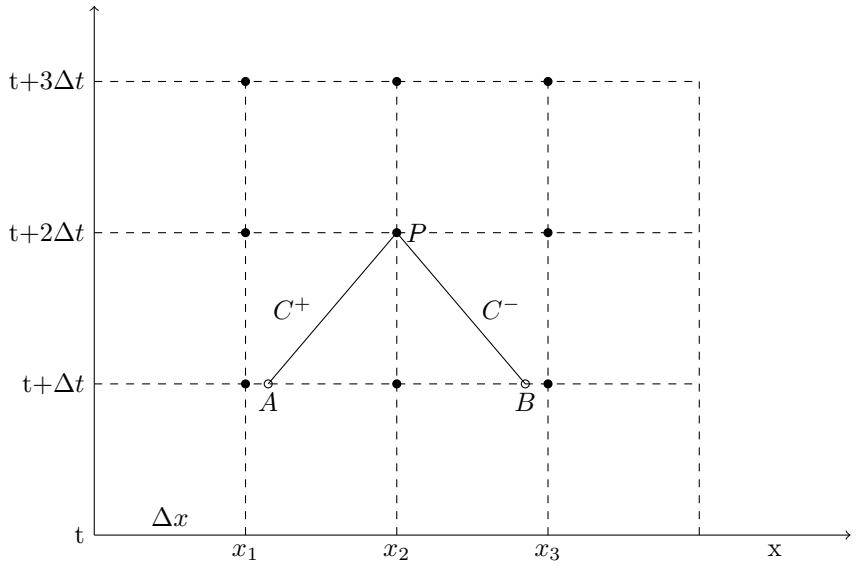

Figure 3.2: Mesh method of characteristics. Flow values at points A and B are found by interpolation from neighboring points.

When determining the flow conditions at P the following equations have to be solved.

$$(p_P - p_A) + \frac{c}{A}(\dot{m}_P - \dot{m}_A) + \frac{fc^3\dot{m}_P|\dot{m}_A|}{2DA^2p_A}\Delta t = 0 \tag{3.14}$$

$$(x_P - x_A) = c(t_P - t_A) \tag{3.15}$$

$$(p_P - p_B) - \frac{c}{A}(\dot{m}_P - \dot{m}_B) + \frac{fc^3\dot{m}_P|\dot{m}_B|}{2DA^2p_B}\Delta t = 0 \tag{3.16}$$

$$(x_P - x_B) = c(t_P - t_B) \tag{3.17}$$

In the friction term the mass flow term is represented by $\dot{m}_A|\dot{m}_P|$ and $\dot{m}_B|\dot{m}_P|$ respectively instead of $\dot{m}_P|\dot{m}_P|$ in order to give a linear equation in $\dot{m}_P$. To ensure that this is a valid approximation the CFL number should be close to, but below 1. In the mesh method of characteristics the time step is kept constant and is set by the user. The only requirement for the time step is that combined with the spatial step Δx it has to fulfill the CFL condition in Equation (3.13). The procedure for finding p_P and $\dot{m}_P$ at time level $t + 2\Delta t$ is as follows.

1. Find the positions x_A and x_B at time level $t+\Delta t$ by solving Equations (3.15) and (3.17) using the fact that $\Delta t = (t_P - t_B) = (t_P - t_A)$.

2. When the positions x_A and x_B are known the values of p_A, $\dot{m}_A$, p_B and $\dot{m}_B$ can be calculated by interpolating between points x_1 and x_2 and points x_2 and x_3 respectively.

3. When p_A, $\dot{m}_A$, p_B and $\dot{m}_B$ are known, the values of p_P and $\dot{m}_P$ can be found using Equations (3.14) and (3.16). Boundaries have to be treated separately.

The procedure above is repeated at each time step. Poloni et al. [13] compared the method of characteristics to explicit finite difference methods. It was stated that finite difference methods were easier to implement compared to the method of characteristics. Also, because of the required interpolation in the method of characteristics, finite difference methods were also found to be computationally faster. Because finite difference methods are a lot more flexible, the method of characteristics is seldom used when modeling one-dimensional compressible pipe flow. Owing to the CFL condition the method of characteristics is limited to small time steps. The method is however valuable in classification of more complex systems of PDEs, and for obtaining criteria for the proper initial and boundary conditions for the fundamental variables in different flow regimes.

3.2 Finite difference methods

Finite difference methods are commonly used when modeling the flow of natural gas through pipelines. The governing equations are transformed from partial differential equations to algebraic expressions in discrete time and space. The basic idea is illustrated in Figure 3.3.

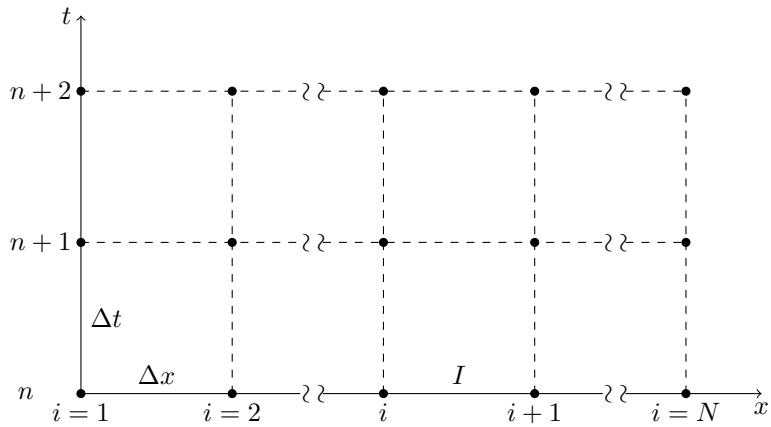

Figure 3.3: Stencil used in the finite difference method.

The pipeline is divided into N grid points with Δx being the distance between points i and $i+1$. Δt is the time step between time levels $n+1$ and n. The discretization can be either explicit or implicit in time. Explicit methods are easy to implement, but as with the method of characteristics are limited to small time steps owing to the stability condition. Implicit methods are more difficult to implement, but are stable for any choice of time and spatial step.

3.2.1 Explicit finite difference methods

Two explicit finite difference methods will be considered. The two step Lax-Wendroff method and the third order TVD Runge-Kutta method.

The two-step differential Lax-Wendroff method is an explicit finite difference method which is second order correct in time and space and was published by Lax and Wendroff in 1960 [45]. It requires that the governing equations can be written on the vector form

$$\frac{\partial \mathbf{A}}{\partial t} + \frac{\partial \mathbf{B}}{\partial x} + \mathbf{C} = 0 \tag{3.18}$$

For Equations (3.4) and (3.5) the vectors in Equation (3.18) are

$$\mathbf{A} = \begin{bmatrix} p \\ \dot{m} \end{bmatrix} \qquad \mathbf{B} = \begin{bmatrix} (c^2/A)\dot{m} \\ (A)p \end{bmatrix} \qquad \mathbf{C} = \begin{bmatrix} 0 \\ -\frac{fc^2|\dot{m}|\dot{m}}{2ADp} \end{bmatrix}$$

where the pipe cross section A and speed of sound c are assumed constant. In the first step the flow values are calculated at half time steps $t^{n+1/2}$ and half spatial steps $x_{i+1/2}$.

$$\mathbf{A}_{i+1/2}^{n+1/2} = \frac{1}{2}(\mathbf{A}_{i+1}^{n} + \mathbf{A}_{i}^{n}) - \frac{\Delta t}{2\Delta x}(\mathbf{B}_{i+1}^{n} - \mathbf{B}_{i}^{n}) - \frac{\Delta t}{4}(\mathbf{C}_{i+1}^{n} + \mathbf{C}_{i}^{n}) \tag{3.19}$$

In the second step the values are calculated at a new time step $n+1$ using the values from the previous step.

$$\mathbf{A}_{i}^{n+1} = \mathbf{A}_{i}^{n} - \frac{\Delta t}{\Delta x}(\mathbf{B}_{i+1/2}^{n+1/2} - \mathbf{B}_{i-1/2}^{n+1/2}) - \frac{\Delta t}{2}(\mathbf{C}_{i+1/2}^{n+1/2} + \mathbf{C}_{i-1/2}^{n+1/2}) \tag{3.20}$$

The method uses centered differences in space. As for the mesh method of characteristics the CFL condition in Equation (3.13) has to be fulfilled to ensure stability.

Higher order accuracy can be achieved by using the third order TVD Runge-Kutta method by Gottlieb and Shu [46] for the time discretization. The governing equations are now required to be on the form

$$\frac{\partial \mathbf{q}}{\partial t} + \mathbf{D}\frac{\partial \mathbf{q}}{\partial x} = \mathbf{S} \tag{3.21}$$

where $\mathbf{q}$ is a vector containing flow variables, $\mathbf{D}$ a coefficient matrix and $\mathbf{S}$ a source term vector. For the hydraulic model these vectors are

$$\mathbf{q} = \begin{bmatrix} p \\ \dot{m} \end{bmatrix} \qquad \mathbf{D} = \begin{bmatrix} 0 & c^2/A \\ A & 0 \end{bmatrix} \qquad \mathbf{S} = \begin{bmatrix} 0 \\ -\frac{fc^2|\dot{m}|\dot{m}}{2ADp} \end{bmatrix}$$

The 3rd order TVD Runge-Kutta method advances the solution to time level $n+1$ by performing the steps

$$\begin{aligned} \mathbf{q}^{(1)} &= \mathbf{q}^n + \Delta t \mathbf{R}(\mathbf{q}^n) \\ \mathbf{q}^{(2)} &= \frac{3}{4}\mathbf{q}^n + \frac{1}{4}(\mathbf{q}^{(1)} + \Delta t \mathbf{R}(\mathbf{q}^{(1)})) \\ \mathbf{q}^{(n+1)} &= \frac{1}{3}\mathbf{q}^n + \frac{2}{3}(\mathbf{q}^{(2)} + \Delta t \mathbf{R}(\mathbf{q}^{(2)})) \end{aligned} \tag{3.22}$$

where $\mathbf{R}$ are the vectors of the right hand side of $(q_i)_t = -(q_i)_x + S_i$. As with the Lax-Wendroff method the spatial derivatives are approximated by centered differences. The second order centered difference scheme for the spatial derivative of a variable y discretized from x_1 to x_N is

$$\frac{\partial \mathbf{y}}{\partial x} = \begin{pmatrix} \frac{dy(x_1)}{dx} \\ \frac{dy(x_2)}{dx} \\ \vdots \\ \frac{dy(x_{N-1})}{dx} \\ \frac{dy(x_N)}{dx} \end{pmatrix} = \frac{1}{2\Delta x} \begin{pmatrix} -3 & 4 & -1 & 0 & \cdots & 0 \\ -1 & 0 & 1 & 0 & \cdots & 0 \\ \vdots & \ddots & \ddots & \ddots & \ldots & \vdots \\ 0 & \cdots & 0 & -1 & 0 & 1 \\ 0 & \cdots & 0 & 1 & -4 & 3 \end{pmatrix} \begin{pmatrix} y(x_1) \\ y(x_2) \\ \vdots \\ y(x_{N-1}) \\ y(x_N) \end{pmatrix} + \mathcal{O}(\Delta x^2) \tag{3.23}$$

One sided differences are used at the boundaries x_1 and x_N. Higher order centered difference schemes can easily be applied. Stencils for such schemes can be found in the book by Gustafsson [47]. The stability domain in slightly larger for the 3rd order TVD Runge-Kutta method compared to the Lax-Wendroff method. However, the computational time of the Runge-Kutta method is greater than the Lax-Wendroff method, as three iterations are required at each time level of the Runge-Kutta method compared to the two iterations of the Lax-Wendroff method.

3.2.2 Implicit finite difference methods

Compared to explicit methods, implicit methods are unconditionally stable and are not limited to small time steps by the CFL condition. In many cases it may be advantageous to take long time steps, and because of its stability properties, implicit finite difference methods are commonly used in commercial tools for one-dimensional compressible flow calculations.

For implicit finite difference schemes, a simple method for the time discretization of a flow variable Y at grid point i is the backward Euler method

$$\frac{\partial Y(x_i, t_{n+1})}{\partial t} = \frac{Y_i^{n+1} - Y_i^n}{\Delta t} + \mathcal{O}(\Delta t) \tag{3.24}$$

Spatial derivatives can be approximated by either upwind or centered differences. The first order one-sided upwind discretization approximates the spatial derivative of a variable Y at point i by

$$\frac{\partial Y(x_i, t_{n+1})}{\partial x} = \frac{Y_i^{n+1} - Y_{i-1}^{n+1}}{\Delta x} + \mathcal{O}(\Delta x) \tag{3.25}$$

and the second order centered difference discretization approximates the spatial derivative of a variable Y at a point i by

$$\frac{\partial Y(x_i, t_{n+1})}{\partial x} = \frac{Y_{i+1}^{n+1} - Y_{i-1}^{n+1}}{2\Delta x} + \mathcal{O}(\Delta x^2) \tag{3.26}$$

Higher order stencils can be used for both the upwind and centered difference approximations. The expressions can be found in the book by Gustafsson [47]. When discretizing all terms in a fully implicit way the governing equations form a system non-linear equations. Both Kiuchi [14] and Abbaspour and Chapman [16] solve the system of non-linear equations by using the Newton-Raphson method. This can be computationally expensive, especially for long pipelines and complicated networks. To avoid having to solve a system of non-linear equations, the non-linear terms can be linearized about the previous time step to give a system of linear equations. The procedure can be found in the article by Luskin [48], and is also illustrated in research article [a].

An alternative to the backward Euler method using either upwind or centered differences for the spatial derivatives is the cell centered method. This method is the same as that of Kiuchi [14], Abbaspour and Chapman [16], Abbaspour et al. [49] and Modisette [39], with the latter referring to the method as the cell centered method. In the cell centered method the partial derivatives for each pipe section, and not for each grid point as in the backward Euler method, are approximated by algebraic expressions. In Figure 3.3 pipe section I is the section between grid points i and $i+1$. For section I the time derivatives are approximated by

$$\frac{\partial Y(x_I, t_{n+1})}{\partial t} = \frac{Y_{i+1}^{n+1} + Y_i^{n+1} - Y_{i+1}^{n} - Y_i^{n}}{2\Delta t} + \mathcal{O}(\Delta t) \tag{3.27}$$

the spatial derivatives by

$$\frac{\partial Y(x_I, t_{n+1})}{\partial x} = \frac{Y_{i+1}^{n+1} - Y_i^{n+1}}{\Delta x} + \mathcal{O}(\Delta x^2) \tag{3.28}$$

and the individual terms by

$$Y(x_I, t_{n+1}) = \frac{Y_{i+1}^{n+1} + Y_i^{n+1}}{2} + \mathcal{O}(\Delta x^2) \tag{3.29}$$

This method is first order correct in time and second order correct in space, and is therefore similar to the backward Euler method with second order centered differences for the spatial derivatives. However, the cell centered method is slightly easier to implement because the boundary conditions are simpler to handle compared to the backward Euler method with centered differences. To illustrate how the cell centered method can be used to solve the governing equations, the hydraulic model is once again considered

$$\frac{\partial p}{\partial t} + \frac{c^2}{A}\frac{\partial \dot{m}}{\partial x} = 0 \tag{3.30}$$

$$\frac{\partial \dot{m}}{\partial t} + A\frac{\partial p}{\partial x} = -\frac{f c^2 \dot{m}|\dot{m}|}{2DAp} \tag{3.31}$$

where the friction term in the momentum equation is the only non-linear term. This term will be linearized in the following. A variable y at time level $n+1$ can be written as a first order Taylor expansion

$$y_i^{n+1} = y_i^n + \Delta t (y_i^n)_t + \mathcal{O}(\Delta t^2) \tag{3.32}$$

Using this approximation, the friction term in the momentum equation can according to Luskin [48] be developed into

$$K\frac{(\dot{m}^{n+1})^2}{p^{n+1}} = K\frac{\dot{m}^n}{p^n}(\dot{m} + 2\Delta t \dot{m}_t) + \mathcal{O}(\Delta t^2) \tag{3.33}$$

where $K = fc^2/2DA$. The pressure is taken from the previous time step and the first order Taylor expansion has been used for the mass flow. Inserting the expression for the spatial derivative (Equation (3.28)) and the individual term (Equation (3.29)) in Equation (3.33), the friction term is further developed into

$$K\frac{(\dot{m}^{n+1})^2}{p^{n+1}} \approx K\frac{(\dot{m}_{i+1}^n + \dot{m}_i^n)}{(p_{i+1}^n + p_i^n)}\left(\dot{m}_{i+1}^{n+1} + \dot{m}_i^{n+1} - \frac{\dot{m}_{i+1}^n + \dot{m}_i^n}{2}\right) \tag{3.34}$$

Using the expression above for the friction term, the governing equations form a system of linear equations which can be solved using linear algebra. The discretized equations are written on the matrix form

$$\mathbf{A}\mathbf{x} = \mathbf{b} \tag{3.35}$$

For a pipeline consisting of 4 grid points like that in Figure 3.4, with inlet mass flow and outlet pressure as boundary conditions, the matrixes in Equation (3.35) take the form as given below.

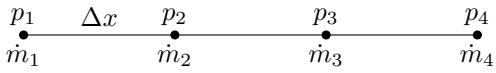

Figure 3.4: A short pipeline discretized by 4 grid points, with pressure and mass flow stored at each grid point.

$$\mathbf{A} = \begin{pmatrix}
\frac{1}{2\Delta t} & \frac{1}{2\Delta t} & 0 & \frac{c^2}{A\Delta x} & 0 & 0 \\
-\frac{A}{\Delta x} & \frac{A}{\Delta x} & 0 & \frac{1}{2\Delta t} + \frac{fc^2}{2DA}\frac{(\dot{m}_1^n + \dot{m}_2^n)}{(p_1^n + p_2^n)} & 0 & 0 \\
0 & \frac{1}{2\Delta t} & \frac{1}{2\Delta t} & -\frac{c^2}{A\Delta x} & \frac{c^2}{A\Delta x} & 0 \\
0 & -\frac{A}{\Delta x} & \frac{A}{\Delta x} & \frac{1}{2\Delta t} + \frac{fc^2}{2DA}\frac{(\dot{m}_2^n + \dot{m}_3^n)}{(p_2^n + p_3^n)} & \frac{1}{2\Delta t} + \frac{fc^2}{2DA}\frac{(\dot{m}_2^n + \dot{m}_3^n)}{(p_2^n + p_3^n)} & 0 \\
0 & 0 & \frac{1}{2\Delta t} & 0 & -\frac{c^2}{A\Delta x} & \frac{c^2}{A\Delta x} \\
0 & 0 & -\frac{A}{\Delta x} & 0 & \frac{1}{2\Delta t} + \frac{fc^2}{2DA}\frac{(\dot{m}_3^n + \dot{m}_4^n)}{(p_3^n + p_4^n)} & \frac{1}{2\Delta t} + \frac{fc^2}{2DA}\frac{(\dot{m}_3^n + \dot{m}_4^n)}{(p_3^n + p_4^n)}
\end{pmatrix}$$

$$\mathbf{x} = \begin{bmatrix} p_1^{n+1} \\ p_2^{n+1} \\ p_3^{n+1} \\ \dot{m}_2^{n+1} \\ \dot{m}_3^{n+1} \\ \dot{m}_4^{n+1} \end{bmatrix} \qquad \mathbf{b} = \begin{bmatrix} \frac{p_1^n + p_2^n}{2\Delta t} + \frac{c^2}{A}\frac{\dot{m}_1^{n+1}}{\Delta x} \\ -\frac{\dot{m}_1^{n+1}}{2\Delta t} - \frac{fc^2}{2DA}\frac{\dot{m}_1^n + \dot{m}_2^n}{p_1^n + p_2^n}\dot{m}_1^{n+1} + \frac{\dot{m}_1^n + \dot{m}_2^n}{2\Delta t} + \frac{1}{2}\frac{fc^2}{2DA}\frac{(\dot{m}_1^n + \dot{m}_2^n)^2}{p_1^n + p_2^n} \\ \frac{p_2^n + p_3^n}{2\Delta t} \\ \frac{\dot{m}_2^n + \dot{m}_3^n}{2\Delta t} + \frac{1}{2}\frac{fc^2}{2DA}\frac{(\dot{m}_2^n + \dot{m}_3^n)^2}{(p_2^n + p_3^n)} \\ \frac{p_3^n + p_4^n}{2\Delta t} - \frac{p_4^{n+1}}{2\Delta t} \\ \frac{\dot{m}_3^n + \dot{m}_4^n}{2\Delta t} + \frac{1}{2}\frac{fc^2}{2DA}\frac{(\dot{m}_3^n + \dot{m}_4^n)^2}{(p_3^n + p_4^n)} - A\frac{p_4^{n+1}}{\Delta x} \end{bmatrix}$$

Chapter 4

Results

This chapter presents results for different flow setups using the numerical methods presented in Chapter 3. In Section 4.1 the method of characteristics and explicit finite difference methods are used to solve the hydraulic isothermal model. Discretization errors for all schemes are presented and the hydraulic model is validated by comparing numerical results to measured values from a short on-shore pipeline. In Section 4.2 implicit finite difference methods are used to solve the full non-isothermal model. Verification and validation of the model is included in Section 4.3. Verification is done by comparing numerical results to other results in the literature, while validation is performed by comparing numerical results to measured values from an offshore pipeline operated by Gassco.

4.1 Method of characteristics and explicit finite difference methods

The method of characteristics was compared to explicit finite difference methods for a horizontal pipeline. Isothermal conditions were assumed, meaning only the hydraulic model introduced at the beginning of Chapter 3 was solved for the flow. Two explicit finite difference methods were considered, the two step Lax-Wendroff method and the 3rd order TVD Runge-Kutta method, both of which use centered differences for the spatial derivatives.

4.1.1 Results isothermal model

A 48 km horizontal pipeline with an inner diameter of $D = 1.016$ m was considered. The constant speed of sound and friction factor were set to 380 m/s and $f = 0.0075$ respectively. The following boundary conditions were used

$$\begin{aligned} p(0,t) &= 6 \text{ MPa} \\ \dot{m}(L,t) &= f(t) \text{ kg/s} \end{aligned} \tag{4.1}$$

where $f(t)$ is depicted in Figure 4.1.

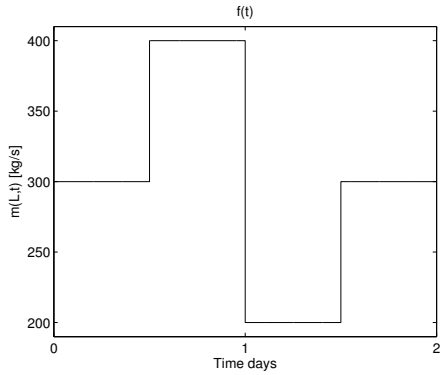

Figure 4.1: Boundary condition for outlet mass flow.

The pipeline was divided into 12 sections, each with a discretization length of $\Delta x = 4000$ m. The time step was set to $\Delta t = 10$ s. With the speed of sound being 380 m/s the CFL number was determined to be 0.95. Results for inlet mass flow and outlet pressure are presented in Figures 4.2 and 4.3 respectively. The difference between the solution strategies is small and not visible to the left in Figures 4.2 and 4.3. A close up view during the transient is shown to the right, where small differences can be observed. The two-step Lax-Wendroff method agrees well with the 3rd order TVD Runge-Kutta method, while the method of characteristics differs slightly compared to the other two. The reason for this discrepancy could be the interpolation errors which are introduced in the mesh method of characteristics. The Lax-Wendroff method had the shortest computational time, followed by the Runge-Kutta method which was slightly longer. For the presented case with 17280 time steps the total computational time was approximately 1 second. For the method of characteristics the computational time was significantly longer and over twice that of the explicit finite difference methods. This result is in agreement with Poloni et al. [13]. This increase in computational time is because of the interpolation which is required at each grid point and time step. The method of characteristics is seldom used owing to the fact that it is less flexible compared to finite difference methods because of the required interpolation, which also makes it computationally more demanding.

4.1.2 Discretization errors

The numerical discretization errors were investigated for all methods presented in Section 4.1.1. Owing to the stability criteria, the CFL number was kept constant at 0.95. This was done by reducing the time step Δt together with the spatial step Δx for each simulation. The local error is defined as

$$e = \frac{1}{N}\left(\sum_{i=1}^{N}\left(\frac{Y_i - Y_{i,h_i}}{Y_{i,h_i}}\right)^2\right)^{1/2} \tag{4.2}$$

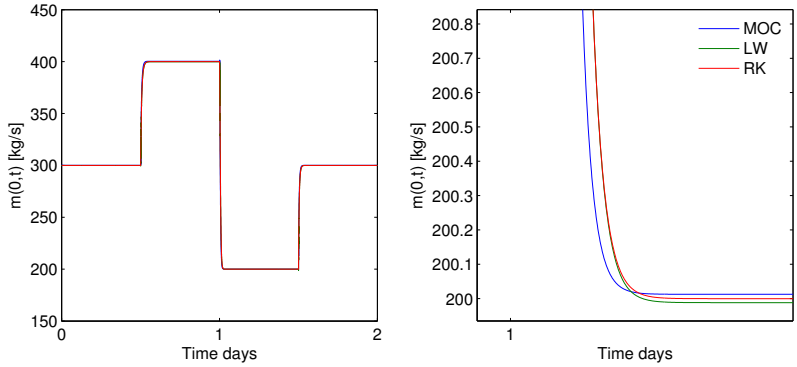

Figure 4.2: Left: Results for inlet mass flow using the method of characteristics (MOC), two-step Lax-Wendroff method (LW) and the 3rd order TVD Runge-Kutta method (RK). Right: Close up view during the transient.

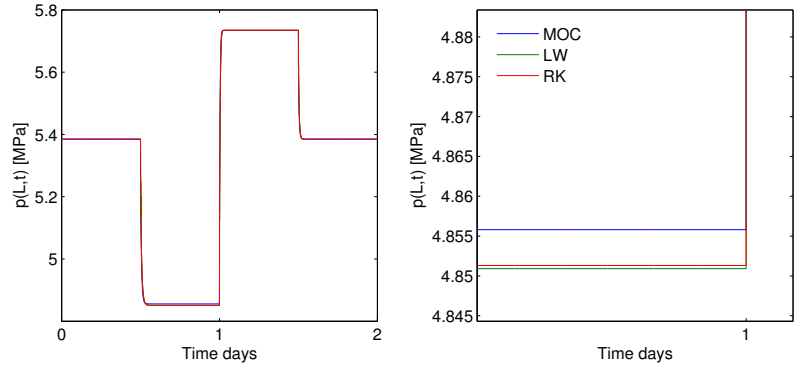

Figure 4.3: Left: Results for outlet pressure using the method of characteristics (MOC), two-step Lax-Wendroff method (LW) and the 3rd order TVD Runge-Kutta method (RK). Right: Close up view during the transient.

where Y represents p and $\dot{m}$ at point i. The summation is done over all grid points N. Y_{i,h_i} is the numerical solution computed using the finest grid and the shortest time step (high resolution solution), and is assumed to be the exact solution. In the case above the high resolution solution was found using a spatial step of $\Delta x = 125$ m and a time step of $\Delta t = 0.3125$ s. The local errors e for both p and $\dot{m}$ averaged over time are presented in Figure 4.4. These are in general small compared to numerical results of p and $\dot{m}$, even for a coarse grid with $N = 13$ ($\Delta x = 4000$ m) and a time step of $\Delta t = 10$ s. The local errors are least for the two-step Lax-Wendroff method, followed by the 3rd order TVD Runge-Kutta method and the method of characteristics. All three methods are found to be approximately second order correct, with the -2 slope indicated in Figure 4.4.

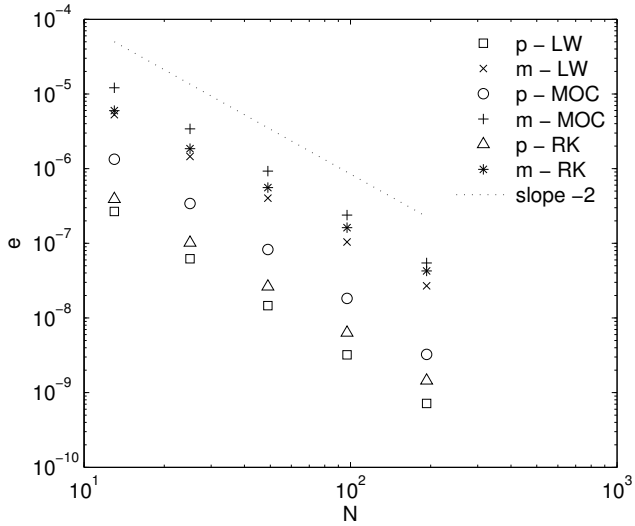

Figure 4.4: Local error e for pressure p and mass flow $\dot{m}$ as a function of grid points N. The local error is computed for the two-step Lax-Wendroff method (LW), the method of characteristics (MOC) and the 3rd order TVD Runge-Kutta method (RK).

4.1.3 Validation isothermal model

The isothermal model is validated by solving Equations (3.4) - (3.5) using operational data from a short transport pipeline. The pipeline considered is a 48 km on-shore pipeline operated by Gassco. The difference between the inlet and outlet temperature is approximately 3 °C, which justifies the isothermal assumption. The internal diameter is 1.016 m and the pipeline was divided into 13 grid points with a spatial discretization length of approximately $\Delta x = 4000$ m. The time step was set to $\Delta t = 10$ s. Inlet pressure and outlet mass flow were given as boundary conditions. The speed of sound was $c = 340$ m/s and the friction factor $f = 0.0075$. Results for a 12 hour period are presented in Figure 4.5, with the inlet mass flow to the left and the outlet pressure to the right. The results were found using the two-step Lax-Wendroff method which was chosen due to its short computational time, but both the 3rd order TVD Runge-Kutta method and the method of characteristics gave almost identical results. Both the computed inlet mass flow and outlet pressure agree well with measured values, indicating that the isothermal approximation is valid for the considered pipeline. However, for longer pipelines operating at high pressure one should, as shown by Osiadacz [17], solve the non-isothermal model. This will be considered in the next section.

Explicit finite difference methods are easy to implement and are fast and efficient. For the pipeline considered in Figure 4.5 they also give acceptable results for the flow. However, for long offshore pipelines the distance between grid points

can be small, especially when there is a steep inclination. Also, it may often be advantageous to use longer time steps than $\Delta t = 10$ s, especially during steady state conditions. Longer time steps and shorter grid spacing means higher CFL numbers. Explicit methods are only stable for CFL numbers less than 1. Implicit finite difference methods are stable for any CFL number, and are therefore often used in commercial tools for one-dimensional compressible flow models. Implicit methods will be considered in the next section.

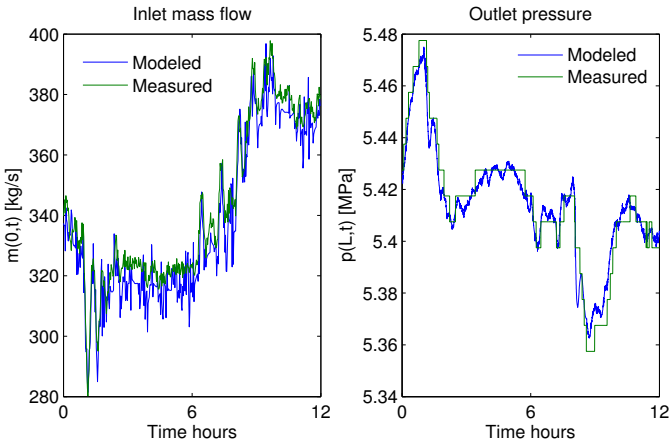

Figure 4.5: Results for 48 km on-shore pipeline. Left: Inlet mass flow. Right: Outlet pressure. Results are compared to measured values.

4.2 Implicit finite difference methods

Two different implicit finite difference solution strategies will be considered. The first case is the cell centered method where the flow values are computed at the midpoint between two grid points. This method is first order correct in time and second order correct in space. In the second case the backward Euler method will be considered, where the spatial derivatives are approximated using both the one sided upwind approximation and the centered difference approximation. This method is first order correct in time and either first, second or forth order correct in space, depending on the selected stencil.

4.2.1 Isothermal model

For the isothermal model the setup and boundary conditions were the same as in Section 4.1.1. Results for inlet mass flow and outlet pressure were identical to those in Figures 4.2 and 4.3. The CFL number of the flow is 0.95. Implicit finite difference methods are unconditionally stable and do not have the same restrictions on the CFL number as explicit methods. However, for a CFL number of 0.95 the

backward Euler method with one sided first order upwind approximation for the spatial derivatives was found to be unstable. In the hydraulic model (Equations (3.4) - (3.5)), information will travel along the characteristic curves with slopes $\pm c$. Using the one sided approximation for the spatial derivatives, information is only taken from points which are upstream of the point where the flow is being computed. While that is correct for the right going acoustic wave with the wave speed c, it is wrong for the left going acoustic wave with wave speed $-c$. The von Neumann stability analysis shows that the backward Euler method with one sided first order upwind approximations for the spatial derivatives becomes unstable for CFL numbers less than 1. When using centered differences information is taken from points lying both upstream and downstream, allowing information to travel along both characteristic curves. Centered differences are therefore a more physically correct way of approximating the spatial derivatives compared to one-sided approximations. The backward Euler method with one-sided first order upwind approximations for the spatial derivatives is a consistent method for modeling one-dimensional compressible flow through pipelines, however, it is not convergent. More details are included in the attached research article [e].

As the backward Euler method with one-sided first order upwind approximations for the spatial derivatives is not convergent, it is not possible to determine the discretization errors for CFL numbers below 1. These have therefore been omitted in the following. Both the spatial and temporal discretization errors for the cell centered method and the backward Euler method with second and forth order centered differences for the spatial derivatives are presented in Figure 4.6. Corresponding values for the spatial discretization errors are given in Tables 4.1 - 4.3.

Table 4.1: Spatial discretization error as a function of grid points N in the isothermal model using the implicit cell centered method. e is the local error and O the order.

		p		$\dot{m}$	
N	Δx [km]	e	O	e	O
13	4	$1.9248 \cdot 10^{-8}$		$4.0496 \cdot 10^{-7}$	
25	2	$3.4097 \cdot 10^{-9}$	2.65	$7.4040 \cdot 10^{-8}$	2.6
49	0.5	$5.9564 \cdot 10^{-10}$	2.62	$1.2929 \cdot 10^{-8}$	2.6
97	0.25	$1.0062 \cdot 10^{-10}$	2.61	$2.1776 \cdot 10^{-9}$	2.6
193	0.125	$1.4273 \cdot 10^{-11}$	2.67	$3.0862 \cdot 10^{-10}$	2.66

Table 4.2: Spatial discretization error as a function of grid points N in the isothermal model using the backward Euler method with second order centered differences for the spatial derivatives. e is the local error and O the order.

		p		$\dot{m}$	
N	Δx [km]	e	O	e	O
13	4	$3.8797 \cdot 10^{-8}$		$1.0624 \cdot 10^{-6}$	
25	2	$1.1691 \cdot 10^{-8}$	1.83	$2.2467 \cdot 10^{-7}$	2.38
49	0.5	$1.9516 \cdot 10^{-9}$	2.25	$3.2400 \cdot 10^{-8}$	2.63
97	0.25	$3.2864 \cdot 10^{-10}$	2.37	$4.5864 \cdot 10^{-9}$	2.71
193	0.125	$5.1955 \cdot 10^{-11}$	2.45	$6.1004 \cdot 10^{-10}$	2.75

Table 4.3: Spatial discretization error as a function of grid points N in the isothermal model using the backward Euler method with forth order centered differences for the spatial derivatives. e is the local error and O the order.

		p		$\dot{m}$	
N	Δx [km]	e	O	e	O
13	4	$8.6265 \cdot 10^{-9}$		$3.1216 \cdot 10^{-7}$	
25	2	$7.6551 \cdot 10^{-9}$	0.18	$2.3675 \cdot 10^{-8}$	3.94
49	0.5	$1.3435 \cdot 10^{-9}$	1.40	$1.1352 \cdot 10^{-9}$	4.23
97	0.25	$2.3456 \cdot 10^{-10}$	1.79	$5.1589 \cdot 10^{-11}$	4.33
193	0.125	$4.2355 \cdot 10^{-11}$	1.97	$4.5962 \cdot 10^{-12}$	4.12

Table 4.4: Temporal discretization error as a function of time step Δt in the isothermal model using the implicit cell centered method. e is the local error and O the order.

	p		$\dot{m}$	
Δt [s]	e	O	e	O
80	$3.9338 \cdot 10^{-6}$		$3.5396 \cdot 10^{-5}$	
40	$1.4327 \cdot 10^{-6}$	1.46	$1.4664 \cdot 10^{-5}$	1.27
20	$5.0897 \cdot 10^{-7}$	1.48	$6.0384 \cdot 10^{-6}$	1.28
10	$1.7456 \cdot 10^{-7}$	1.50	$2.4436 \cdot 10^{-6}$	1.29
5	$5.5810 \cdot 10^{-8}$	1.53	$9.4143 \cdot 10^{-7}$	1.31
2.5	$1.5025 \cdot 10^{-8}$	1.61	$3.2566 \cdot 10^{-7}$	1.35

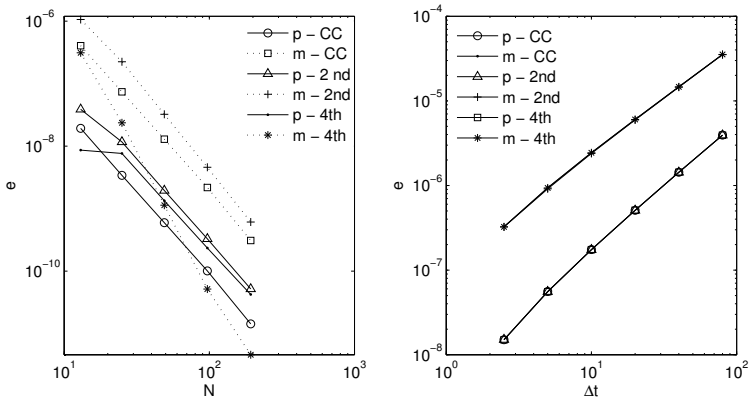

Figure 4.6: Discretization errors for the implicit cell centered method (CC), backward Euler method with 2nd order centered differences (2nd) and 4th order centered differences (4th) for the spatial derivatives. Left: Spatial discretization error as a function of grid points N. Right: Temporal discretization error as a function of time step Δt.

For the cell centered method both the pressure and mass flow converge to an order of approximately 2.6. A similar result for the backward Euler method with second order centered differences was found. For the backward Euler method with forth order centered differences the mass flow converges to the expected forth order, while the pressure only converged to second order. The temporal discretization error is presented to the right in Figure 4.6, with values given in Table 4.4. Results in Table 4.4 were computed using the cell centered method. As can be seen in Figure 4.6, the temporal discretization error for the backward Euler method with second and forth order centered differences were almost identical to those of the cell centered method, and are therefore not listed in separate tables.

4.2.2 Non-isothermal model

In the full non-isothermal model Equations (2.6) - (2.8) are solved for the flow. First an on-shore pipeline buried under ground with a length of 650 km and inner diameter of 1 m is considered. The following boundary conditions were used:

$$\dot{m}(0,t) = f(t) \text{ kg/s} \tag{4.3}$$

$$\begin{aligned} T(0,t) &= 30\ ^\circ\text{C} \\ p(L,t) &= 9 \text{ MPa} \end{aligned} \tag{4.4}$$

where $f(t)$ is depicted in Figure 4.7.

The distance from the ground surface to the pipe centerline was 2 m, with the ambient temperature being 5 °C. The gas composition (mole fraction) was set to:

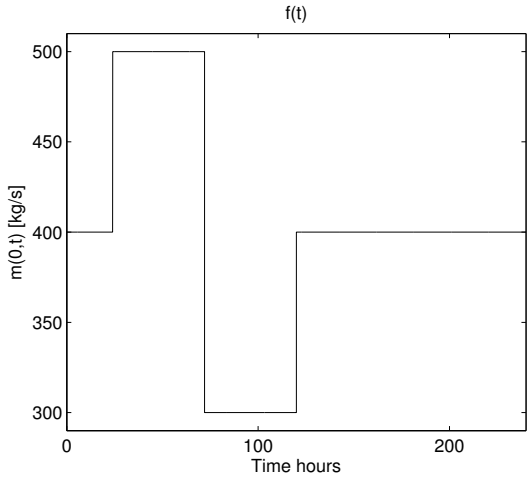

Figure 4.7: Boundary condition for inlet mass flow in full non-isothermal model.

$CH_4 - 89.16\%$, $C_2H_6 - 7.3513\%$, $C_3H_8 - 0.5104\%$, $nC_4H_{10} - 0.0251\%$, $iC_4H_{10} - 0.0311\%$, $nC_5H_{12} - 0.0009\%$, $iC_5H_{12} - 0.0024\%$, $N_2 - 0.6980\%$, $CO_2 - 2.2208\%$. The tuned BWRS equation of state was used to determine the compressibility factor while the heat exchange between the gas and the pipeline surroundings was modeled with the steady external heat transfer model. The pipe wall consists of a single steel layer with a thickness of 25 mm, density $\rho = 7850$ kg/m^3, heat capacity $c_p = 500$ J/(kg·K) and thermal conductivity $\lambda = 45$ W/(m·K). The surrounding soil had a density of $\rho = 2650$ kg/m^3, heat capacity $c_p = 950$ J/(kg·K) and thermal conductivity $\lambda = 3$ W/(m·K). The pipeline was divided into 101 grid points with a grid spacing of $\Delta x = 6.5$ km. The time step was set to $\Delta t = 60$ s. The governing equations were solved using the implicit cell centered method. Results for inlet pressure, outlet mass flow and outlet temperature are presented in Figure 4.8. For a 650 km pipeline under the given operating conditions it takes almost 50 hours for the mass flow at the outlet to reach that of the inlet.

In Figure 4.9 the temperature profile along the pipeline at the final time step ($t = 240$ hours) is shown. The gas temperature is equal to the ambient temperature of 5 °C after approximately 250 km. After this the gas temperature is lower than the ambient due to the Joule-Thomson effect, which is cooling upon expansion.

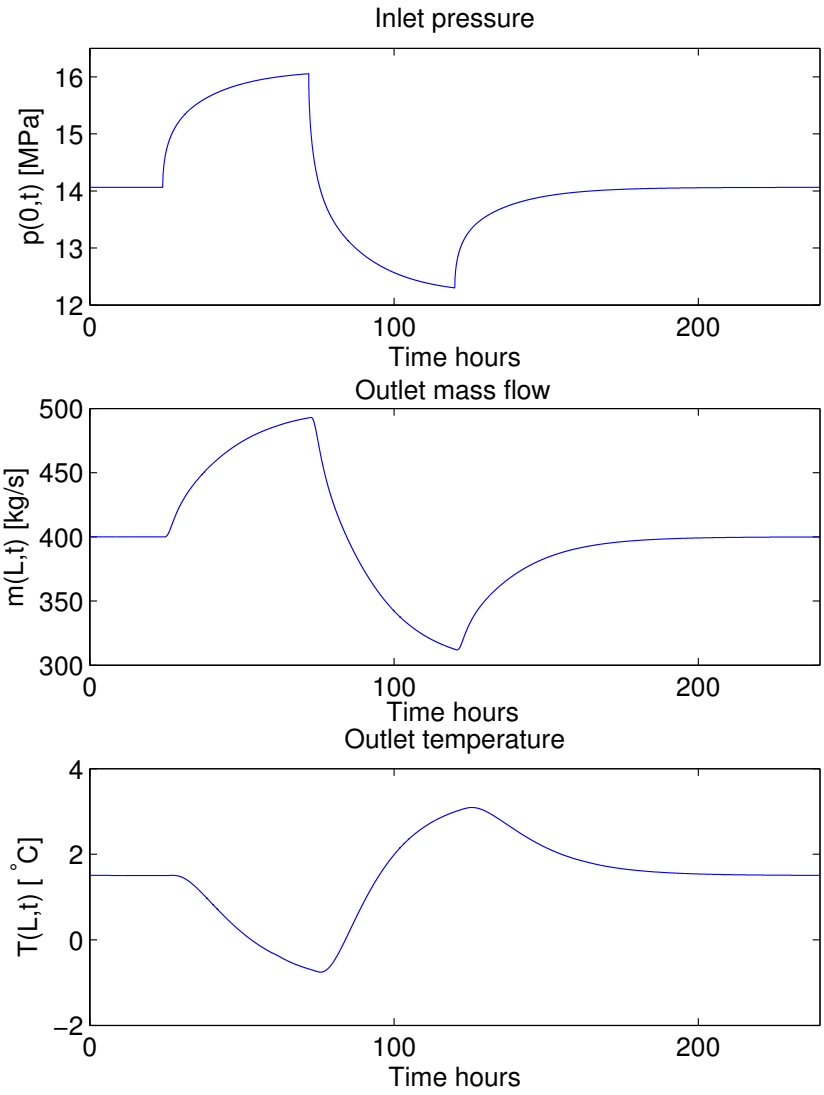

Figure 4.8: Results non-isothermal model. Top inlet pressure, middle outlet mass flow and bottom outlet temperature.

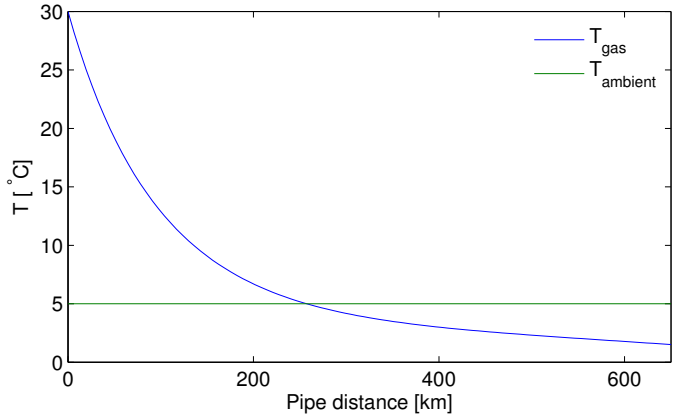

Figure 4.9: Temperature profile along the pipeline at the final time step. Gas temperature is equal the ambient temperature after approximately 250 km.

4.2.3 Discretization errors

Both the temporal and spatial discretization errors using the cell centered method are presented in Figure 4.10, with corresponding values given in Tables 4.5 and 4.6.

Table 4.5: Spatial discretization error as a function of grid points N in the non-isothermal model using the implicit cell centered method. e is the local error and O the order.

		p		$\dot{m}$		T	
N	Δx [km]	e	O	e	O	e	O
26	26	$9.1177 \cdot 10^{-7}$		$4.0748 \cdot 10^{-6}$		$2.6242 \cdot 10^{-6}$	
51	13	$1.1964 \cdot 10^{-7}$	3.01	$1.1655 \cdot 10^{-6}$	1.86	$6.1345 \cdot 10^{-7}$	2.16
101	6.5	$7.6746 \cdot 10^{-9}$	3.52	$3.4679 \cdot 10^{-7}$	1.82	$1.6496 \cdot 10^{-7}$	2.04
201	3.25	$2.6177 \cdot 10^{-9}$	2.86	$9.6424 \cdot 10^{-8}$	1.83	$4.4347 \cdot 10^{-8}$	2.00
401	1.625	$8.2002 \cdot 10^{-10}$	2.56	$2.2285 \cdot 10^{-8}$	1.90	$1.0205 \cdot 10^{-8}$	2.03
801	0.825	$1.9715 \cdot 10^{-10}$	2.46	$3.5674 \cdot 10^{-9}$	2.05	$1.6375 \cdot 10^{-9}$	2.15

Table 4.6: Temporal discretization error in the non-isothermal model using the implicit cell centered method. e is the local error and O the order.

	p		$\dot{m}$		T	
Δt [s]	e	O	e	O	e	O
120	$2.4966 \cdot 10^{-7}$		$2.2741 \cdot 10^{-6}$		$1.0633 \cdot 10^{-7}$	
60	$8.8016 \cdot 10^{-8}$	1.50	$9.8274 \cdot 10^{-7}$	1.21	$5.3836 \cdot 10^{-8}$	0.98
30	$3.0543 \cdot 10^{-8}$	1.52	$4.2808 \cdot 10^{-7}$	1.20	$2.6541 \cdot 10^{-8}$	1.00
15	$1.0289 \cdot 10^{-8}$	1.53	$1.8693 \cdot 10^{-7}$	1.20	$1.1811 \cdot 10^{-8}$	1.06
7.5	$3.2524 \cdot 10^{-9}$	1.57	$8.0447 \cdot 10^{-8}$	1.21	$4.4550 \cdot 10^{-9}$	1.14
3.75	$8.8397 \cdot 10^{-10}$	1.63	$3.3314 \cdot 10^{-8}$	1.22	$1.3276 \cdot 10^{-9}$	1.26

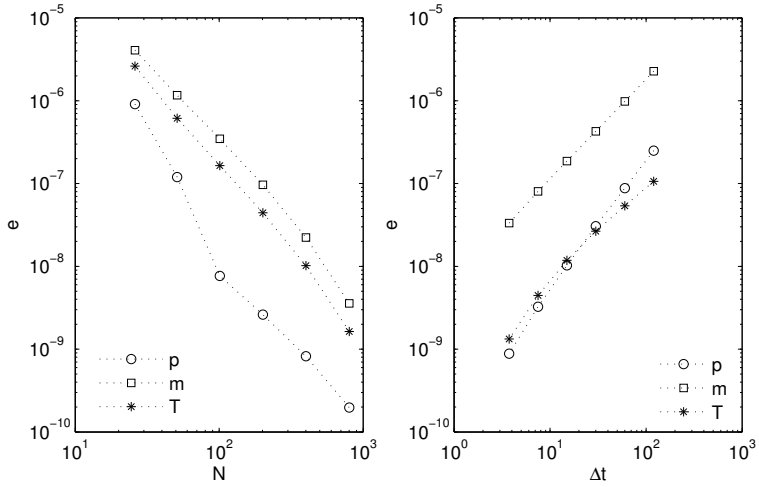

Figure 4.10: Local discretization errors in the non-isothermal model. Left: Spatial discretization error for pressure, mass flow and temperature as a function of grid points N. Right: Temporal discretization error as a function of time step Δt. Corresponding values are given in Tables 4.5 and 4.6.

4.3 Verification and validation

In the article by Oberkampf and Trucano [50] model verification in computational fluid dynamics is defined as "substantiation that a computerized model represents a conceptual model within specified limits of accuracy". Verification determines if the programming and computational implementation of the model is correct, and that one is solving the equations correct. Verification involves examining the convergence of the numerical method and determining the spatial and temporal

discretization errors. A key point in verification is also to compare computed results with either an exact analytical solution or other numerical benchmark results in the literature. Discretization errors were investigated in previous sections. In the following computed results will be compared to other numerical results in the literature.

Model validation is defined as "substantiation that a computerized model within its domain of applicability possesses a satisfactory range of accuracy consistent with the intended application of the model". It is the process of determining the degree to which a model is an accurate representation of the real world, and is a check that one is solving the correct equations. In this work model validation is performed by comparing numerical results to measured values on one of Gassco's offshore pipelines.

4.3.1 Verification with literature

In order to verify the model and numerical method used, simulations were run using the same setup and boundary conditions as in the work by Chaczykowski [19]. The boundary conditions used by Chaczykowski were arbitrary selected, but represent typical flow conditions for on-shore natural gas pipelines. The pipeline considered has a length of $L = 363$ km with an internal diameter of $D = 1.3836$ m. The average roughness of the pipe was $\epsilon = 1.5 \cdot 10^{-6}$ m. The following gas composition (mole fraction) was used: $CH_4 - 98.3455\%$, $C_2H_6 - 0.6104\%$, $C_3H_8 - 0.1572\%$, $iC_4H_{10} - 0.0299\%$, $nC_4H_{10} - 0.0253\%$, $iC_5H_{12} - 0.0055\%$, $nC_5H_{12} - 0.004\%$, $N_2 - 0.0303\%$, $CO_2 - 0.7918\%$. The ground thermal properties were $T_a = 3.1$ °C, soil thermal conductivity $\lambda = 1$ W/(m·K), density $\rho = 1640$ kg/m^3, heat capacity $c_p = 1530$ J/(kg·K) and burial depth 1.5 m. Thermal properties of the pipe wall are given in Table 4.7.

Table 4.7: Thermal properties of pipe wall.

Material	Thickness [mm]	ρ [kg/m^3]	λ [W/(m·K)]	c_p [J/(kg·K)]
Internal coating	0.5	1800	0.52	1050
Steel	19.22	7830	45.3	500
External coating	3	940	0.4	1900

The following bounray conditions were used

$$\begin{aligned} p(0,t) &= 8.4 \text{ MPa} \\ T(0,t) &= 296.65 \text{ K} \\ Q(L,t) &= f(t) \text{ m}^3/\text{h} \end{aligned} \tag{4.5}$$

where $f(t)$ is shown in Figure 4.11. Note that the flow is given in m^3/h (cubic meters per hour) and not kg/s as in the previous sections. The GERG 88 equation of state was used to determine the compressibility factor. Results for inlet flow rate, outlet pressure and outlet temperature are presented in Figures 4.12, 4.13 and 4.14

respectively. The computed results, using both the steady and unsteady external heat transfer model, show good agreement with those of Chaczykowski [19]. The implicit cell centered method was used in this study, while Chaczykowski uses the implicit multistep Gears method [51] for the time integration and centered differences for the spatial derivatives.

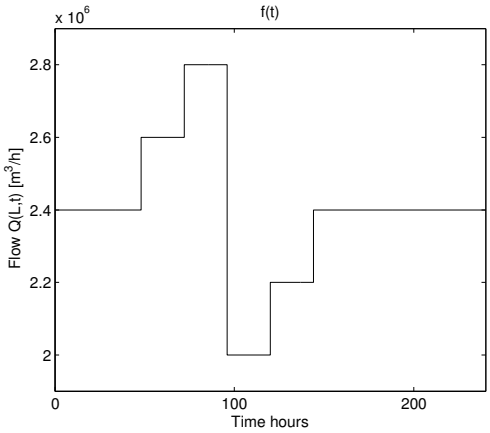

Figure 4.11: Boundary condition for outlet flow rate.

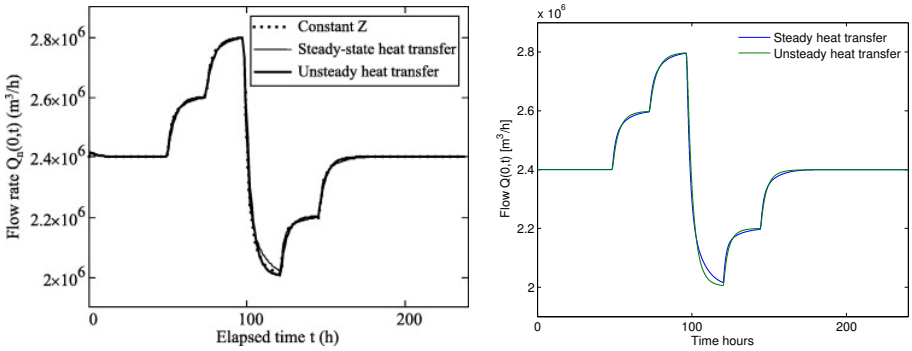

Figure 4.12: Results inlet flow rate. Left: results from Chaczykowski [19]. Right: Results in this study. Results computed using both the steady and unsteady external heat transfer model.

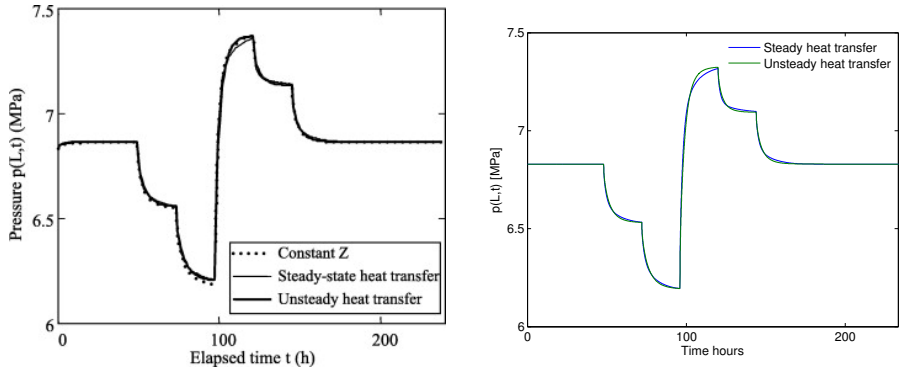

Figure 4.13: Results outlet pressure. Left: Results from Chaczykowski [19]. Right: Results in this study. Results computed using both the steady and unsteady external heat transfer model.

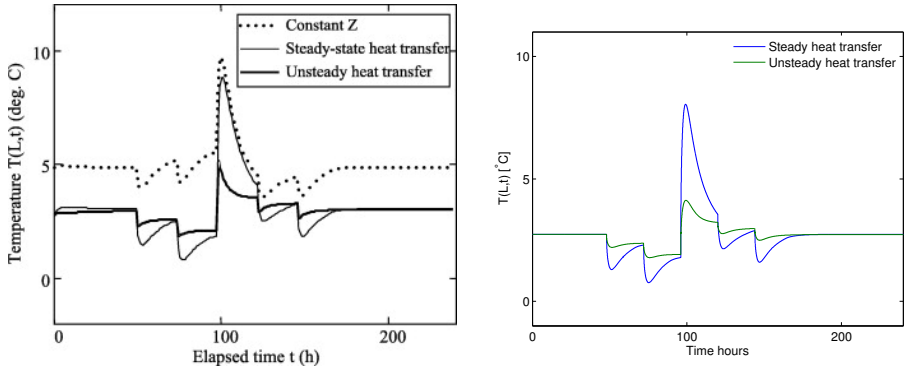

Figure 4.14: Results outlet temperature. Left: Results from Chaczykowski [19]. Right: Results in this study. Results computed using both the steady and unsteady external heat transfer model.

4.3.2 Model Validation

The model was validated by running simulations on one of Gasscos offshore pipelines. The pipeline considered has a length of 650 km and internal diameter of 1.016 m. Three different cases, each spanning a four day time period, were investigated. Inlet mass flow, inlet temperature and outlet pressure were given as boundary conditions.

Simulations were run using similar parameters and correlations which Gassco currently uses today. The tuned BWRS equation of state was used to determine the compressibility factor while the friction factor was computed from the Colebrook-White correlation. The heat exchange between the gas and the surroundings was modeled using both a steady external heat transfer model which Gassco currently uses, and an unsteady external heat transfer model which includes heat accumulation in the ground. The pipeline was divided into 98 grid points with a varying Δx. For steep inclination the distance between two grid points was short, while for little or no inclination the grid size was larger. The time step was $\Delta t = 60$ s. The pipe wall consists of three different layers, with thermal properties given in Table 4.8.

Table 4.8: Thermal properties of pipe wall.

Material	Thickness [mm]	ρ [kg/m^3]	λ [W/(m·K)]	c_p [kJ/(kg·K)]
Steel	24	7800	50	0.5
Asphalt	7	1300	0.74	1.9
Concrete	80	2500	2.9	0.65

The ground thermal conductivity was $\lambda = 2$ W/(m·K), density $\rho = 2000$ kg/m^3, heat capacity $c_p = 1420$ J/(kg·K) and burial depth approximately 1.5 m. Results are presented below.

Case 1

Boundary conditions for case 1 are given in Figure 4.15, and represent typical transient conditions in offshore natural gas pipelines. Results for inlet pressure, outlet mass flow and outlet temperature are presented in Figure 4.16. Both the inlet pressure and outlet mass flow agree well with measured values over the entire four day time period. However, considerable discrepancies between modeled and measured outlet temperature are observable. The steady external heat transfer model over predicts the amplitude of temperature changes in the flow compared to the unsteady external heat transfer model. The difference between the modeled and measured temperature is presented at the bottom right in Figure 4.16. For the unsteady heat transfer model, the difference between the modeled and measured temperature is fairly constant during the entire simulation, while for the steady heat transfer approach it varies a lot more. This result indicates that using an unsteady heat transfer model where the pipeline is buried under ground is a more

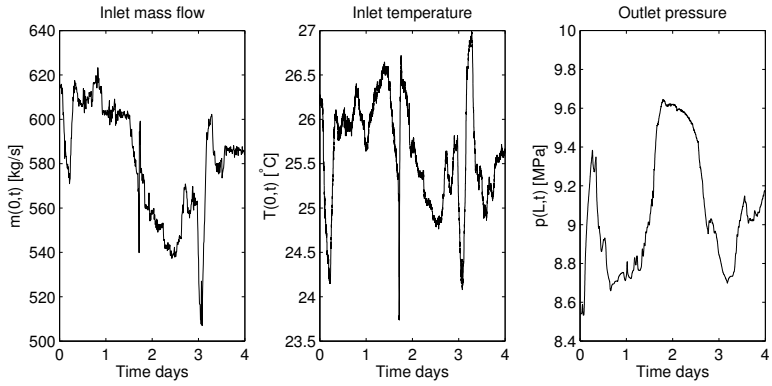

Figure 4.15: Boundary conditions for 650 km offshore pipeline for case 1. Left inlet mass flow, middle inlet temperature, right outlet pressure.

correct approach to model the heat transfer between the gas and the environment compared to a steady heat transfer approach. However, the modeled temperature using the unsteady heat transfer model is approximately $1.5 - 1.75$ °C lower than the measured value. This deviation between modeled and measured outlet gas temperature is investigated and discussed in Chapter 5. For the modeled inlet pressure and outlet mass flow, only small differences between the unsteady and steady external heat transfer models were observed.

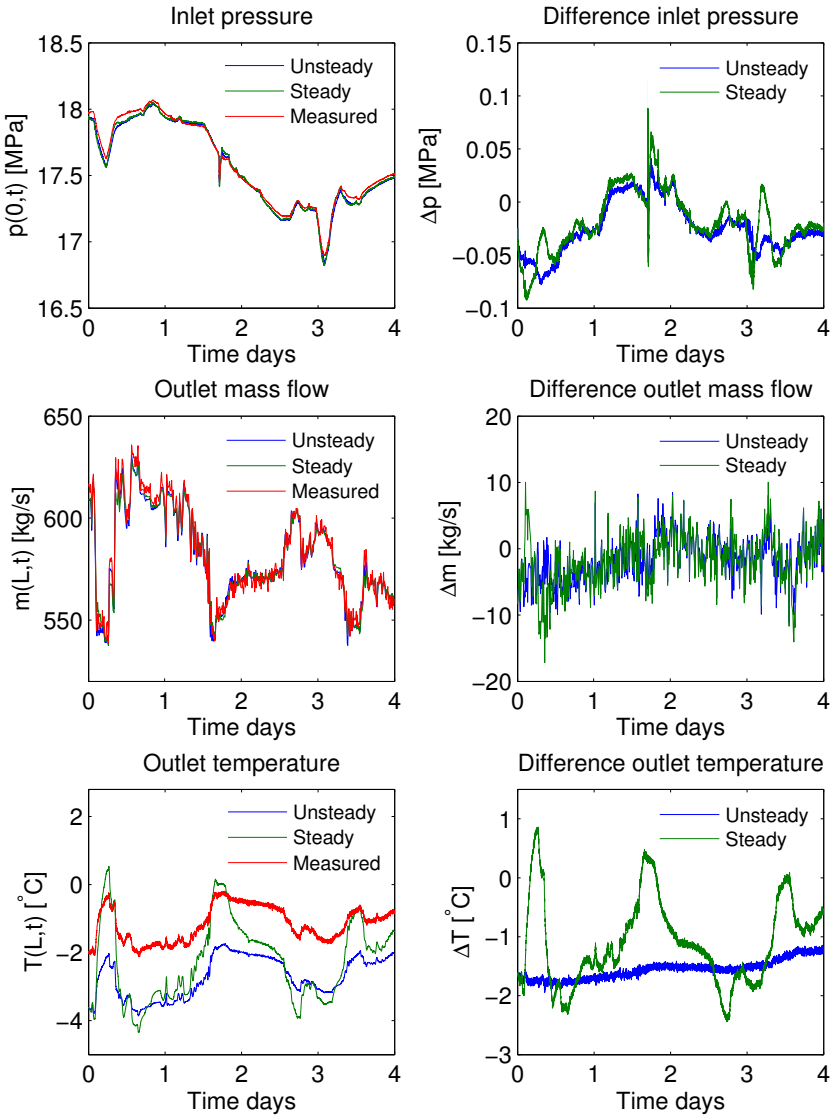

Figure 4.16: Case 1. Results for 650 km offshore pipeline operated by Gassco for boundary conditions in Figure 4.15. Top inlet pressure, middle outlet mass flow and bottom outlet temperature. Results computed using both the steady and unsteady external heat transfer model. To the left computed results are compared to measured values, while the difference between computed and measured values are presented to the right.

Case 2

Boundary conditions for case 2 are presented in Figure 4.17. Results for inlet pressure, outlet mass flow and outlet temperature are presented in Figure 4.18. As in case 1, the modeled inlet pressure and outlet mass flow agree well with measured values. For the outlet temperature the steady heat transfer model over predicts the amplitude of temperature changes in the flow compared to the unsteady heat transfer approach. The modeled outlet temperature is approximately 0.5 °C below the measured temperature. For the inlet pressure and outlet mass flow, using an unsteady heat transfer model improves the results compared to the steady heat transfer model. During the transient, a major difference in modeled inlet pressure was observed. The difference between the two model approaches was 0.3 MPa (3 bar). For the outlet mass flow the unsteady heat transfer model agrees better with measured values, especially after abrupt changes in the flow.

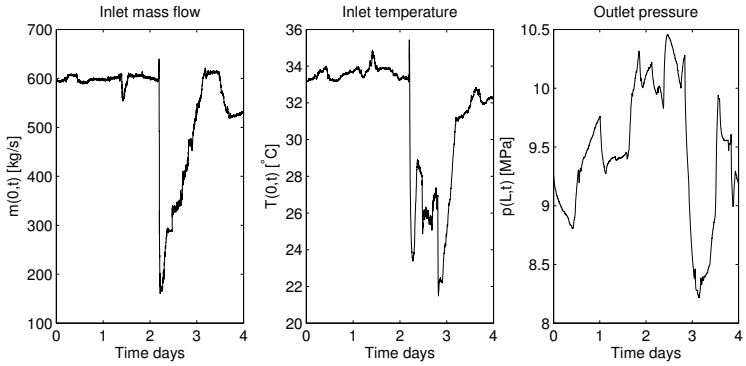

Figure 4.17: Boundary conditions for 650 km offshore pipeline for case 2. Left inlet mass flow, middle inlet temperature, right outlet pressure.

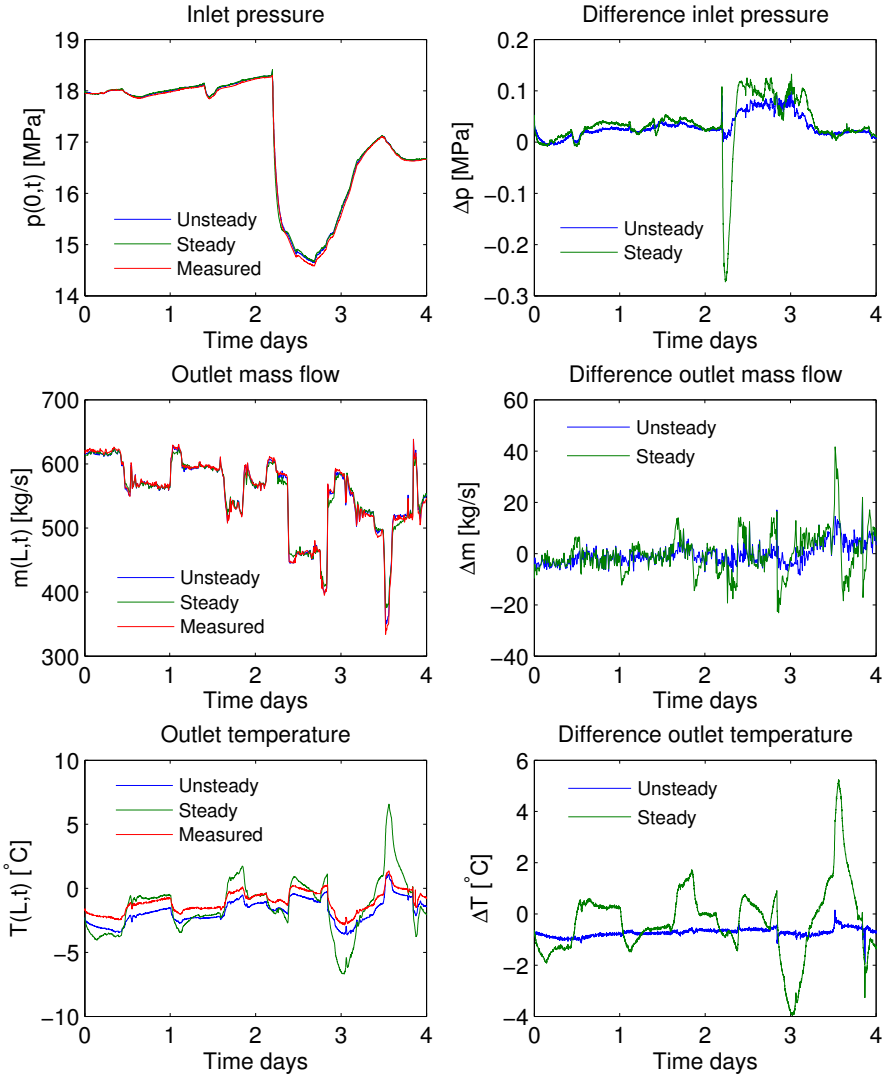

Figure 4.18: Case 2. Results for 650 km offshore pipeline operated by Gassco for boundary conditions in Figure 4.17. Top inlet pressure, middle outlet mass flow and bottom outlet temperature. Results computed using both the steady and unsteady external heat transfer model. To the left computed results are compared to measured values, while the difference between computed and measured values are presented to the right.

Case 3

Boundary conditions for case 3 are presented in Figure 4.19. Results for inlet pressure, outlet mass flow and outlet temperature are presented in Figure 4.20. For the inlet pressure and outlet mass flow there is a small deviation between modeled and measured values at the beginning of the simulation. As the governing flow equations form a system of hyperbolic partial differential equations, initial values for pressure, mass flow and temperature are needed along with appropriate boundary conditions before running simulations. In Figure 4.20 initial conditions were not correct, however after a short time period the computed flow values showed good agreement with measured values. As in both the previous cases, the steady heat transfer model over predict the amplitude of temperature changes in the flow compared to the unsteady heat transfer model.

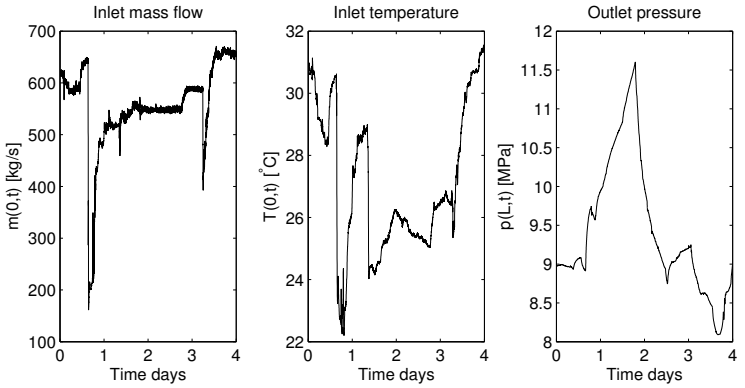

Figure 4.19: Boundary conditions for 650 km offshore pipeline for case 3. Left inlet mass flow, middle inlet temperature, right outlet pressure.

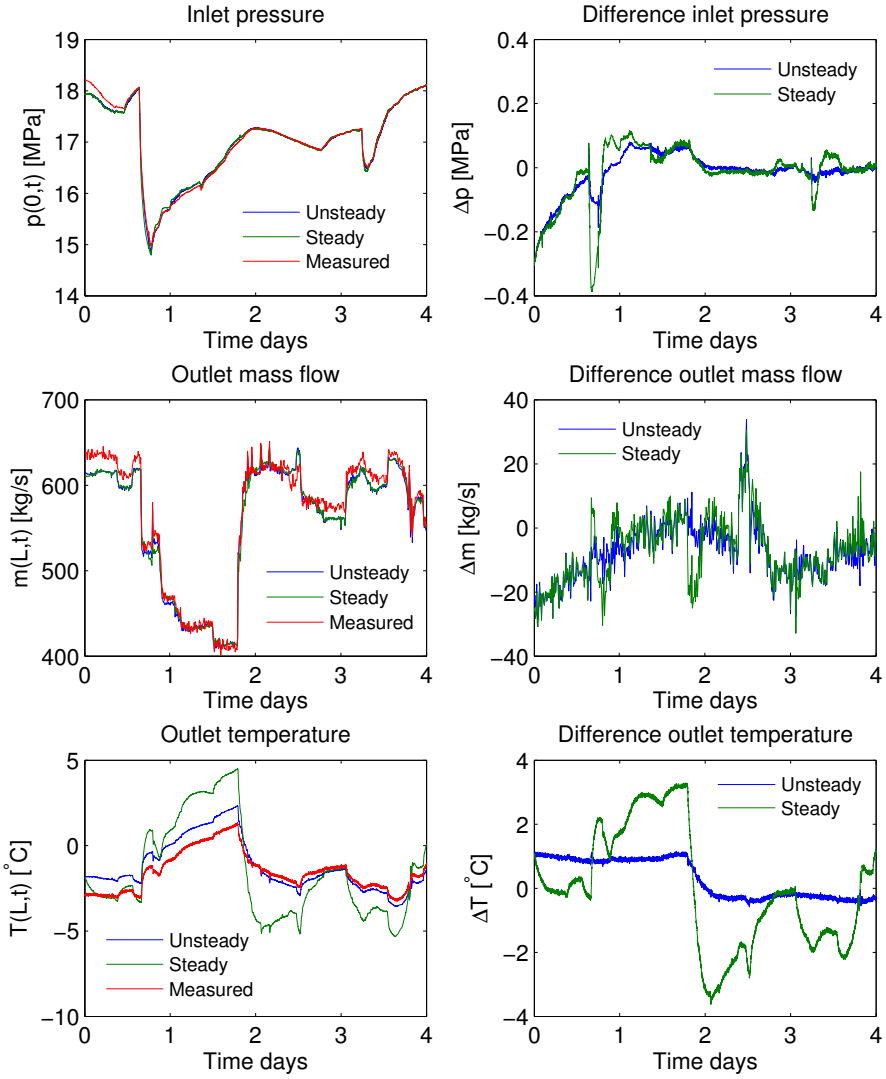

Figure 4.20: Case 3. Results for 650 km offshore pipeline operated by Gassco for boundary conditions in Figure 4.19. Top inlet pressure, middle outlet mass flow and bottom outlet temperature. Results computed using both the steady and unsteady external heat transfer model. To the left computed results are compared to measured values, while the difference between computed and measured values are presented to the right.

Chapter 5

Discussion

Results for the one-dimensional flow model were presented in Chapter 4. In Section 4.3.2 the model was validated by running simulations on one of Gassco's offshore natural gas pipelines, with results presented in Figures 4.16, 4.18 and 4.20. Modeled inlet pressure and outlet mass flow agree well with measured values, with only small discrepancies present. There are however some deviations between modeled and measured outlet temperature, with the difference being in the region $1 - 1.5$ °C. Such a deviation has also been observed by Gassco in their models.

In this Chapter errors and uncertainties in the model are discussed in detail. It is claimed that discrepancies between modeled and measured values are not due to numerical errors, but rather physical approximation errors of different processes which are incorporated into the model. These processes, which include the friction factor, equation of state and the heat exchange between the gas and the pipeline surroundings will be discussed in detail. A detailed sensitivity analysis of the heat transfer model is presented at the end of the chapter.

5.1 Errors and uncertainties

Computed results in Section 4.3.2 agree well with measured flow values from Gassco's offshore pipeline. However, small discrepancies are present, especially in the outlet gas temperature, but also in the case of inlet pressure and outlet mass flow. In this section numerical errors and simplifications in the one-dimensional flow model will be discussed.

According to AIAA (American Institute of Aeronautics and Astronautics) guidelines [52] errors in computational fluid dynamics are defined as "A recognizable deficiency in any phase or activity of modeling and simulation that is not due to lack of knowledge", meaning that the deficiency is present and identifiable in the model. Errors can be classified as acknowledged or unacknowledged. Acknowledged errors include

- Physical modeling error

- Computer round off error
- Iterative convergence error
- Discretization error

while unacknowledged errors include

- Computer programming error
- Usage error

Possible unacknowledged errors can be prevented through verification, as was done in Section 4.3.1.

Computer round off errors occur because numbers on the computer are stored with a certain precision, while iterative convergence errors occur because iterative methods which are used in the model have a stopping criteria. None of these are considered important in this work.

Discretization errors arise due to the fact that the governing equations are represented as algebraic equations in discrete time and space. For unsteady flow calculations discretization errors are present due to both spatial and temporal discretization schemes. In previous Sections (4.1.2 and 4.2.3) an estimate for the spatial and temporal discretization errors for pressure, mass flow and temperature are given. For a correct choice of spatial step Δx and time step Δt discretization errors do not introduce noticeable errors in the flow field solution.

Physical modeling errors are due to uncertainty in the formulation of the model and deliberate simplifications which are made. Several parameters which are incorporated into the model have to be estimated. Some of these parameters, such as the friction factor and compressibility factor, can not be determined from exact relations, but rather from correlations which are based on empirical observations. The uncertainties in these parameters are discussed later in this chapter. Deliberate simplifications of the flow model are necessary in order to solve the governing equations in a fast and efficient way. The most important simplification are discussed below.

One-dimensional assumption

Even though the flow is three-dimensional, a one-dimensional model is the only feasible way to model the flow of natural gas through long distance high pressure natural gas pipelines. The governing equations for one-dimensional compressible viscous heat conducting flow presented in Section 2.1 are the result of averages of the three-dimensional equations across the pipe cross-section. In the attached research article [c] the process of transforming the energy equation into the one-dimensional representation for turbulent flow was studied in detail. Using a turbulent velocity profile it is shown that the dissipation term in Equation (2.3) is over simplified. It was determined that a correction factor, close to unity, should be included in the representation of the dissipation term in the energy equation. This

dimensionless factor depends on the Reynolds number of the flow and the pipe surface roughness. For low Reynolds numbers ($\mathrm{Re} \simeq 10^4$) it reduces the dissipation by as much as 7%, irrespective of roughness. For high Reynolds numbers ($\mathrm{Re} \geq 10^7$) and roughness in the high range of the micron decade, the dissipation is increased by 10%.

For a 150 km pipeline with roughness 10 μm operating at a Reynolds number of $5 \cdot 10^7$ it was shown that including a correction factor on the dissipation term in the energy equation gave an increase in outlet gas temperature of 1 °C compared to no correction. For pipelines operated by Gassco the surface roughness is typically $2 - 3$ μm. For such smooth pipes the correction factor will be close to unity, even for high Reynolds numbers. In this case, including a correction factor on the dissipation term in the energy equation has almost no effect on the computed temperature compared to no correction. The usual expression for the dissipation term in Equation (2.3) can therefore safely by used.

Linearized model

The governing equations for one-dimensional compressible flow are non-linear. When using finite differences to compute the numerical solution, and all terms are discretized in a fully implicit way, the governing equations form a system of non-linear equations. These can be solved using the Newton-Raphson method, as was done by Kiuchi [14] and Abbaspour and Chapman [16]. This is however time consuming, especially for long pipelines and complicated networks. A much more efficient way to solve the governing equations is to linearize the non-linear terms about the previous time step. The procedure can be found in the article by Luskin [48].

In the attached research article [a] a linearized model is compared to a non-linear model. For the hydraulic model in Chapter 3 (Equations (3.4)-(3.5)) the friction term in the momentum equation is the only non-linear term. It is shown in detail how this term is approximated in the linearized model. For both the hydraulic and full non-isothermal there is no observable difference between solving the linearized model or the full non-linear model. The computational time is greatly reduced when linearizing the non-linear terms about the previous time step. A linear model is therefore a valid approximation for natural gas flow in long pipelines, even under transient conditions.

Decoupling hydraulic and thermal model

The governing equations for continuity, momentum and energy are in general coupled and have to be solved simultaneously at each time step. This is also done in most of the simulations in this work. However, it could be advantageous to solve the thermal model separately from the hydraulic model in order to reduce the computational time for each time step. This was investigated in the attached research article [b]. Solving the hydraulic model (continuity and momentum equations) separately one time step ahead of the thermal model (energy equation) simplifies the governing equations and reduces the computational time. This was shown to only

introduce small errors in the solution. Similar results were reported in the article by Barley [53].

However, in most cases it is just as convenient to solve all equations simultaneously at each time step, as was done in the majority of this work. It should however be noted that in some special cases it could be necessary to solve the hydraulic model separately from the thermal model, which is shown in research article [e]. Using the cell centered method it is shown that when a discontinuous change in inlet temperature is given as a boundary condition, unphysical oscillations in the temperature are introduced into the flow. This can be avoided by solving the thermal model separately from the hydraulic model using a different discretization than the cell centered method.

A possible source of error which is not listed above is incorrect boundary conditions. When modeling the flow through natural gas pipelines, operational data is used as boundary values in the flow model. These data have been measured by flow metering devices, and contain some uncertainty. In the work by Langelandsvik [5] it is claimed that the measurement uncertainty for pressure is $0.03 - 0.04\%$, mass flow 0.5% and temperature 0.04%. In the following it is assumed that the measurement uncertainty is so small that it does not effect the modeled results in any significant way.

5.2 Test case setup

In order to investigate and discuss different physical processes in the flow model, a test case scenario is constructed. The pipeline considered is a 650 km pipeline with a diameter of 1 m, with the setup shown in Figure 5.1.

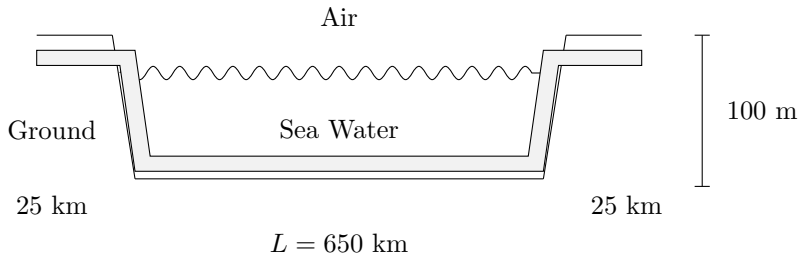

Figure 5.1: Offshore natural gas pipeline which is buried under ground on-shore for the first and final 25 km. The sea bottom is at a depth of 100 m below sea level. The total length is 650 km.

Offshore natural gas pipelines are typically buried under ground for the first and final parts of the pipe length where the gas departs the processing terminal and arrives at the receiving terminal. In Figure 5.1 this has been included by assuming that the pipeline is buried under ground for the first and final 25 km. Between this the pipeline is lying on the seabed at an elevation of 100 m below sea level. Unless stated otherwise, the pipeline is lying on the seabed fully exposed to sea

water like that in Figure 5.1. The boundary conditions used for inlet mass flow, inlet temperature and outlet pressure are shown in Figure 5.2. These represent typical transient conditions, with a large reduction in mass flow and temperature occurring after one day.

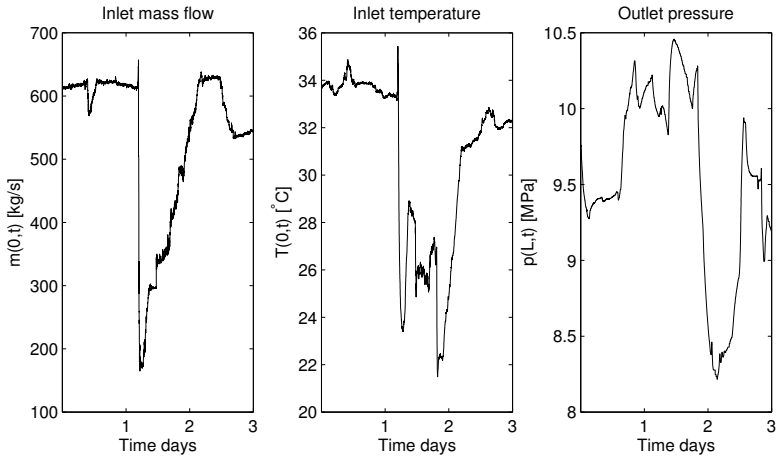

Figure 5.2: Boundary conditions used in test case scenario. Left inlet mass flow, middle inlet temperature and right outlet pressure.

The equivalent sand grain roughness was 3 μm while the gas composition was the same as previously: $CH_4 - 89.16\%$, $C_2H_6 - 7.3513\%$, $C_3H_8 - 0.5104\%$, $nC_4H_{10} - 0.0251\%$, $iC_4H_{10} - 0.0311\%$, $nC_5H_{12} - 0.0009\%$, $iC_5H_{12} - 0.0024\%$, $N_2 - 0.6980\%$, $CO_2 - 2.2208\%$. Thermal properties of the pipe wall were the same as in Section 4.3.2 and are given in Table 5.1. The ground thermal conductivity was $\lambda = 2$ W/(m·K), density $\rho = 2000$ kg/m^3, heat capacity $c_p = 1420$ J/(kg·K) and burial depth (ground level to top of pipe) 1 m. The ambient air temperature was 6 °C while the sea bottom temperature was 4 °C.

Table 5.1: Thermal properties of pipe wall.

Material	Thickness [mm]	ρ [kg/m^3]	λ [W/(m·K)]	c_p [kJ/(kg·K)]
Steel	24	7800	50	0.5
Asphalt	7	1300	0.74	1.9
Concrete	80	2500	2.9	0.65

5.3 Friction factor and surface roughness

Transport pipelines operated by Gassco are made of steel and usually have a layer of concrete and asphalt on the outside. Before being put into service the pipelines

are coated on the inside. Internal coating reduces the friction between the gas and the pipe wall, therefore reducing the cost of the operating compressor. When determining the friction factor f from the Colebrook-White correlation in Equation (2.9) the equivalent sand grain roughness of the pipeline surface is required. The equivalent sand grain roughness corresponds to that which Nikuradse used in his experiments when measuring the pressure drop in pipelines [54]. Based on these results he developed the friction factor correlation for rough turbulent pipe flow, which is the first term in the Colebrook-White correlation in Equation (2.9). Based on the discussion in the thesis by Langelandsvik [5] there does not seem to be a clear way of how to determine the equivalent sand grain roughness. Measurements by Langelandsvik on pipelines operated by Gassco suggest an equivalent sand grain roughness of approximately 6 μm. However, both Langelandvik [5] and Piggott [55] show by examples how the roughness changes over time, especially before and after pigging of the pipeline. In Gassco's case, when performing capacity tests in offshore pipelines the effective roughness is estimated by operating the pipeline at steady state conditions, with stable flow rate, inlet pressure, outlet pressure, inlet temperature and gas composition. The wall roughness is then used to tune the model so that the simulated results coincide with measured values. How the equivalent sand grain roughness effects the flow is illustrated in Figure 5.3, which shows the modeled inlet pressure for the pipeline described in Section 5.2. Three different roughness values were used, 2, 3 and 4 μm. The difference in inlet pressure between 3 and 4 μm is approximately 0.15 MPa (1.5 bar). The same was found for the difference between 2 and 3 μm. For outlet mass flow and outlet temperature there was no observable difference between the different roughness values.

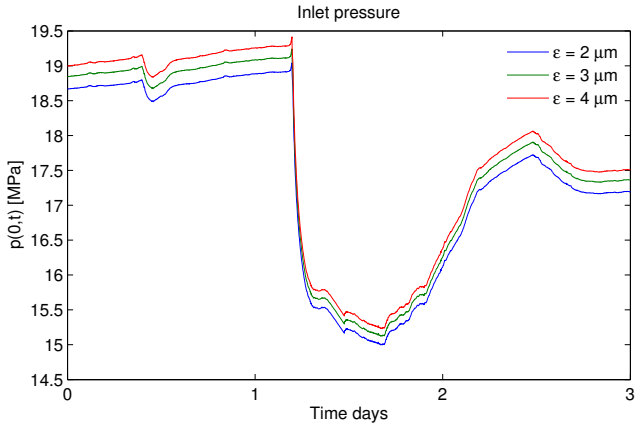

Figure 5.3: Results inlet pressure using an equivalent sand grain roughness of 2, 3 and 4 μm in the Colebrook-White formula. Difference between each curve is approximately 0.15 MPa.

An equivalent sand grain roughness of 2, 3 and 4 μm is somewhat lower than that measured by Langelandsvik on coated transport pipelines. However, Langelandsvik shows by example [5] (page 142) how the measured friction factor from a long distance offshore pipeline all lie on a Colebrook-White curve with an equivalent sand grain roughness of $1-2$ μm. In other words, running a simulation under steady state conditions and tuning the sand grain roughness in order to match the simulated results with measured values corresponds to a sand grain roughness of $1-2$ μm, considerably lower compared to measured values of the surface roughness.

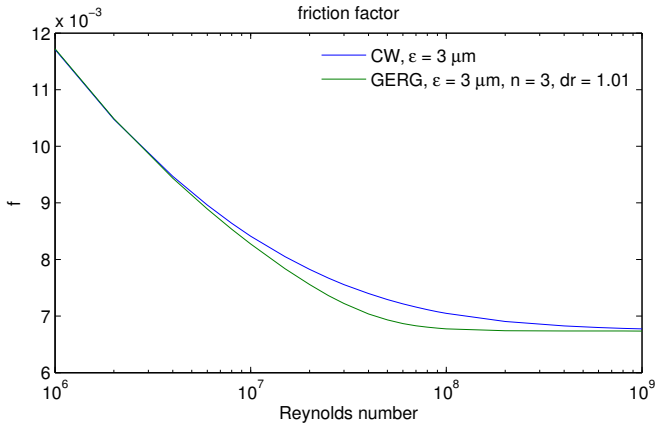

Figure 5.4: Friction factor f as a function of Reynolds number using the Colebrook-White (CW) and GERG friction factor formulas for an equivalent sand grain roughness of 3 μm.

Having run several steady state simulations tuning the surface roughness in order to match computed result with measured values, a similar conclusion was drawn by the author. Even though the surface roughness was claimed to be approximately 5 μm, after tuning the equivalent sand roughness was determined to be approximately 2 μm. For results in Section 4.3.2 the equivalent sand grain roughness was 2 μm. Experimental results from Langelandsvik et al. [22] suggest a more abrupt transition from smooth to rough turbulent flow compared to that predicted by Colebrook-White. This transition takes place in the Reynolds number range which Gassco typically operates in ($\mathrm{Re} \sim 5 \cdot 10^7$). In Section 2.2 the GERG friction factor formula (Equation (2.10)) is claimed to give a more abrupt transition from smooth to rough turbulent flow. For an equivalent sand grain roughness of 3 μm the friction factor f as a function of Reynolds number using both the Colebrook-White and GERG formula is shown in Figure 5.4. In the GERG friction factor formula the transition and draught factor were set to $n = 3$ and $dr = 1.01$ respectively. In the Reynolds number range $10^7 - 10^8$ these two relations show quite different behaviors, with the GERG formula predicting a considerably lower friction factor compared

to the Colebrook-White formula.

In Figure 5.5 the modeled inlet pressure using the Colebrook-White formula with an equivalent sand grain roughness of 3 μm is shown. When using the GERG friction factor formula with the same equivalent sand grain roughness, the modeled inlet pressure is lower compared to that computed using the Colebrook-White formula. In order to get similar results using the GERG friction factor formula, the equivalent sand grain roughness had to be increased to 5 μm. The corresponding modeled inlet pressure is also shown in Figure 5.5. This result agrees well with that computed using the Colebrook-White formula with an equivalent sand grain roughness of 3 μm. In this work it has been observed that in order to match the modeled pressure with measured values, the equivalent sand grain roughness has to be approximately 2 μm. This is considerably lower than measured values of approximately $5 - 6$ μm [5]. Owing to the more abrupt transition from smooth to rough turbulent flow, results in Figure 5.5 suggest that the GERG formula can be used to give similar results as the Colebrook-White formula with a larger equivalent sand grain roughness. Results in Figures 5.4 and 5.5 are not sufficient to suggest that the GERG friction factor formula is more correct than Colebrook-White. However, compared to Colebrook-White the GERG formula can be used with an equivalent sand grain roughness closer to the measured surface roughness. Although several others ([5], [24], [55]) have stated that the transition from smooth to rough turbulent flow is more abrupt than that predicted by Colebrook-White, it still seems to be the preferred choice when determining the friction factor in natural gas pipelines.

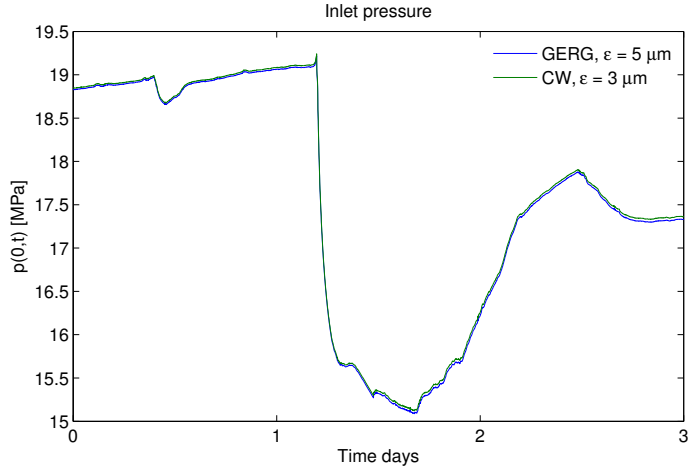

Figure 5.5: Modeled inlet pressure using Colebrook-White and GERG friction factor formulas. The equivalent sand grain roughness had to be increased from 3 to 5 μm for the GERG friction formula in order to get similar results to those using the Colebrook-White formula.

5.4 Equation of state

Different equations of states commonly used when modeling the flow through natural gas pipelines were presented in Section 2.3. These included SRK, Peng-Robinson, BWRS, GERG 88 and GERG 2004. Gassco currently uses a version of BWRS which is especially tuned for hydrocarbons. Results for the compressibility factor Z as a function of pressure at different temperatures were presented in Figure 2.2. As commented on previously, up to 10 MPa the different equations predict similar values for the compressibility factor Z. But in the range $10 - 25$ MPa there is a considerable difference between the computed values. To investigate the effect of the different equations of state, simulations were run using all the presented correlations.

Results for inlet pressure using all the different equations of state are presented at the top of Figure 5.6, with BWRS* being the tuned BWRS currently used by Gassco. At the bottom the difference in inlet pressure between the indicated equation of state and the tuned BWRS* is shown. The GERG 2004 equation of state is the most recently developed, and the only one which is explicitly stated to be valid for pressures up to 30 MPa. It is therefore assumed to be the most accurate equation of state presented in this work. Off all the equations of state presented here, the tuned BWRS* shows the best agreement with GERG 2004. The GERG 2004 gives an inlet pressure which is approximately 0.1 MPa (1 bar) below the tuned BWRS*. This difference is fairly constant over the entire simulation period during both steady and transient conditions. Results for outlet mass flow and outlet temperature are given in Figure 5.7. Only small differences in outlet mass flow and outlet temperature can be observed between the different equations of state, and the sensitivity of the selection of the equation of state is not that dominant as in the case of the modeled inlet pressure. Referring to Figure 2.2 in Section 2.3, the different equations of state do not differ that greatly for pressures up to 10 MPa. Above this the difference is more dominant. As the outlet pressure of the pipeline lies in the region $9 - 10$ MPa (Figure 5.2), it is expected that the sensitivity of the equation of state on the outlet is not that significant as on the inlet.

As the GERG 2004 equation of state is valid up to 30 MPa, it would be the preferred choice when modeling the flow through high pressure natural gas pipelines. It can also be used to calculate other thermodynamical properties such as heat capacities, enthalpy, entropy and internal energy, and can handle a gas mixture with up to 18 different components. However, it is computationally demanding compared to other equations of state such as BWRS and GERG 88. For the examples above, the computational time for GERG 2004 was almost ten times that of BWRS and GERG 88. The reason for this great increase in computational time is the vast amount of coefficients which are required in the GERG 2004 equation of state. Therefore, owing to its considerably shorter computational time compared to GERG 2004, the tuned BWRS would still be the preferred choice when modeling the flow of natural gas through long distance pipelines. The difference in inlet pressure between GERG 2004 and the tuned BWRS in Figure 5.6 is approximately 0.1 MPa. However, since this difference is fairly constant over the entire simulation

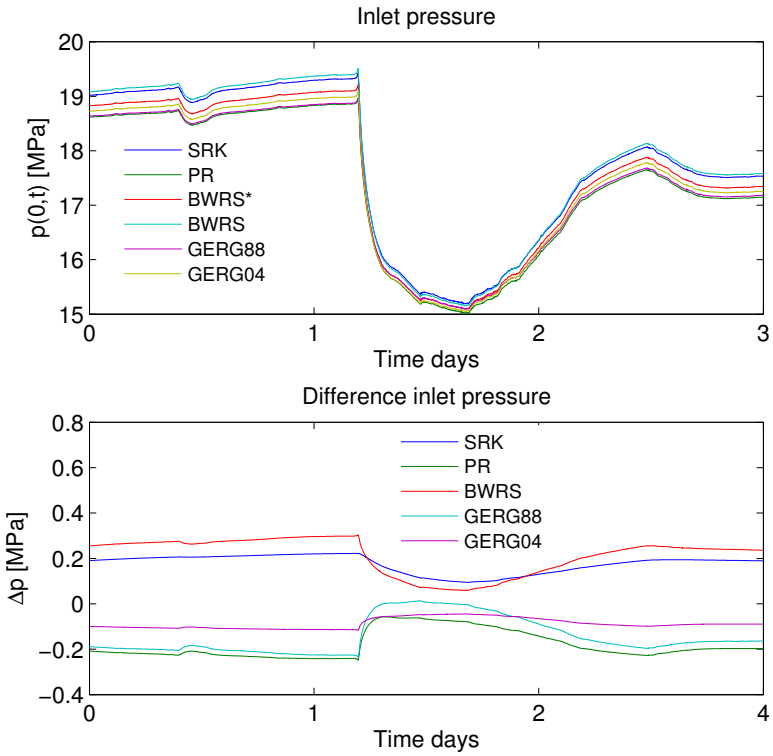

Figure 5.6: Top: Results inlet pressure using the different equations of state. BWRS* is the tuned BWRS currently used by Gassco. Bottom: Difference inlet pressure between indicated equation of state and the tuned BWRS*.

period during both steady and transient conditions, it can be compensated for by tuning the equivalent sand grain roughness in order to match the inlet pressure of the BWRS and GERG 2004 equation of state.

The Joule-Thomson effect is cooling upon expansion, with the Joule-Thomson coefficient defined in Equation (2.29). This coefficient depends on the partial derivative of Z with respect to T at constant p. Small differences in computed outlet temperature in Figure 5.7 indicate that the Joule-Thomson effect is not sensitive to the selection of the equation of state. Even though the numerical values of the partial derivatives of Z are small, they still have a large influence on the flow. In Figure 5.8 this was investigated by setting all the partial derivatives equal to zero. For the modeled inlet pressure no difference during steady state conditions was observed. However, during the transient, setting the partial derivatives of Z equal to zero gave a much higher inlet pressure. For the outlet mass flow small differences can be seen in Figure 5.8. For the outlet temperature, setting the partial derivatives equal zero and neglecting the Joule-Thomson effect gave an

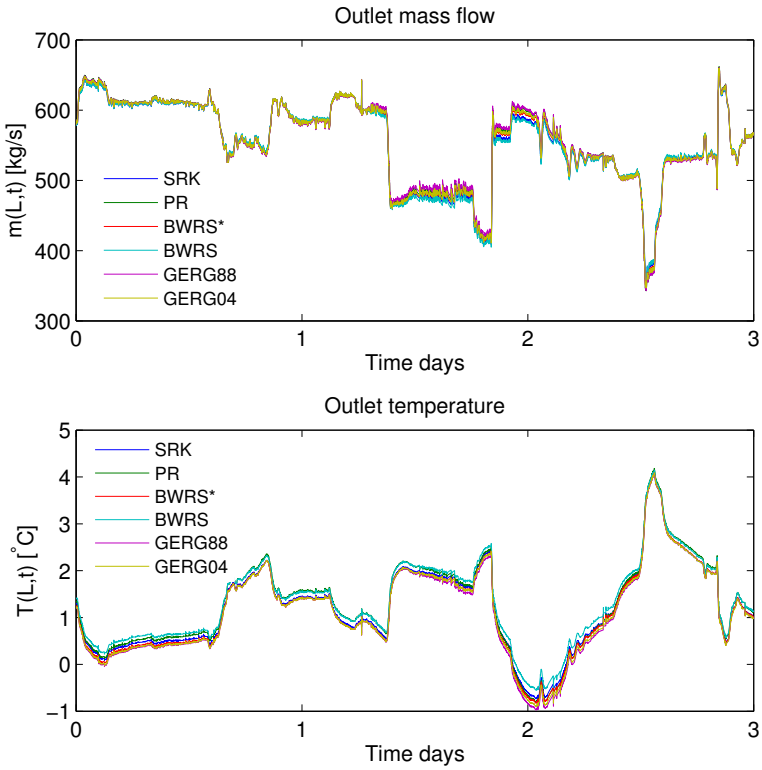

Figure 5.7: Results for outlet mass flow (top) and outlet temperature (bottom) using the different equations of state.

outlet temperature which was approximately 5 °C higher. For the considered case, during expansion the Joule-Thomson effect cools the gas by approximately 5 °C. The partial derivatives of Z can not be neglected in the detailed flow model.

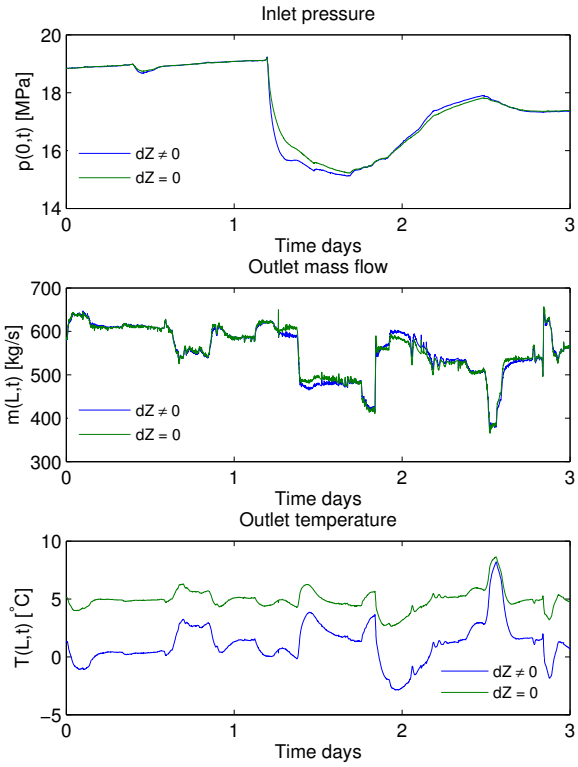

Figure 5.8: Results setting partial derivatives of Z equal zero ($dZ = 0$). Top inlet pressure, middle outlet mass flow and bottom outlet temperature. Result compared to simulation where partial derivatives of Z were not equal to zero ($dZ \neq 0$).

5.5 Effect of varying composition

Results in Section 4.3.2 were computed using a varying gas composition. The composition was given as a boundary condition at the inlet and was tracked along the pipeline until it reached the outlet. The basic principle of how to model the flow with a varying composition is illustrated in Figure 5.9.

A pipeline is discretized by N nodes from $i = 1$ to $i = N$. At time t_0 there is no information available about the composition of the gas along the pipeline. The composition at each node is therefore assumed to be the same as that of the inlet. During a time step Δt the gas has moved a distance $d_1 = u_1 \cdot \Delta t$, where u_1 is the velocity at node 1. The distance d_1 corresponds to the length of the first batch with a composition corresponding to that of the inlet at time t_0. At time $t_2 = t_0 + 2\Delta t$

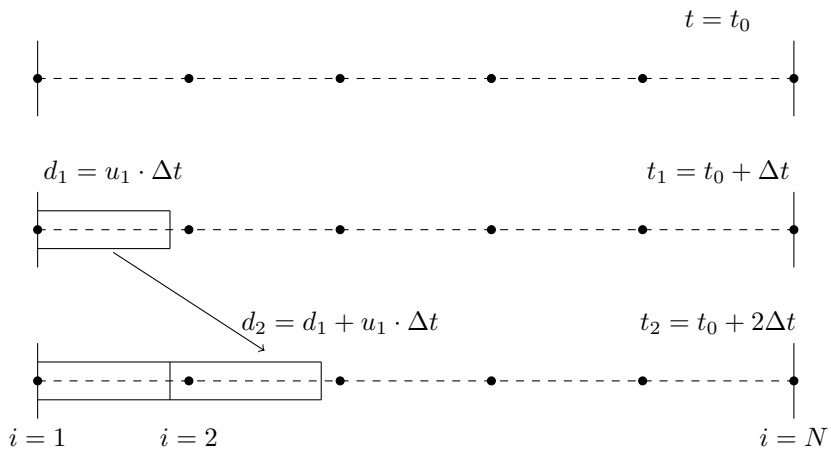

Figure 5.9: Principle behind how to model the flow with a varying composition. Gas is divided into batches, each with a separate composition.

the first batch has moved a distance d_2, while a new batch has entered the pipeline directly behind the first batch. At t_2, the first batch which entered the pipeline has now passed node $i = 2$. The composition at $i = 2$ has now been updated with the composition of batch 1. By advancing the solution further in time, the process is repeated until the batch reaches the end of the pipeline. In Figure 5.10 a typical North Sea natural gas mixture is presented. The composition varies in time, with data for a three day period given. Methane (C1) is the dominating component and is presented to the left. After one day there is a considerable decrease in methane, which is compensated for by an increase in ethane (C2), which is presented in the middle in Figure 5.10. Other dominating components are propane (C3), nitrogen (N2) and carbon dioxide (CO2), which are also presented in the middle graph. Heavier components such as butane (C4) and pentane (C5) are only present in small amounts, and are presented to the right in Figure 5.10.

Using the setup in Section 5.2, simulations were run with a varying and constant composition. For the constant composition, the composition at time step 1 in Figure 5.10 was used. Results for inlet pressure and outlet mass flow are presented in Figure 5.11. For the inlet pressure, a small difference of approximately 0.1 MPa can be observed during the transient, which occurs when the methane amount decreases and is compensated for by a larger amount of ethane. As ethane is a heavier component than methane, using a varying composition will give a higher inlet pressure, as the gas in the pipeline has a higher molecular weight. Apart from the period where the methane content decreases significantly, no observable difference between using a constant and varying composition was observed. For the outlet mass flow to the right in Figure 5.11, a small difference of 10 kg/s at the end of the simulation was observed, while for the outlet temperature there was no difference.

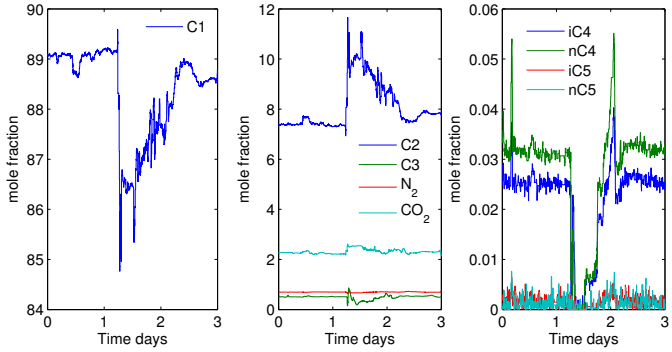

Figure 5.10: Gas composition in mole fraction. Left: C1. Middle: C2, C3, N2 and CO2. Right: iC4, nC4, iC5 and nC5.

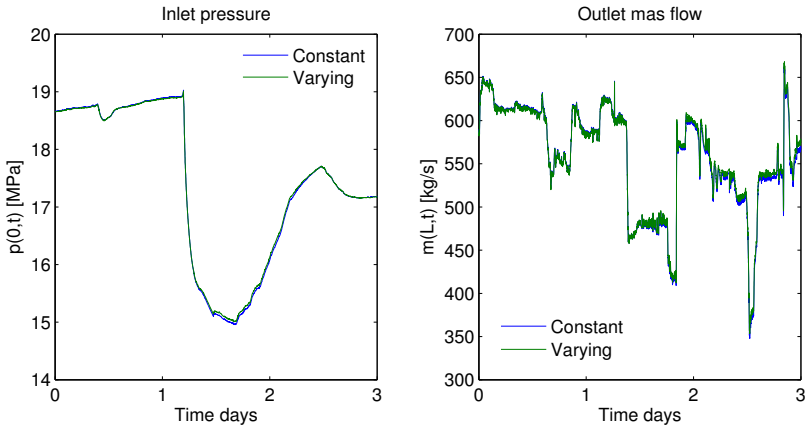

Figure 5.11: Effect of varying composition. Left inlet pressure, right outlet mass flow. Simulation were run using a varying composition (that in Figure 5.10) and a constant composition. For the constant composition, the composition at time step one in Figure 5.10 was used.

5.6 Heat transfer model

In Section 2.4 the external heat transfer model which predicts the heat exchange between the gas and the surrounding environment was presented. Currently Gassco uses a steady heat transfer model, based on a total heat transfer coefficient U, to model the heat exchange. In Section 4.3.1, where the flow model was verified with results from Chaczykowski [19], the steady heat transfer model over predicts the amplitude of temperature changes in the flow compared to an unsteady heat transfer model. This was also observed in the model validation case in Section 4.3.2. The difference between the steady and unsteady external heat transfer model

is that the unsteady model takes into account heat accumulation in the ground. All results in previous sections suggest that heat accumulation in the ground and pipe wall should be included in the model. This statement may also be supported by considering the Fourier number of the heat equation. The radial heat equation which is solved in the domain surrounding the pipeline takes the form

$$\rho c_p \frac{\partial T}{\partial t} = \frac{\lambda}{r} \frac{\partial}{\partial r} \left(r \frac{\partial T}{\partial r} \right) \tag{5.1}$$

which can be expressed on dimensionless form as

$$\frac{\partial T^*}{\partial t^*} = \frac{Fo}{r^*} \frac{\partial}{\partial r^*} \left(r^* \frac{\partial T^*}{\partial r^*} \right) \tag{5.2}$$

where * represents a dimensionless variable. Fo is the Fourier number which is defined as

$$Fo = \frac{\alpha t}{L^2} \tag{5.3}$$

where $\alpha = \lambda / \rho c_p$ is the thermal diffusivity, t the characteristic time and L the characteristic length through which heat conduction occurs. The Fourier number is the ratio of the heat conduction rate to the heat storage rate. For small Fourier numbers (much less than 1) the heat storage rate is greater than the heat conduction rate, underlining that heat accumulation should be included in the model. For the example in Section 4.3.1, the thermal diffusivity was approximately $4 \cdot 10^{-7}$ m^2/s, the characteristic length 1.5 m and the characteristic time 25 hours, giving a Fourier number of approximately 0.02. For such a small Fourier number the heat storage is much great than the heat conduction rate, underlining that heat accumulation in the ground and pipe wall should be included in the model.

Results in Section 4.3.2 show that when using an unsteady external heat transfer model, the profile of the outlet gas temperature agrees well with the measured temperature, and is a considerable improvement compared to the steady external heat transfer model which over predicts the amplitude of temperature changes in the flow. An unsteady heat transfer model also gives improved results for the modeled inlet pressure and outlet mass flow during transient conditions. This can especially be observed in Figure 4.18. For the inlet pressure, only small differences were observed during steady state conditions. However, during the transient there is a considerable difference of 0.3 MPa (3 bar) between the two solution strategies. To the right in Figure 4.18 the difference between the modeled and measured pressure is presented, with the unsteady heat transfer model showing better agreement with measured values. For the outlet mass flow there is also a noticeable improvement, especially when there are abrupt changes in the flow. The significant improvement in modeled pressure and mass flow further underlines the need for an unsteady heat transfer model. Although the unsteady heat transfer model agrees well with respect to the amplitude of temperature changes in the flow, discrepancies between the modeled and measured gas temperature are still present. Possible causes behind these discrepancies will be discussed in the following sections.

5.6.1 Sensitivity of heat transfer model

For the unsteady external heat transfer model the most important parameters are; the thermal conductivity, heat capacity and density of each thermal layer, the burial depth and whether the pipeline is buried under ground or not, and the ambient temperature. The sensitivity of these parameters will be investigated. Two cases will be considered. In the first case the setup is the same as that in Section 5.2, with the ambient air and sea bottom temperature being 6 °C and 4 °C respectively. This case corresponds to typical winter conditions. In the second case the ambient air and sea bottom temperatures are 15 °C and 7 °C respectively, corresponding to conditions during the summer season.

Case 1 - winter

For case 1 during the winter season the outlet gas temperature corresponds to that in Figure 5.7. In Table 5.2 and Table 5.3 the results of increasing the thermal conductivity λ and heat capacity c_p of each thermal element separately by a factor two is presented. ΔT is the difference in outlet gas temperature, Δp the difference in inlet pressure and $\Delta \dot{m}$ the difference in outlet mass flow. In all cases the difference is the average of the last two days.

Table 5.2: Sensitivity of thermal conductivity in unsteady heat transfer model. λ is increased by a factor 2. ΔT, Δp and $\Delta \dot{m}$ is the difference in outlet temperature, inlet pressure and outlet mass flow.

	λ [W/(m·K)]	factor	ΔT [°C]	Δp [MPa]	$\Delta \dot{m}$ [kg/s]
Steel	50	2	0.0108	$4.64 \cdot 10^{-5}$	0.0045
Asphalt	0.74	2	0.2131	$6.67 \cdot 10^{-4}$	0.0795
Concrete	2.9	2	0.6060	0.0016	0.2141
Soil	2	2	0.4987	-0.0092	-0.0546

Table 5.3: Sensitivity of heat capacity in unsteady heat transfer model. c_p is increased by a factor 2. ΔT, Δp and $\Delta \dot{m}$ is the difference in outlet temperature, inlet pressure and outlet mass flow.

	c_p [J/(kg·K)]	factor	ΔT [°C]	Δp [MPa]	$\Delta \dot{m}$ [kg/s]
Steel	500	2	-0.0127	$3.1 \cdot 10^{-5}$	0.037
Asphalt	1900	2	-0.002	$5.7 \cdot 10^{-5}$	0.0047
Concrete	650	2	-0.0146	$-2.0 \cdot 10^{-4}$	0.0136
Soil	1420	2	-0.0464	0.0017	0.059

Although increasing the thermal conductivity and heat capacity by a factor two is a considerable amount, the difference in computed outlet temperature was not that significant. For the heat capacity c_p, the difference in outlet temperature was of the

order 0.01 °C. For the thermal conductivity λ, the change in outlet temperature was more noticeable. By increasing the thermal conductivity of the concrete and soil by a factor two, the outlet temperature was determined to be approximately 0.5 °C higher. For the pipe wall, the thermal properties are believed to be fairly accurate, with an increase in thermal conductivity of the concrete by 100% an unlikely scenario. However, the thermal conductivity of the soil contains more uncertainty, and most likely contains seasonal variation. An increase (or decrease) in thermal conductivity of the soil by a factor 2 is therefore not that unlikely. Increasing the density ρ by a factor two would give the same result as increasing the heat capacity c_p by a factor two, as it is the product of the heat capacity and density which enters into the model. The results of an increase in density by a factor two is therefore the same as the results of an increase in heat capacity by a factor two in Table 5.3. For the inlet pressure and outlet mass flow the difference in computed results were not that significant as for the temperature.

The burial depth, being the distance from the ground level to the outer wall of the pipeline was originally 1 m. The effect of varying the burial depth is presented in Table 5.4. For a shorter burial depth, the outlet temperature increases, while for a larger burial depth it decreases. The burial depth is only significant for the sections where the pipeline is buried under ground, which for the setup considered is the first and final 25 km.

The effect of increasing and decreasing the length in which the pipeline is buried under ground was investigated, with results presented in Table 5.5. By increasing the length in which the pipeline is buried under ground at the inlet and outlet to 30 km, the outlet gas temperature is reduced by approximately 0.5 °C, while decreasing the length to 20 km increased the gas temperature by approximately 0.6 °C. The burial length is an important parameter to know in order to model the correct temperature at the outlet.

Table 5.4: Effect of burial depth. ΔT, Δp and $\Delta \dot{m}$ is the difference in outlet temperature, inlet pressure and outlet mass flow. The original burial depth was 1 m.

Burial depth [m]	ΔT [°C]	Δp [MPa]	$\Delta \dot{m}$ [kg/s]
0.4	0.5466	-0.01	-0.0843
0.6	0.2737	-0.0052	-0.0481
0.8	0.1089	-0.0021	-0.0186
1	0	0	0
1.2	-0.0780	0.0016	0.0128
1.4	-0.1370	0.0028	0.0214
1.6	-0.1831	0.0038	0.0266

Table 5.5: Effect of distance which pipeline is buried under ground. ΔT, Δp and $\Delta \dot{m}$ is the difference in outlet temperature, inlet pressure and outlet mass flow. The original burial length was 25 km.

Burial length [km]	ΔT [°C]	Δp [MPa]	$\Delta \dot{m}[kg/s]$
20	0.6640	-0.0087	0.0565
25	0	0	0
30	-0.5233	0.0084	-0.0519

The effect of the ambient temperature was investigated, with results given in Table 5.6. The original air temperature was 6 °C and sea bottom temperature 4 °C. A change in sea bottom temperature was more significant than a change in ambient air temperature. An increase in sea bottom temperature of 1 °C gave an increased outlet gas temperature of 0.26 °C, while for an increase in ambient air temperature of 1 °C the difference in outlet gas temperature was 0.08 °C. Results in Table 5.6 indicate that the model is more sensitive to the ambient sea bottom temperature towards the end of the pipeline compared to the beginning. For a 1 °C increase in sea bottom temperature for the first 300 km, the difference in outlet gas temperature was -0.0029 °C, while for a corresponding increase along the final 300 km the difference was 0.2672 °C. When only increasing the ambient temperature along the final 150 km, the difference in outlet temperature was 0.2652 °C. When increasing the ambient sea bottom temperature from 4 °C to 6 °C along the final 300 km, the difference in outlet gas temperature was approximately 0.5 °C. The same difference was found when increasing the temperature along the final 150 km.

Table 5.6: Effect of change in ambient temperature. ΔT, Δp and $\Delta \dot{m}$ is the difference in outlet temperature, inlet pressure and outlet mass flow.

	Old T [°C]	New T [°C]	ΔT [°C]	Δp [MPa]	$\Delta \dot{m}$ [kg/s]
Air	6	7	0.0825	$6.2{\cdot}10^{-4}$	0.0137
Air	6	9	0.2480	0.0018	0.041
Air	6	4	-0.1648	-0.0012	-0.0274
Sea	4	5	0.2644	0.0435	-0.0207
Sea	4	6	0.5262	0.0867	-0.0456
Sea	4	3	-0.2671	-0.0438	0.0164
Sea first 300 km	4	5	-0.0029	0.0203	0.0381
Sea final 300 km	4	5	0.2672	0.0232	-0.0596
Sea final 150 km	4	5	0.2652	0.0097	-0.0358
Sea final 300 km	4	6	0.5314	0.0463	-0.1190
Sea final 150 km	4	6	0.5275	0.0193	-0.0711

Case 2

In the second case the ambient air and sea bottom temperature were set to 15 °C and 7 °C respectively. These values correspond to typical conditions during the summer season. Apart from this, the flow setup was the same as in Section 5.2. The outlet gas temperature is shown in Figure 5.12. Compared to Figure 5.7, the outlet temperature of the gas is approximately 5 °C higher.

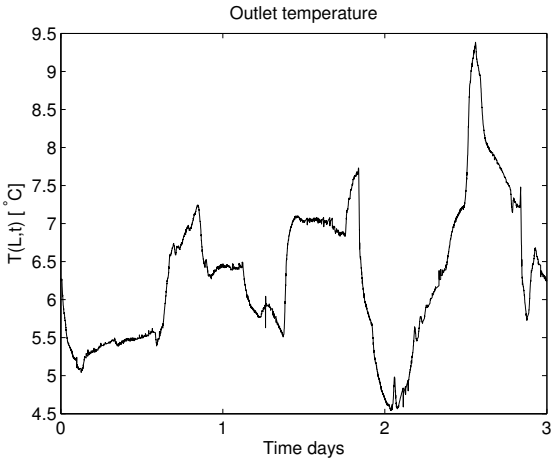

Figure 5.12: Outlet gas temperature for case 2 with ambient air and sea bottom temperature of 15 °C and 7 °C respectively.

As in case 1, the sensitivity of parameters which enter into the heat transfer model were investigated in detail. The sensitivity of the thermal conductivity and heat capacity of each thermal layer is presented in Table 5.7 and Table 5.8. The thermal conductivity was increased by a factor 2, with the most noticeable difference being observed for the concrete and soil layer. As commented on earlier, the thermal conductivity of the concrete is thought to be relatively accurate, and an increase by a factor 2 is therefore very unlikely. However, the thermal conductivity of the soil is more uncertain. For an increase in soil thermal conductivity by a factor 2, the difference in outlet gas temperature is approximately 1 °C. Results in Table 5.8 again confirm that the model is not sensitive to a change in heat capacity and density of the medium surrounding the pipeline. Even for an increase in heat capacity by a factor 2, the difference in outlet gas temperature was less than 0.1 °C.

The effect of burial depth and length are presented in Table 5.9 and Table 5.10. It can be observed that, compared to case 1, the model is not that sensitive to a change in burial length of the pipeline. When decreasing the burial length to 20 km, the difference in outlet gas temperature was 0.24 °C, while in case 1 it was 0.66 °C. The most likely reason for this is that the difference between the ambient and the gas temperature at the outlet is a lot more in case 2 compared to case 1. As the ambient temperature at the outlet is a lot more compared to the gas, there

will be energy transferred from the surroundings to the gas. This compensates for the Joule-Thomson effect, which is cooling upon expansion. Because of the large temperature difference, the heat exchange rate at the outlet is high, and the gas is not cooled by the Joule-Thomson effect to the same extent as when the temperature difference between the gas and the ambient is small. For a shorter burial length, this leads to an increase in outlet gas temperature.

The sensitivity of the ambient temperature is presented in Table 5.11. As in case 1, the model is more sensitive to a change in ambient temperature along the final part of the pipeline compared to the first part. For all computations in this case, the difference in inlet pressure and outlet mass flow is not that significant as for the outlet temperature.

Table 5.7: Sensitivity of thermal conductivity in unsteady heat transfer model. λ is increased by a factor 2. ΔT, Δp and $\Delta \dot{m}$ is the difference in outlet temperature, inlet pressure and outlet mass flow.

	λ [W/(m·K)]	factor	ΔT [°C]	Δp [MPa]	$\Delta \dot{m}$ [kg/s]
Steel	50	2	0.0167	$8.8 \cdot 10^{-5}$	0.0038
Asphalt	0.74	2	0.3336	0.0015	0.0674
Concrete	2.9	2	0.9792	0.0041	0.181
Soil	2	2	1.0198	-0.0045	-0.0119

Table 5.8: Sensitivity of heat capacity in unsteady heat transfer model. c_p is increased by a factor 2. ΔT, Δp and $\Delta \dot{m}$ is the difference in outlet temperature, inlet pressure and outlet mass flow.

	c_p [J/(kg·K)]	factor	ΔT [°C]	Δp [MPa]	$\Delta \dot{m}$ [kg/s]
Steel	500	2	-0.0182	$2.9 \cdot 10^{-4}$	0.0349
Asphalt	1900	2	-0.0029	$5.3 \cdot 10^{-5}$	0.0044
Concrete	650	2	-0.0223	$-2.0 \cdot 10^{-4}$	0.0132
Soil	1420	2	-0.0666	0.0015	0.0544

Table 5.9: Effect of burial depth. ΔT, Δp and $\Delta \dot{m}$ is the difference in outlet temperature, inlet pressure and outlet mass flow. The original burial depth was 1 m.

Burial depth [m]	ΔT [°C]	Δp [MPa]	$\Delta \dot{m}$ [kg/s]
0.4	1.1010	-0.0056	-0.0596
0.6	0.5551	-0.003	-0.0343
0.8	0.2230	-0.0012	-0.0129
1	0	0	0
1.2	-0.1606	$9.2{\cdot}10^{-4}$	0.0082
1.4	-0.2818	0.0016	0.0133
1.6	-0.3760	0.0022	0.0156

Table 5.10: Effect of distance which pipeline is buried under ground. ΔT, Δp and $\Delta \dot{m}$ is the difference in outlet temperature, inlet pressure and outlet mass flow. The original burial length was 25 km.

Burial length [km]	ΔT [°C]	Δp [MPa]	$\Delta \dot{m}$ [kg/s]
20	0.2405	-0.0101	0.0596
25	0	0	0
30	-0.2084	0.0095	-0.0527

Table 5.11: Effect of change in ambient temperature. ΔT, Δp and $\Delta \dot{m}$ is the difference in outlet temperature, inlet pressure and outlet mass flow.

	Old T [°C]	New T [°C]	ΔT [°C]	Δp [MPa]	$\Delta \dot{m}$ [kg/s]
Air	15	16	0.0850	$6.1{\cdot}10^{-4}$	0.0131
Air	15	18	0.2551	0.0018	0.0393
Air	15	14	-0.0850	$-6.1 \cdot 10^{-4}$	-0.0131
Sea	7	8	0.3432	0.0425	-0.0286
Sea	7	9	0.6835	0.0858	-0.0612
Sea	7	6	-0.2609	-0.0438	0.0254
Sea first 300 km	7	8	-0.0033	0.0194	0.0287
Sea final 300 km	7	8	0.3462	0.0227	-0.0556
Sea final 150 km	7	8	0.3446	0.0095	-0.0317
Sea final 300 km	7	9	0.6894	0.0457	-0.1132
Sea final 150 km	7	9	0.6861	0.0194	-0.0653

5.6.2 One-dimensional approximation

The unsteady external heat transfer model presented in Section 2.4.2 is a one-dimensional model, with the setup shown in Figure 2.7. Each thermal layer is represented by a coaxial cylindrical shell, with the boundary condition on the outer most shell being the ambient temperature T_a. This implies that the boundary condition along the entire circular domain is T_a, which in general is not correct, as the temperature at a distance D_0 above the pipeline will in general be different from that at a distance D_0 below. In the one-dimensional external heat transfer model, the heat flow is assumed to be the same in all radial directions.

In order to set correct boundary conditions, the two-dimensional heat conduction equation has to be solved in the domain surrounding the pipeline, as in the work by Barletta et al. [56]. It is shown that the temperature field in the soil surrounding the pipeline is not symmetric, and that the one-dimensional assumption in general is not valid. This is also illustrated in research article [d] in the Appendix. The heat flux from a natural gas pipeline is computed by solving both the one-dimensional and two-dimensional heat conduction equation. The computed heat flux between the gas and the surroundings was determined to be approximately 50% more in the one-dimensional model compared to the two-dimensional model. To determine how this will effect the flow, the one-dimensional flow model should in future be coupled to a two-dimensional external heat transfer model.

Chapter 6

Conclusions and Outlook

6.1 Conclusions

Transmission of natural gas through long distance high pressure offshore pipelines was modeled by numerically solving the governing equations for one-dimensional compressible viscous heat conducting flow. The governing equations are solved using an implicit finite difference scheme. The cell centered method where the flow values are computed at the midpoint between two grid points was used. Boundary conditions can easily be handled and the method uses centered differences to approximate the partial derivatives in space. Centered differences are preferred over one-sided approximations as these are stable for any CFL number. When discretizing all terms in a fully implicit way, the governing equations form a system of non-linear equations. To avoid having to solve a system of non-linear equations, the non-linear terms are linearized about the previous time step to give a system of linear equations.

Both the spatial and temporal discretization errors for pressure, mass flow and temperature were computed and are determined to be small compared to typical flow values. Other model simplifications, such as the one-dimensional assumption, model linearization and thermal decoupling are discussed in detail. These do not effect the results in any significant way. The model was validated by running simulations on a long distance offshore natural gas pipeline operated by Gassco. Computed results agreed well with measured values, but some discrepancies were observed, especially in the outlet gas temperature. These discrepancies are most likely due to physical approximation errors. Three different parameters which enter into the model are discussed in detail; the friction factor, equation of state and heat transfer term.

The friction factor was determined from the traditional Colebrook-White correlation, which is currently used by Gassco today. It has previously been stated that the transition from smooth to fully rough turbulent flow is more abrupt than that suggested by Colebrook-White. The alternative friction factor formula suggested by GERG was investigated. This formula gives a more abrupt transition com-

pared to Colebrook-White, however it contains two additional parameters, with little information available as to what numerical values these should be assigned. Because of this it is difficult to claim whether the GERG friction factor formula is an improvement of the Colebrook-White formula. A possible improvement of the Colebrook-White formula would only be possible by performing experiments in large scale test laboratories, something which has not been covered by the scope of this work.

The sensitivity of the selection of the equation of state for high pressure pipelines was investigated by comparing the SRK, Peng-Robinson, BWRS, GERG 88 and GERG 2004 equations of state. Gassco currently uses a BWRS equation of state with coefficients which are especially tuned for hydrocarbons. GERG 2004 is the most recently developed equation of state, and also believed to be the most accurate at high pressures (18 - 20 MPa). When modeling the flow of natural gas through high pressure pipelines, the major difference between the different equations of state was observed in the modeled inlet pressure. Comparison between GERG 2004 and the tuned BWRS currently used by Gassco gave a difference in inlet pressure of 0.1 MPa. This difference was observed during both steady state and transient conditions. The major disadvantage of GERG 2004 is its computational time, which is significantly longer compared to BWRS. Taking this into account, the tuned BWRS equation of state is most likely still the best alternative in Gassco's case. As the difference in computed inlet pressure between GERG 2004 and BWRS was fairly constant during both steady and transient conditions, the difference can be compensated for by tuning the equivalent sand grain roughness in such a way that the inlet pressure when using BWRS matches that of GERG 2004.

An unsteady external heat transfer model, which takes into account heat accumulation in the ground, was compared to a steady external heat transfer model currently used by Gassco. It is shown by example that the steady external heat transfer model over predicts the amplitude of temperature changes in the flow. Even for an offshore pipeline, which is only buried under ground for a short distance at the beginning and end of the pipeline, including heat accumulation in the ground is important in order to model the correct outlet gas temperature. The unsteady heat transfer model also improves the modeled inlet pressure and outlet mass flow. Compared to the steady heat transfer model the unsteady heat transfer model significantly improves the modeled outlet gas temperature. However, there is still a discrepancy between modeled and measured outlet gas temperature. The difference was observed to be in the region $1 - 1.5$ °C. Such a deviation has also been observed by Gassco in their models. The most important parameters identified that can account for this discrepancy is the ambient sea bottom temperature, soil thermal conductivity and pipeline burial length.

6.2 Outlook

In order to achieve better agreement between modeled and measured outlet gas temperature, the following key points should be addressed in future research.

- Thermal properties of the pipe wall and soil are important when modeling

the outlet gas temperature, especially the concrete and soil thermal conductivity. While data for the concrete thermal conductivity is believed to be fairly accurate, the soil thermal conductivity is thought to be more uncertain. Accurate data for the soil thermal conductivity at both the inlet and outlet of the pipeline could improve the modeled gas temperature.

- The unsteady external heat transfer model is a one-dimensional model. Correct ambient boundary conditions in the domain surrounding the pipeline is not possible in a one-dimensional model, only in the two-dimensional case. To investigate how this effects the flow, a two-dimensional external heat transfer model should be coupled to a one-dimensional flow model. In a real time application, solving the two-dimensional heat transfer model at every grid point would most likely not be feasible owing to the increase in computational time. However, it still important to know how a two-dimensional external heat transfer model would effect the flow compared to a one-dimensional model. It could be possible to derive an expression for the one-dimensional external heat transfer model which compensates for the one-dimensional assumption. Such an expression should be valid for both steady and unsteady flow conditions.

- In this work, only pipelines which were buried under ground or fully exposed to sea water were considered. Partially buried pipelines were not covered in this work. This is a key point which should be considered in detail, as many offshore pipelines lying on the seabed are partially buried. Heat transfer from a partially buried pipeline was investigated by Morud and Simonsen [57], however they only considered the steady one-dimensional heat transfer model. By implementing a two-dimensional heat transfer model, the domain surrounding the pipeline can be constructed such that it replicates a partially buried pipeline. By doing this it can be determined how the heat transfer from partially buried pipelines, including heat accumulation in the ground, effects the flow.

Chapter 7

Summary of research articles

Article [a]

J.F. Helgaker. An implicit method for 1D unsteady flow in a high pressure transmission pipeline. In Proceedings of *First ECCOMAS Young Investigators Conference 2012*, Aveiro, 2012.

Explicit and implicit finite difference are implemented in order to numerically solve the governing equations for unsteady one-dimensional compressible flow. Implicit finite difference methods are unconditionally stable and are therefore often used when modeling the flow of natural gas through high pressure transmission pipelines. As the governing equations are non-linear, discretizing the equations in a fully implicit way gives a system of non-linear equations which has to be solved at every time step. This can be computationally expensive, especially for long pipelines and complicated networks. In this article it shown by example how the governing equations can be linearized to give a system of linear equations, which can be solved using linear algebra.

The computational time of the linear model is compared to that of the non-linear model, and shown to be considerably less. For transient flow through a 650 km pipeline there was no observable difference in results between the linear and non-linear model. This confirms that a linear assumption when modeling the flow of natural gas through long distance pipelines is valid. Also, the simple hydraulic model is compared to the full non-isothermal model. A clear difference in modeled pressure and mass flow was observed, confirming that a full non-isothermal model should be used when modeling the flow of natural gas through long distance high pressure pipelines.

Article [b]

J.F. Helgaker and T. Ytrehus. Coupling between Continuity/Momentum and Energy Equation in 1D Gas Flow. Energy Procedia **26** (2012), pages 82-89, In Pro-

ceedings of *2nd Trondheim Gas Technology Conference*, Trondheim 2011.

Transportation of natural gas through high pressure offshore transmission pipelines is simulated by numerically solving the governing equations for one-dimensional compressible viscous heat conducting flow. Since the flow is compressible and viscous, and the temperature is a function of pressure and density, the continuity, momentum and energy equation should be solved simultaneously at each time step when using an implicit finite difference method to solve the governing equations. However, in some cases it may be advantageous to solve thermal model (energy equation) separately from the hydraulic model (continuity and momentum equations). In this article, solving the energy equation separately one time step after the continuity and momentum equations is investigated.

Decoupling the thermal model from the hydraulic model makes the resulting system of equations easier to solve and reduces the computational time for each time step. It is shown by example that this simplification does not effect the results in any major way, indicating that the changes in temperature are sufficiently slow to allow the energy equation to be solved separately one time step after the continuity and momentum equations. For a pipeline discretized by N points, solving all three governing equations simultaneously implies finding the inverse of a $(3N-3)\times(3N-3)$ matrix at each time step. When solving the thermal model separately from the hydraulic model, the inverse of a $(2N-2)\times(2N-2)$ and $(N-1)\times(N-1)$ matrix is required at each time step. This procedure reduces the computational time of each time step.

Article [c]

T. Ytrehus and J.F. Helgaker. Energy Dissipation Effect in the One-Dimensional Limit of the Energy Equation in Turbulent Compressible Flow. Journal of Fluids Engineering - Transactions of The ASME, Vol. **135** (6) (2013).

When modeling the flow of natural gas through long distance pipelines, the governing equations for one-dimensional compressible flow are found by averaging the three-dimensional equations over the pipe cross-section.

In this article a turbulent velocity profile is used when deriving the one-dimensional version of the energy equation in turbulent compressible flow. The result is a correction factor, close to unity, on the usual expression of the dissipation term in the energy equation. This factor, which depends on the Reynolds number of the flow and the pipe surface roughness, will to some extent affect the temperature distribution along the pipeline. For low Reynolds numbers ($Re \simeq 10^4$) it reduces the dissipation by as much as 7%, irrespective of roughness. For high Reynolds numbers ($Re \geq 10^7$) and roughness in the high range of the micron decade, the dissipation is increased by 10%. If the pipeline is also thermally isolated such that the flow can be considered adiabatic, the effect of turbulent dissipation gains further importance.

It is shown by examples how a correction factor can give changes in outlet

temperature of up to $1°C$ or more, depending upon thermal insulation and the length of the pipe. However, for pipelines operated by Gassco the surface roughness is typically in the range $3-5\ \mu m$. In this roughness range and for Reynolds numbers of approximately 10^7 the correction factor is so close to unity that it does not effect the temperature distribution along the pipeline in any significant way. In this case the usual expression for the dissipation term in the energy equation may be used.

Article [d]

J.F. Helgaker, A. Oosterkamp and T. Ytrehus. Transmission of Natural Gas through Offshore Pipelines - Effect of unsteady heat transfer model. In B. Skallerud and H. Andersson, editors, *MekIT'13: Seventh national conference on Computational Mechanics*, pages 113-131, Akademika Publishing 2013

The heat exchange between the gas and the pipeline surroundings in investigated in detail. A steady state external heat transfer model, based on using a total heat transfer coefficient U, is compared to an unsteady external heat transfer model which takes into account heat accumulation in the ground. It is shown by example that a steady heat transfer model over predicts the amplitude of temperature changes in the flow compared to an unsteady heat transfer model. Results are compared to measured values from an offshore natural gas pipeline. These confirm that the steady heat transfer model over predicts the amplitude of temperature changes in the flow compared to an unsteady heat transfer model, even for an offshore pipeline which is only buried under ground for a short length at the beginning and end of the pipeline. It is also shown by example that during large transients a considerable difference in modeled inlet pressure is observed between the steady and unsteady external heat transfer model.

The considered heat transfer model is one-dimensional. This implies that the boundary condition along the entire circular domain is the ambient temperature T_a, which in general is not correct, as the temperature at a distance D_0 above the pipeline will in general be different from that at a distance D_0 below. In the one-dimensional external heat transfer model, the heat flow is assumed to be the same in all radial directions. Correct boundary conditions can only be set in a two-dimensional model. The heat flux from a two-dimensional model was therefore compared to the heat flux from the one-dimensional model. For the considered case, it was determined that the one-dimensional heat transfer model over predicts the heat flux by approximately 50% compared to a two-dimensional model.

Article [e]

J.F. Helgaker, B. Müller and T. Ytrehus. Transient Flow in Natural Gas Pipelines using Implicit Finite Difference Schemes. Submitted to Journal of Fluids Engineering, June 2013.

The transmission of natural gas through high pressure pipelines is modeled by numerically solving the governing equations using implicit finite difference schemes. Two main approaches are considered. In the first case the backward Euler method is considered, with spatial derivatives being approximated by both first order one-sided upwind and second order centered differences. In the second case the implicit cell centered method is considered, where flow values are computed at the midpoints between two grid points.

The backward Euler method with upwind approximations for the spatial derivatives is unstable for CFL numbers less than 1. The von Neumann stability analysis confirms this. The backward Euler method with centered differences and the implicit cell centered method are stable for any CFL number. However, for a discontinuous change in inlet temperature both methods introduce unphysical oscillations in the temperature profile along the pipeline. A solution strategy where the thermal model is solved separately from the hydraulic model using a different discretization technique is suggested. The hydraulic model is solved using the implicit cell centered method, while the thermal model is solved using the backward Euler upwind method. This solution strategy is stable for any CFL number and does not introduce unphysical oscillations for a discontinuous changes in inlet temperature.

Article [f]

J.F. Helgaker, A. Oosterkamp, L.I. Langelandsvik and T. Ytrehus. Validation of 1D Flow Model for Transmission of Natural Gas through Offshore Pipelines. Submitted to Journal of Natural Gas Science and Engineering, June 2013

The 1D flow model is validated by running simulations on an offshore natural gas pipeline operated by Gassco. Modeled results agree well with measured values, however some discrepancies are present, which most likely are due to physical approximation errors. The influence of different physical processes which enter into the flow model are discussed in detail. These include the friction factor, equation of state and the heat exchange between the gas and the surroundings.

The influence of the equation of state for high pressure natural gas pipelines is investigated. The SRK, Peng-Robinson, BWRS, GERG 88 and GERG 2004 equations of state are investigated. The most noticeable difference was observed in inlet pressure, with the difference between GERG 2004 and BWRS being 0.1 MPa (1 bar).

The heat exchange between the gas and the surroundings was modeled using both a steady external heat transfer model and an unsteady external heat transfer model. By comparing computed results to measured values the steady heat transfer model over predicts the amplitude of temperature changes in the flow, while the unsteady model agrees a lot better with measured values. Including heat accumulation in the ground gives improved results for the modeled temperature.

Bibliography

[1] BP p.l.c London, "BP Statistical Review of World Energy," 2012. `bp.com/statisticalreview`.

[2] "Natural Gas Supply Association," 2013. `naturalgas.org/environment`.

[3] International Gas Union (IGU), "Global Vision for Gas - The Pathway towards a Sustainable Energy Future," 2012.

[4] L. I. Langelandsvik, W. Postvoll, B. Aarhus, K. K. Kaste, "Accurate calculations of pipeline transport capacity," *Proceedings to 24th World Gas Conference, Buenos Aires, Argentina*, 2009.

[5] L. I. Langelandsvik, *Modeling of natural gas transport and friction factor for large-scale pipelines*. PhD thesis, Norwegian University of Science and Technology, Trondheim, Norway, 2008.

[6] J. Ramsen, S. E. Losnegaard, L. I. Langelandsvik, A. J. Simonsen, W. Postvoll, "Important Aspects of Gas Temperature Modeling in Long Subsea Pipelines," *Proceedings to 40th PSIG Annual Meeting, Galvestone, Texas, USA*, 2009.

[7] P. H. G. M. Hendriks, W. Postvoll, M. Mathiesen, R. P. Spiers, J. Siddorn, "Improved Capacity Utilization by Integrating Real-time Sea Bottom Temperature Data," *Proceedings to 37th PSIG Annual Meeting, Williamsburg, Virginia, USA*, 2006.

[8] L. I. Langelandsvik, S. Solvang, M. Rousselet, I. N. Metaxa, M. J. Assael, "Dynamic Viscosity Measurements of Three Natural Gas Mixtures - Comparison against Prediction Models," *International Journal of Thermophysics*, vol. 28, pp. 1120–1130, 2007.

[9] L. I. Langelandsvik, S. Solvang, M. Rousselet, M. J. Assael, "New Viscosity Measurements of Three Natural Gas Mixtures and an Improved Tuning of the LGE-Correlation," *Proceedings of the Asian Thermophysical Properties Conference, Fukuoka, Japan*, 2007.

[10] A. R. D. Thorley, C. H. Tiley, "Unsteady and transient flow of compressible fluids in pipelines - a review of theoretical and some experimental studies," *International Journal of Heat and Fluid Flow*, vol. 8, no. 1, pp. 3–15, 1987.

[11] R. I. Issa, D. B. Spalding, "Unsteady One-Dimensional Compressible Frictional Flow with Heat Transfer," *Journal of Mechanical Engineering Science*, vol. 14, no. 6, pp. 365–369, 1972.

[12] E. B. Wylie, V. L. Streeter, M. A. Stoner, "Unsteady-State Natural-Gas Calculations in Complex Pipe Systems," *Society of Petroleum Engineering*, vol. 14, pp. 35–43, 1974.

[13] M. Poloni, D. E. Winterbone, J. R. Nichols, "Comparison of Unsteady Flow Calculations in a Pipe by the Method of Characteristics and the Two-step Differential Lax-Wendroff Method," *Int. J. Mech. Sci*, vol. 29, no. 5, pp. 367–378, 1987.

[14] T. Kiuchi, "An implicit method for transient gas flows in pipe networks," *International Journal of Heat and Fluid Flow*, vol. 15, pp. 378–383, 1994.

[15] A. J. Osiadacz, "Different Transient Models - Limitations, Advantages and Disadvantages," *Proceedings to 28th PSIG Annual Meeting, San Francisco, California, USA*, 1996.

[16] M. Abbaspour, K. S. Chapman, "Nonisothermal Transient Flow in Natural Gas Pipeline," *ASME Journal of Applied Mechanics*, vol. 75, pp. 0310181–0310188, 2008.

[17] A. J. Osiadacz, M. Chaczykowski, "Comparison of isothermal and non-isothermal pipeline gas flow model," *Chemical Engineering Journal*, vol. 81, pp. 41–51, 2001.

[18] M. Chaczykowski, "Sensitivity of pipeline gas flow model to the selection of the equation of state," *Chemical Engineering Research and Design*, vol. 87, pp. 1596–1603, 2009.

[19] M. Chaczykowski, "Transient flow in natural gas pipeline - The effect of pipeline thermal model," *Applied Mathematical Modelling*, vol. 34, pp. 1051–1067, 2010.

[20] C. F. Colebrook, "Turbulent flow in pipes, with particular reference to the transition region between the smooth and rough pipe laws," *J. Inst. Civil. Eng*, vol. 11, pp. 133–156, 1939.

[21] L. I. Langelandsvik, W. Postvoll, P. Svendsen, J. M. Øverli, T. Ytrehus, "An Evaluation of the Friction Factor Formula based on Operational Data," *Proceedings to 37th PSIG Annual Meeting, San Antonio, Texas, USA*, 2005.

[22] L. I. Langelandsvik, G. J. Kunkel, A. J. Smits, "Flow in a commercial steel pipe," *Journal of Fluid Mechanics*, vol. 595, pp. 323–339, 2008.

[23] K. Gersten, H. D. Papenfuss, T. H. Kurschat, P. H. Genillon, F. Fernandez Perez, N. Revell, "New transmission-factor formula proposed for gas pipelines," *Oil and Gas Journal*, pp. 58–62, feb 2000.

[24] E. Sletfjerding, *Friction factor in smooth and rough gas pipelines*. PhD thesis, Norwegian University of Science and Technology, Trondheim, Norway, 1998.

[25] S. E. Haaland, "Simple and Explicit Formulas for the Friction Factor in Turbulent Pipe Flow," *Journal of Fluids Engineering*, vol. 105, pp. 89–91, 1983.

[26] G. Soave, "Equilibrium constants from a modified Redlich-Kwong equation of state," *Chemical Engineering Science*, vol. 27, pp. 1197–1203, 1972.

[27] O. Redlich, J. N. S. Kwong, "On the Thermodynamics of Solutions. V. An Equation of State. Fugacities of Gaseous Solutions," *Chem. Rev*, vol. 44, pp. 233–244, 1944.

[28] D. Y. Peng, D. B. Robinson, "A New Two-Constant Equation of State," *Industrial and Engineering Chemical Fundamentals*, vol. 15, pp. 59–64, 1976.

[29] J. L. Modisette, "Equation of State Tutorial," *Proceedings to 32nd PSIG Annual Meeting, Savannah, Georgia, USA*, 2000.

[30] K. E. Starling, *Fluid Thermodynamic Properties for Light Petroleum Systems*. Gulf Publishing Company, 1973.

[31] M. Jaeschke, S. Audlbert, P. Caneghem, A. E. Humphreys, R. J. Rosmalen, Q. Pellel, J. A. Schouten, J. P. J. Michels, "Accurate Prediction of Compressibility Factor by the GERG Virial Equation," *SPE Production Engineering*, 1991.

[32] O. Kunz, R. Klimeck, W. Wagner, M. Jaeschke, *The GERG-2004 Wide-Range Equation of State for Natural Gases and Other Mixtures*, 2007. GERG Technichal Monograph TM15.

[33] O. Kunz, W. Wagner, "The GERG-2008 Wide-Range Equation of State for Natural Gases and Other Mixtures: An Expansion of GERG-2004," *Journal of chemical & engineering data*, vol. 57, no. 11, pp. 3032–3091, 2012.

[34] Z. Nagy, A. I. Shirkovskiy, "Mathematical Simulation of Natural Gas Condensation Processes using the Peng-Robinson Equation of State," *Society of Petroleum Engineers*, 1982.

[35] F. P. Incropera, D. P. DeWitt, T. L. Bergman, A. S. Lavine, *Fundamentals of Heat and Mass Transfer*. Wiley, 6 ed., 2007.

[36] A. F. Mills, *Heat and Mass Transfer*. Irwin, 1995.

[37] A. L. Lee, M. H. Gonzalez, B. E. Eakin, "The Viscosity of Natural Gases," *Journal of Petroleum Technology*, vol. 18, no. 8, pp. 997–1000, 1966.

[38] G. P. Greyvenstein, "An implicit method for the analysis of transient flows in pipe networks," *International Journal for Numerical Methods in Engineering*, vol. 53, pp. 1127–1143, 2001.

[39] J. Modisette, "Instability and other numerical problems in finite difference pipeline models," *Proceedings to 43rd PSIG Annual Meeting, Santa Fe, New Mexico, USA*, 2012.

[40] C. Bisgaard, H. H. Sørensen, S. Spangenberg, "A Finite Element Method for Transient Compressible Flow in Pipelines," *International Journal for Numerical Methods in Fluids*, vol. 7, pp. 291–303, 1987.

[41] M. A. Chaiko, "A finite-volume approach for simulation of liquid-column separation in pipelines," *ASME Journal of Fluids Engineering*, vol. 128, pp. 1324–1335, 2006.

[42] L. M. C. Gato, J. C. C. Henriques, "Dynamic behaviour of high-pressure natural-gas flow in pipelines," *International Journal of Heat and Fluid Flow*, vol. 26, pp. 817–825, 2005.

[43] A. J. Osiadacz, M. Yedroudj, "A comparison of a finite element method and a finite difference method for transient simulation of a gas pipeline," *Applied Mathematical Modelling*, vol. 13, pp. 79–85, 1987.

[44] E. B. Wylie, V. Streeter, *Fluid Transients in Systems*. Prentice Hall, 1993.

[45] P. Lax, B. Wendroff, "Systems of Conservation Laws," *Communications on Pure and Applied Mathematics*, vol. 13, pp. 217–237, 1960.

[46] S. Gottlieb, C. W. Shu, "Total variation diminishing Runge-Kutta schemes," *Mathematics of Computation*, vol. 67, pp. 73–85, 1998.

[47] B. Gustafsson, *High Order Difference Methods for time dependent PDE*. Springer Series in Computational Mathematics, 2008.

[48] M. Luskin, "An Approximate Procedure for Nonsymmetric Nonlinear Hyperbolic Systems with Integral Boundary Conditions," *SIAM Journal on Numerical Analysis*, vol. 16, pp. 145–164, 1979.

[49] M. Abbaspour, K. S. Chapman, L. A. Glasgow, "Transient modeling of non-isothermal, dispersed two-phase flow in natural gas pipelines," *Applied Mathematical Modelling*, vol. 34, pp. 495–507, 2010.

[50] W. L. Oberkampf, T. G. Trucano, "Verification and Validation in Computational Fluid Dynamics," *Progress in Aerospace Sciences*, vol. 38, pp. 209–272, 2002.

[51] C. W. Gear, *Numerical Initial Value Problems in Ordinary Differential Equations*. Prentice-Hall, Englewood Cliffs, NJ, 1971.

[52] AIAA, "Guide for the verification and validation of computational fluid dynamics simulations," Tech. Rep. AIAA-G-077-1998, American Institute of Aeronautics and Astronautics, Reston VA, 1998.

[53] J. Barley, "Thermal decoupling: An investigation," *Proceedings to 43rd PSIG Annual Meeting, Santa Fe, New Mexico, USA*, 2012.

[54] J. Nikuradse, "Stromungsgesetze in rauhen rohren," *Forschungsheft 361, volume B, VDI Verlag Berlin*, 1950. Translated in NACA Technical Memorandum nr.1292.

[55] J. Piggott, N. Revell, T. Kurschat, "Taking the rough with the Smooth - a new look at transmission factor formulae," *Proceedings to 34th PSIG Annual Meeting, Portland, Oregon, USA*, 2002.

[56] A. Barletta, E. Zanchini, S. Lazzari, A. Terenzi, "Numerical study of heat from an offshore buried pipeline under steady-periodic thermal boundary conditions," *Applied thermal engineering*, vol. 28, pp. 1168–1176, 2008.

[57] J. C. Morud, A. Simonsen, "Heat transfer from partially buried pipelines," *Proceedings to 16th Australasian Fluid Mechanics Conference*, 2007.

Appendix

Derivation of Governing Eq. for 1D flow

The governing equations for 1D unsteady compressible viscous heat conducting flow are

Continuity

$$\frac{\partial \rho}{\partial t} + \frac{\partial (\rho u)}{\partial x} = 0 \tag{7.1}$$

Momentum

$$\frac{\partial (\rho u)}{\partial t} + \frac{\partial (\rho u^2 + p)}{\partial x} = -\frac{f \rho u^2}{2D} - \rho g \sin\theta \tag{7.2}$$

Energy

$$\rho c_v \left(\frac{\partial T}{\partial t} + u \frac{\partial T}{\partial x} \right) + T \left(\frac{\partial p}{\partial T} \right)_\rho \frac{\partial u}{\partial x} = \frac{f \rho u^3}{2D} - \frac{4U}{D}(T - T_a) \tag{7.3}$$

The energy equation is in the non-conservative internal energy form. The density ρ can be exchanged for the pressure p using a real gas equation of state

$$\frac{p}{\rho} = ZRT \tag{7.4}$$

The mass flow rate is defined as

$$\dot{m} = \rho u A \tag{7.5}$$

Continuity Equation

The equation of state (Equation (7.4)) can be written as

$$\ln \rho = \ln p - \ln Z - \ln R - \ln T \tag{7.6}$$

Taking the derivative of Equation (7.6) with respect to time

$$\frac{1}{\rho}\frac{\partial \rho}{\partial t} = \frac{1}{p}\frac{\partial p}{\partial t} - \frac{1}{Z}\frac{\partial Z}{\partial t} - \frac{1}{T}\frac{\partial T}{\partial t} \tag{7.7}$$

The compressibility factor is a function of pressure and temperature, $Z = Z(p, T)$

$$\frac{\partial Z}{\partial t} = \left(\frac{\partial Z}{\partial p}\right)_T \frac{\partial p}{\partial t} + \left(\frac{\partial Z}{\partial T}\right)_p \frac{\partial T}{\partial t} \tag{7.8}$$

Equation (7.7) can now be written

$$\frac{1}{\rho}\frac{\partial \rho}{\partial t} = \left[\frac{1}{p} - \frac{1}{Z}\left(\frac{\partial Z}{\partial p}\right)_T\right] - \left[\frac{1}{T} + \frac{1}{Z}\left(\frac{\partial Z}{\partial T}\right)_p\right] \tag{7.9}$$

The continuity equation can now be written

$$\begin{aligned} \frac{\partial p}{\partial t} &= \left[\frac{1}{T} + \frac{1}{Z}\left(\frac{\partial Z}{\partial T}\right)_p\right]\left[\frac{1}{p} - \frac{1}{Z}\left(\frac{\partial Z}{\partial p}\right)_T\right]^{-1}\frac{\partial T}{\partial t} \\ &- \frac{ZRT}{pA}\left[\frac{1}{p} - \frac{1}{Z}\left(\frac{\partial Z}{\partial p}\right)_T\right]^{-1}\frac{\partial \dot{m}}{\partial x} \end{aligned} \tag{7.10}$$

Momentum Equation

For the momentum equation the expression for the gas velocity is needed

$$u = \frac{\dot{m} Z R T}{pA} \tag{7.11}$$

which can be rewritten

$$\ln u = \ln \dot{m} + \ln Z + \ln R + \ln T - \ln p - \ln A \tag{7.12}$$

Taking the derivative of Equation (7.12) with respect to time

$$\frac{1}{u}\frac{\partial u}{\partial x} = \frac{1}{\dot{m}}\frac{\partial \dot{m}}{\partial x} + \frac{1}{Z}\frac{\partial Z}{\partial x} + \frac{1}{T}\frac{\partial T}{\partial x} - \frac{1}{p}\frac{\partial p}{\partial x} \tag{7.13}$$

The derivative of the compressibility factor with respect to x is

$$\frac{\partial Z}{\partial x} = \left(\frac{\partial Z}{\partial p}\right)_T \frac{\partial p}{\partial x} + \left(\frac{\partial Z}{\partial T}\right)_p \frac{\partial T}{\partial x} \tag{7.14}$$

Inserting this into Equation (7.13)

$$\frac{1}{u}\frac{\partial u}{\partial x} = \frac{1}{\dot{m}}\frac{\partial \dot{m}}{\partial x} + \left[\frac{1}{T} + \frac{1}{Z}\left(\frac{\partial Z}{\partial T}\right)_p\right]\frac{\partial T}{\partial x} - \left[\frac{1}{p} - \frac{1}{Z}\left(\frac{\partial Z}{\partial p}\right)_T\right]\frac{\partial p}{\partial x} \tag{7.15}$$

Assuming a constant pipe cross-section A, the momentum equation can be written

$$\frac{1}{A}\frac{\partial \dot{m}}{\partial t} + \frac{1}{A}\left(u\frac{\partial \dot{m}}{\partial x} + \dot{m}\frac{\partial u}{\partial x}\right) + \frac{\partial p}{\partial x} = -\frac{f \dot{m} u}{2D} - \rho g \sin\theta \tag{7.16}$$

Inserting the expressions for u, ρ and $\partial u/\partial x$ gives the final result for the momentum equation

$$\begin{aligned}\frac{\partial \dot{m}}{\partial t} &= \frac{\dot{m}ZRT}{pA}\left(-2\frac{\partial \dot{m}}{\partial x}+\dot{m}\left[\frac{1}{p}-\frac{1}{Z}\left(\frac{\partial Z}{\partial p}\right)_T\right]\frac{\partial p}{\partial x}-\dot{m}\left[\frac{1}{T}+\frac{1}{Z}\left(\frac{\partial Z}{\partial T}\right)_p\right]\frac{\partial T}{\partial x}\right)\\ &- A\frac{\partial p}{\partial x}-\frac{fZRT\dot{m}|\dot{m}|}{2DAp}-\frac{pA}{ZRT}g\sin\theta \end{aligned} \tag{7.17}$$

The momentum equation was derived from the conservative form, opposed to Chaczykowski [19] who derived it from the non-conservative form. The momentum equation derived from the non-conservative form is

$$\begin{aligned}\frac{\partial \dot{m}}{\partial t} &= -\frac{\dot{m}ZRT}{pA}\frac{\partial \dot{m}}{\partial x}+\dot{m}\left[\frac{1}{p}-\frac{1}{Z}\left(\frac{\partial Z}{\partial p}\right)_T\right]\times\left(\frac{\partial p}{\partial t}+\frac{\dot{m}ZRT}{pA}\frac{\partial p}{\partial x}\right)\\ &- \dot{m}\left[\frac{1}{T}+\frac{1}{Z}\left(\frac{\partial Z}{\partial T}\right)_p\right]\times\left(\frac{\partial T}{\partial t}+\frac{\dot{m}ZRT}{pA}\frac{\partial T}{\partial x}\right)\\ &- A\frac{\partial p}{\partial x}-\frac{fZRT\dot{m}|\dot{m}|}{2DAp}-\frac{pA}{ZRT}g\sin\theta \end{aligned} \tag{7.18}$$

Equation (7.17) and (7.18) look different, but mathematically they are the same. In Equation (7.18) all the terms in the continuity equation (Equation (7.10)) can be identified. The sum of these terms is zero, meaning Equation (7.18) can be simplified to (7.17). Equation (7.17) is thought to be easier to work with as there is only one time derivative, opposed to Equation (7.18) which has three.

Energy Equation

In the energy equation (Equation (7.3)) an expression has already been found for the gas velocity u and the derivative of the velocity $\partial u/\partial x$. In the Joule-Thomson term an expression is needed for the derivative of the pressure with respect to temperature. Using the real gas equation of state

$$\left(\frac{\partial p}{\partial T}\right)_\rho = \rho R\left[Z+T\left(\frac{\partial Z}{\partial T}\right)_\rho\right] \tag{7.19}$$

Using this the internal energy equation is developed into

$$\begin{aligned}\frac{\partial T}{\partial t} &= -\frac{\dot{m}ZRT}{pA}\frac{\partial T}{\partial x}-\frac{\dot{m}(ZRT)^2}{pAc_v}T\left[\frac{1}{T}+\frac{1}{Z}\left(\frac{\partial Z}{\partial T}\right)_\rho\right]\\ &\times\left(\frac{1}{\dot{m}}\frac{\partial \dot{m}}{\partial x}-\left[\frac{1}{p}-\frac{1}{Z}\left(\frac{\partial Z}{\partial p}\right)_T\right]\frac{\partial p}{\partial x}+\left[\frac{1}{T}+\frac{1}{Z}\left(\frac{\partial Z}{\partial T}\right)_p\right]\frac{\partial T}{\partial x}\right)\\ &+ \frac{f}{2c_vD}\left(\frac{ZRT|\dot{m}|}{pA}\right)^3-4U\frac{ZRT}{pc_vD}(T-T_a)\end{aligned} \tag{7.20}$$

Research articles in full text

Article [a]

An implicit method for 1D unsteady flow in a high pressure transmission pipeline

J.F. Helgaker

In Proceedings of First ECCOMAS Young Investigators Conference, Aveiro, 2012.

YIC2012 — Universidade de Aveiro
First ECCOMAS Young Investigators Conference
A. Andrade-Campos, N. Lopes, R.A.F. Valente, H. Varum (editors)
24–27 April 2012, Aveiro. Portugal.

AN IMPLICIT METHOD FOR 1D UNSTEADY FLOW IN A HIGH PRESSURE TRANSMISSION PIPELINE

J.F. Helgaker [a,b,⋆]

[a]Polytec R&D Institute
Sorhauggt 128
5527 Haugesund, Norway

[b]NTNU - Norwegian University of Science and Technology
Dept. Energy and Process Engineering
Kolbjorn Hejes vei 1B
7491 Trondheim, Norway

⋆Corresponding author: jan.fredrik.helgaker@polytec.no

Abstract. *Explicit and implicit finite difference methods have been used to numerically solve the governing equations for one-dimensional compressible viscous heat conducting flow. For the implicit method, to avoid having to solve a system of non-linear equations, the non-linear terms are linearized about the previous time step. The linearized model is shown to give just as good results as the non-linear model and the computational time is greatly reduced. Accurate, efficient and stable methods for compressible 1D unsteady flow calculations are desirable for industrial applications. The presented model was validated using operational data from high pressure natural gas transmission pipelines.*

Keywords: CFD; numerical methods; unsteady compressible 1D flow.

1 INTRODUCTION

Natural gas is an important energy resource in Europe and the rest of the world and can be transported over long distances through high pressure transmission pipelines. For offshore pipelines lying on the seabed, measurements of the state of the gas, such as pressure, flow rate, composition and temperature are usually done only at the inlet and outlet. To know the state of the gas between these two points one has to rely on computer models. These models are used to monitor the gas, providing estimated time of arrival for unwanted quality disturbances and predicting the pipeline hydraulic capacity. It is crucial that these models are as accurate as possible, but at the same time they have to be fast and efficient as conditions in the pipeline are usually transient. As offshore transport pipelines are becoming longer and longer, the need for mathematical models which are both accurate and fast is becoming more important.

The simulation of natural gas in pipelines involves the numerical solution of a system of initial valued partial differential equations which are of hyperbolic type. An overview of different numerical techniques used to solve the governing equations for 1D unsteady compressible flow can be found in base literature articles, for instance by Thorley and Tiley [1].

The method of characteristics was popular a few decades ago, see for example the article by Wylie [2]. It is however slow compared to other methods such as finite difference and the time step is restricted by the CFL condition. Finite difference methods are commonly used to solve 1D unsteady flow problems. Poloni [3] used the explicit finite difference method which is fast and easy to implement, but as with the method of characteristics the time step is limited by the CFL condition. The implicit finite difference method is unconditionally stable and is therefore commonly used in commercial tools. It can however be computationally more expensive, especially if one has to solve a system of non-linear equations at each time step. The fully implicit model was solved by Kiuchi [4] and Abbaspour and Chapman [5].

The model by Kiuchi assumes isothermal conditions, while Abbaspour and Chapman solve the non-isothermal model. If changes in temperature along the pipeline are small one can assume an isothermal model, which means only the continuity and momentum equations have to be solved for the flow. However, for large pipelines operating at high pressures one has to, as shown by Osiadacz [6], solve the non-isothermal model.
Both Kiuchi and Abbaspour and Chapman discretize the equations in a fully implicit way and use the Newton-Raphson technique to solve the system of non-linear equations. Although the method is stable and gives good results [5], it is computationally expensive and becomes impractical for long pipelines and complex networks. In the following a linearized implicit finite difference method will be investigated. The non-linear terms are linearized about the previous time step as in the article by Luskin [7]. It will be compared to the non-linear method and validated using operational data from offshore high pressure transmission pipelines.

2 MATHEMATICAL MODEL

2.1 Governing Equations

The governing equations for 1D unsteady compressible viscous heat conducting flow are

Continuity

$$\frac{\partial \rho}{\partial t} + \frac{\partial (\rho u)}{\partial x} = 0 \tag{1}$$

Momentum

$$\frac{\partial (\rho u)}{\partial t} + \frac{\partial (\rho u^2 + p)}{\partial x} = -\frac{f \rho u^2}{2D} - \rho g \sin\theta \tag{2}$$

Energy

$$\rho c_v \left(\frac{\partial T}{\partial t} + u \frac{\partial T}{\partial x} \right) + T \left(\frac{\partial p}{\partial T} \right)_\rho \frac{\partial u}{\partial x} = \frac{f \rho u^3}{2D} + \rho q \tag{3}$$

The continuity and momentum equations are expressed in conservative form while the energy equation is in the non-conservative internal energy form. The density ρ can be exchanged for the pressure p by using a real gas equation of state

$$\frac{p}{\rho} = ZRT \tag{4}$$

where $Z = Z(p, T)$ is the compressibility factor. The ratio between pressure p and density ρ is the speed of sound squared, i.e. $p/\rho = c^2$. $\sin\theta$ is the pipe inclination angle, f the friction factor which can be found from the Colebrook-White [8] correlation

$$\frac{1}{\sqrt{f}} = -2 \log \left(\frac{\epsilon}{3.7D} + \frac{2.51}{Re\sqrt{f}} \right) \tag{5}$$

where ϵ is the surface roughness, D the pipeline diameter and Re the Reynolds number of the flow. The last term in the energy equation is the heat transfer term between the gas and the medium surrounding the pipeline

$$\rho q = -\frac{4U}{D}(T - T_a) \tag{6}$$

where U is the total heat transfer coefficient and T_a the ambient temperature.

2.2 Simple model

A simple model (SM) for 1D unsteady flow is based on the model by Kiuchi [4]. Trading the density ρ for the pressure p and introducing the mass flow rate $\dot{m} = \rho u A$ (A being the pipeline cross-section) the continuity and momentum equations are developed into

$$\frac{\partial p}{\partial t} + \frac{c^2}{A} \frac{\partial \dot{m}}{\partial x} = 0 \tag{7}$$

$$\frac{\partial \dot{m}}{\partial t} + A \frac{\partial p}{\partial x} = -\frac{f c^2 \dot{m} |\dot{m}|}{2DAp} \tag{8}$$

The pipeline is assumed to be horizontal and the convective term in the momentum equation has been neglected. Kiuchi assumed an isothermal model and therefore a constant speed of sound. In this article the SM is a non-isothermal model and the energy Equation (3) is solved together with Equations (7) and (8) to determine the temperature along the pipeline. The speed of sound is then determined at every point and is not assumed constant.

2.3 Full model

In the full model (FM) no terms are neglected when finding the partial differential equations for pressure, mass flow and temperature. The procedure can be found in the article by Chaczykowski [9]. The result is

$$\frac{\partial p}{\partial t} = \left[\frac{1}{T}+\frac{1}{Z}\left(\frac{\partial Z}{\partial T}\right)_p\right]\left[\frac{1}{p}-\frac{1}{Z}\left(\frac{\partial Z}{\partial p}\right)_T\right]^{-1}\frac{\partial T}{\partial t}-\frac{ZRT}{pA}\left[\frac{1}{p}-\frac{1}{Z}\left(\frac{\partial Z}{\partial p}\right)_T\right]^{-1}\frac{\partial \dot{m}}{\partial x} \tag{9}$$

$$\begin{aligned}\frac{\partial \dot{m}}{\partial t} &= \frac{\dot{m}ZRT}{pA}\left(-2\frac{\partial \dot{m}}{\partial x}+\dot{m}\left[\frac{1}{p}-\frac{1}{Z}\left(\frac{\partial Z}{\partial p}\right)_T\right]\frac{\partial p}{\partial x}-\dot{m}\left[\frac{1}{T}+\frac{1}{Z}\left(\frac{\partial Z}{\partial T}\right)_p\right]\frac{\partial T}{\partial x}\right)\\ &- A\frac{\partial p}{\partial x}-\frac{fZRT\dot{m}|\dot{m}|}{2DAp}-\frac{pA}{ZRT}g\sin\theta\end{aligned} \tag{10}$$

$$\begin{aligned}\frac{\partial T}{\partial t} &= -\frac{\dot{m}ZRT}{pA}\frac{\partial T}{\partial x}-\frac{\dot{m}(ZRT)^2}{pAc_v}T\left[\frac{1}{T}+\frac{1}{Z}\left(\frac{\partial Z}{\partial T}\right)_p\right]\\ &\times \left(\frac{1}{\dot{m}}\frac{\partial \dot{m}}{\partial x}-\left[\frac{1}{p}-\frac{1}{Z}\left(\frac{\partial Z}{\partial p}\right)_T\right]\frac{\partial p}{\partial x}+\left[\frac{1}{T}+\frac{1}{Z}\left(\frac{\partial Z}{\partial T}\right)_p\right]\frac{\partial T}{\partial x}\right)\\ &+ \frac{f}{2c_vD}\left(\frac{ZRT|\dot{m}|}{pA}\right)^3+\frac{q}{c_v}\end{aligned} \tag{11}$$

Equations (9-11) are almost identical to the ones in the article by Chaczykowski, the only difference is that the momentum equation is derived from the conservative form, while Chaczykowski derives it from the non-conservative substantial derivative form.

3 NUMERICAL METHODS

The governing equations form a system of initial valued partial differential equations which are of hyperbolic type and have to be solved numerically. Explicit and implicit finite difference methods will be investigated.

3.1 Explicit finite difference method

There are several different explicit methods which can be used for 1D unsteady flow. First order approximations are in general not sufficient when modeling transients in gas pipelines as these are unstable [1]. Higher order methods are therefore needed, e.g. the Lax-Wendroff or MacCormack scheme which are both 2nd order multistep methods. Poloni [3] used the two step differential Lax-Wendroff method, while Liang [10] used the TVD-MacCormack scheme to solve the 1D shallow water equations, but the method can be applied to 1D unsteady pipe flows. In this article the 3rd order TVD Runge-Kutta method by Gottlieb and Chu [11] was used for the time derivatives, while 2nd order centered differences were used for the spatial derivatives. For the SM in Section (2.2), Equations (7) and (8) can be written in the form

$$\frac{\partial \mathbf{q}}{\partial t}+\mathbf{A}\frac{\partial \mathbf{q}}{\partial x}=\mathbf{S} \tag{12}$$

where $\mathbf{q}=[p,\dot{m}]^T$, $\mathbf{A}$ is a 2x2 coefficient matrix and $\mathbf{S}$ the source term vector. The 3rd order TVD Runge-Kutta method advances the solution to time level $n+1$ by performing the steps

$$\begin{aligned}\mathbf{q}^{(1)} &= \mathbf{q}^n+\Delta t\mathbf{R}(\mathbf{q}^n)\\ \mathbf{q}^{(2)} &= \frac{3}{4}\mathbf{q}^n+\frac{1}{4}(\mathbf{q}^{(1)}+\Delta t\mathbf{R}(\mathbf{q}^{(1)}))\\ \mathbf{q}^{n+1} &= \frac{1}{3}\mathbf{q}^n+\frac{2}{3}(\mathbf{q}^{(2)}+\Delta t\mathbf{R}(\mathbf{q}^{(2)}))\end{aligned} \tag{13}$$

where $\mathbf{R}$ are the vectors of the right hand side of $(q_i)_t = -(q_i)_x + S_i$. The 2nd order centered difference scheme for spatial derivatives of a variable y discretized from x_1 to x_N is

$$\frac{\partial \mathbf{y}}{\partial x} = \begin{pmatrix} \frac{dy(x_1)}{dx} \\ \frac{dy(x_2)}{dx} \\ \vdots \\ \frac{dy(x_{N-1})}{dx} \\ \frac{dy(x_N)}{dx} \end{pmatrix} = \frac{1}{2\Delta x} \begin{pmatrix} -3 & 4 & -1 & 0 & \cdots & 0 \\ -1 & 0 & 1 & 0 & \cdots & 0 \\ \vdots & \ddots & \ddots & \ddots & \dots & \vdots \\ 0 & \cdots & 0 & -1 & 0 & 1 \\ 0 & \cdots & 0 & 1 & -4 & 3 \end{pmatrix} \begin{pmatrix} y(x_1) \\ y(x_2) \\ \vdots \\ y(x_{N-1}) \\ y(x_N) \end{pmatrix} + O(\Delta x^2) \tag{14}$$

One sided differences are used at the boundaries x_1 and x_N. The time step Δt in the explicit method is restricted by the stability condition of the 3rd order TVD Runge-Kutta method.

3.2 Fully implicit finite difference method

Fully implicit methods are unconditionally stable. Compared to explicit methods the time step is not restricted by the CFL condition. Both Kiuchi [4] and Abbaspour and Chapman [5] discretize the equations in a fully implicit way. The partial derivatives with respect to time are approximated by

$$\frac{\partial y}{\partial t} = \frac{y_{i+1}^{n+1} + y_i^{n+1} - y_{i+1}^n - y_i^n}{2\Delta t} \tag{15}$$

the partial derivatives in space are approximated by

$$\frac{\partial y}{\partial x} = \frac{y_{i+1}^{n+1} - y_i^{n+1}}{\Delta x} \tag{16}$$

and the individual terms by

$$y = \frac{y_{i+1}^{n+1} + y_i^{n+1}}{2} \tag{17}$$

where y represents p, T and $\dot{m}$. The method is claimed to be first order correct in space and second order correct in time [5]. For a pipe which is discretized by N nodes there will be 3N values of p, T and $\dot{m}$ and (3N-3) equations. A boundary value is assigned each variable, meaning there are (3N-3) unknowns at each time level n+1. Whether applied to the SM in Section (2.2) or the FM in Section (2.3) the governing equations for the fully implicit method form a system of non-linear equations. Kiuchi and Abbaspour and Chapman use the Newton-Raphson technique to solve the system of non-linear equations. In this article the fsolve function in MATLAB which uses the Trust-Region-Dogleg Algorithm was used.

3.3 Linear implicit finite difference model

While the explicit method in Section (3.1) is easy and efficient to solve, the time step is limited to small values by the stability condition. The fully implicit method in Section (3.2) is stable, but because the discretized equations form a system of non-linear equations the method is time consuming. It would be favorable to have a method which is both fast and stable. The solution is to linearize the non-linear terms in the fully implicit method about the previous time step and solve the linear system of equations. A variable y at time level n+1 can be written as a first order Taylor expansion

$$y_i^{n+1} = y_i^n + \Delta t (y_i^n)_t + O(\Delta t^2) \tag{18}$$

For the SM in Section (2.2) the only non-linear term is the friction term in the momentum equation. This term can according to Luskin [7] be (assuming $\dot{m} > 0$) written as

$$K\frac{(\dot{m}^{n+1})^2}{p^{n+1}} = K\frac{\dot{m}^n}{p^n}\left(\dot{m}^n + 2\Delta t \dot{m}_t\right) + O(\Delta t^2) \tag{19}$$

where $K = fc^2/2DA$. The pressure has been taken from the previous time step and the first order Taylor expansion has been used for the mass flow. Inserting Equations (15) and (17) for the spatial derivative and the individual terms in Equation (19), the friction term is developed into

$$K\frac{(\dot{m}^{n+1})^2}{p^{n+1}} \approx K\frac{(m_{i+1}^n + m_i^n)}{(p_{i+1}^n + p_i^n)}\left(m_{i+1}^{n+1} + m_i^{n+1} - \frac{m_{i+1}^n + m_i^n}{2}\right) \tag{20}$$

Using this result, Equations (7) and (8) now form a system of linear equations, which can be solved in an efficient way using simple linear algebra.

4 RESULTS

The presented numerical methods will be investigated for both the SM and FM. In Section(4.1) a 650 km pipe with constructed boundary conditions has been investigated. In Section(4.2) the FM has been validated using operational data from high pressure natural gas transmission pipelines.

4.1 Comparison of models and numerical methods

A 650 km pipeline transporting natural gas with a molecular weight of 18 was divided into 100 sections with a discretization length of 6.5 km. The diameter was 1 meter and the inclination angle was set to zero. The setup was similar to that of Chaczykowski [12]. The following boundary conditions were assigned.

$$\begin{aligned} p(0,t) &= 16MPa \\ T(0,t) &= 25°C \\ \dot{m}(L,t) &= f(t) \end{aligned} \tag{21}$$

$f(t)$ is shown in Figure 1.

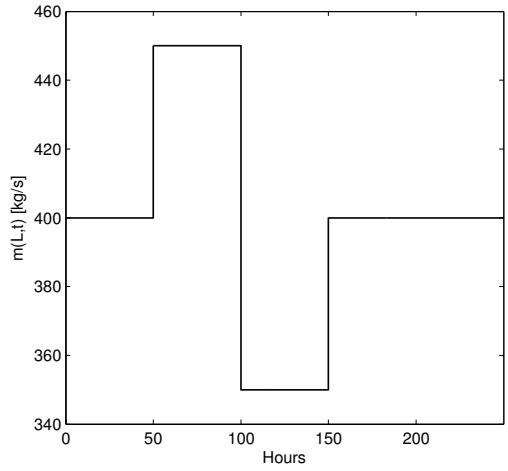

Figure 1: Boundary condition for the outlet mass flow.

The total heat transfer coefficient was set to 4 W/m^2K and the ambient temperature to 4 $°C$. The SM in Section (2.2) was solved by both the explicit, linearized implicit and the non-linear implicit method. Figure 2 shows the computed outlet pressure for the linearized and non-linear implicit methods. The two methods gave almost identical results, but the computational time was substantially less for the linearized method compared to the non-linear method. Comparison of computational times are given in Table 1. For the SM the linear implicit method was over 90 times faster than the non-linear implicit method. A close up view of the pressure drop during the transient is shown to the right in Figure 4. The difference between the two is less than 0.01 MPa and shows that the non-linear terms can be linearized about the previous time step without effecting the results in any major way.
An estimation of the local spatial discretization error for the pressure in the SM using the linear implicit finite difference method is given to the left in Figure 3. The numerical error has been plotted at two different times, t=100h

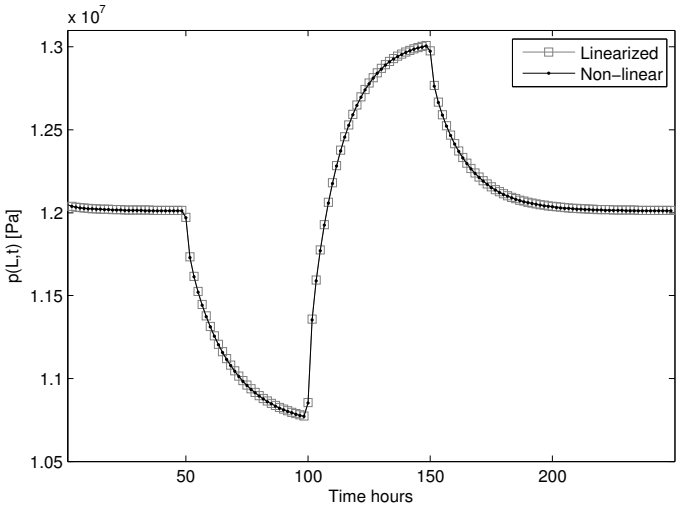

Figure 2: Outlet pressure for the SM using the linearized and non-linear implicit finite difference method. The two methods give almost identical results. The computational time is greatly reduced using the linear method.

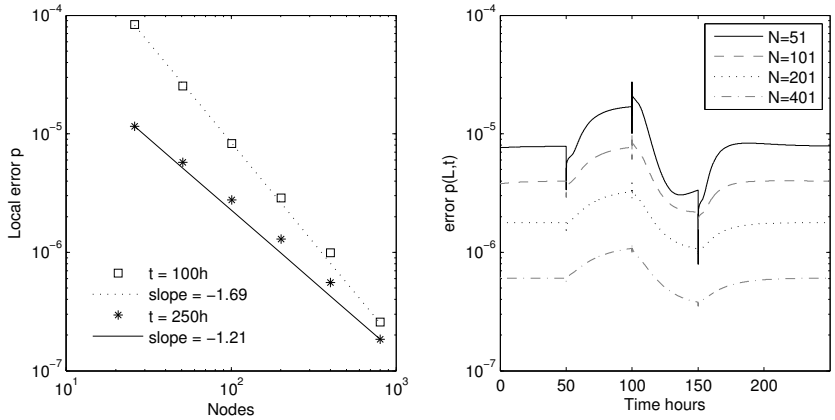

Figure 3: Left: Spatial discretization error scaling for pressure in the SM using the linearized implicit method. The error has been plotted at two different times, t = 100h when the conditions are transient and t = 250h when the conditions are steady state. The local error is higher during the transient. Right: Error in outlet pressure as a function of time for different number of grid points N. In both figures the error has been scaled with the outlet pressure for the finest grid.

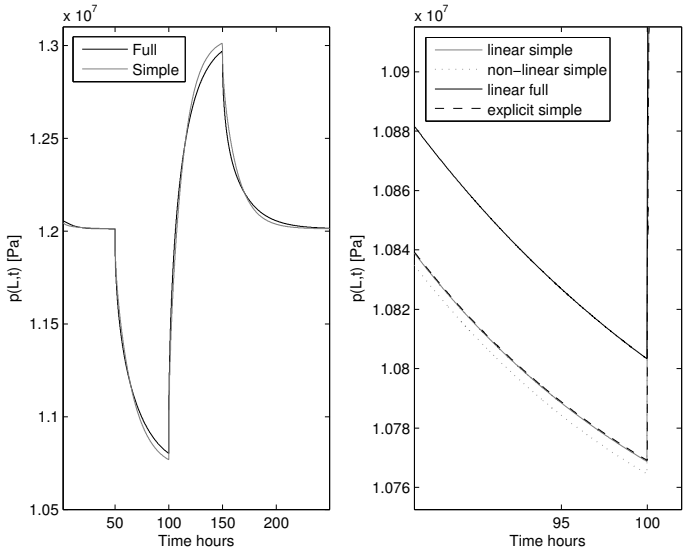

Figure 4: Left: Outlet pressure for the SM and FM using the linearized implicit finite difference method. Right: Close up view of outlet pressure during the transient.

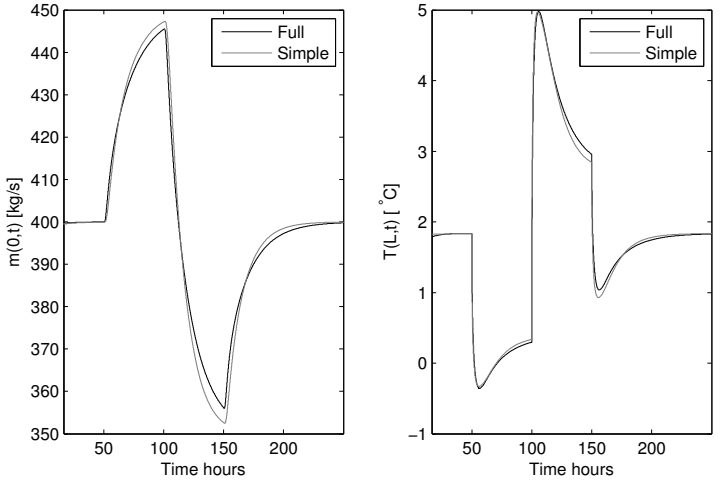

Figure 5: Comparison of the SM and FM using the linearized implicit finite difference method. Left: Inlet mass flow. Right: Outlet temperature.

during transient conditions and t=250h during steady state conditions. The error is larger when the conditions are transient. The spatial discretization error for the outlet pressure as a function of time for different grid sizes is shown to the right. The temporal discretization error was found to be of the same order of magnitude as the spatial. Similar estimates for the discretization errors were also found using the FM.
The difference between the SM and FM using the linear implicit method is shown to the left in Figure 4. During steady state the two models give almost identical results, while during the transient there is a noticeable difference in outlet pressure which at most is approximately 0.04 MPa. Figure 5 shows the inlet mass flow and outlet temperature for the SM and FM. The computational time for the FM was only a factor 1.1 larger than for the SM. To get as accurate results as possible the FM should be used instead of the SM.
Results for the SM using the explicit method is shown to the right in Figure 4. As expected it is similar to the linear and non-linear implicit method. The reason why it is slightly different compared to the non-linear implicit method is that the explicit method is third order correct in time and second order correct in space, while the non-linear method is second order correct in time and first order correct in space. Because the time step in the explicit method is restricted by the CFL condition, Δt in the explicit method was smaller than in the implicit methods. The computational time for each time step is shorter for the explicit method, but because the total number of time steps is larger for the explicit method compared to the implicit method the total computational time is shorter for the implicit method. This, combined with the fact that the implicit method is unconditionally stable makes the linear implicit finite difference method the preferred choice.

Table 1: Ratio of computational times for different methods in Section (4.1). The SM using the linear implicit finite difference method was used as the reference.

Method	**Time step Δ t**	**Ratio computational time**
Linearized implicit SM	60 s	1
Explicit SM	10 s	3.3
Linearized implicit FM	60 s	1.1
Non-linear implicit SM	60 s	92.1

4.2 Validation with operational data

The implicit methods were validated using operational data from high pressure natural gas pipelines. Data was taken from offshore pipelines in the North Sea transporting natural gas from Norway to continental Europe and the UK. Simulated results were compared to measured data for a 650 km pipeline with a diameter of approximately 1 meter. When modeling the flow of natural gas in offshore pipelines the gravity term in the momentum equation can not be neglected due to the height difference between the sea level and the sea bottom. Close attention needs to be paid to the discretization length. When the inclination angle is large the discretized length needs to be small, and when the inclination angle is small the length can be larger. This leads to problems with explicit methods, because the CFL condition depends on the discretization length Δx. When the inclination angle is large, the discretization length is so small that the CFL condition would require a very small time step Δt, which would be impractical. Therefore, implicit methods are used when simulating transportation of natural gas in offshore pipelines.
Inlet mass flow and temperature and outlet pressure were given as boundary conditions. Results were found using both the linearized and the non-linear implicit finite difference method. Figure 6 shows the results for inlet pressure and outlet mass flow and temperature. The difference between the linearized and the non-linear method is very small. The computational time for the non-linear method was over 100 times longer than for the linearized method. Inlet pressure and outlet mass flow agree well with measured data. There is a noticeable deviation in outlet temperature. This is most likely due to uncertainty in the total heat transfer coefficient U and the ambient sea bottom temperature T_a.

5 CONCLUSIONS

The objective of this article was to derive a fast and accurate method for unsteady 1D compressible flow of natural gas in long pipelines. Implicit finite difference methods should be used to ensure stability. The governing equations form a system of non-linear equations which have to be solved at each time step. Previous articles which have discretized the equations in a fully implicit way have used numerical techniques to solve the resulting system of non-linear equations. This is shown to be very time consuming and impractical for industrial applications. This

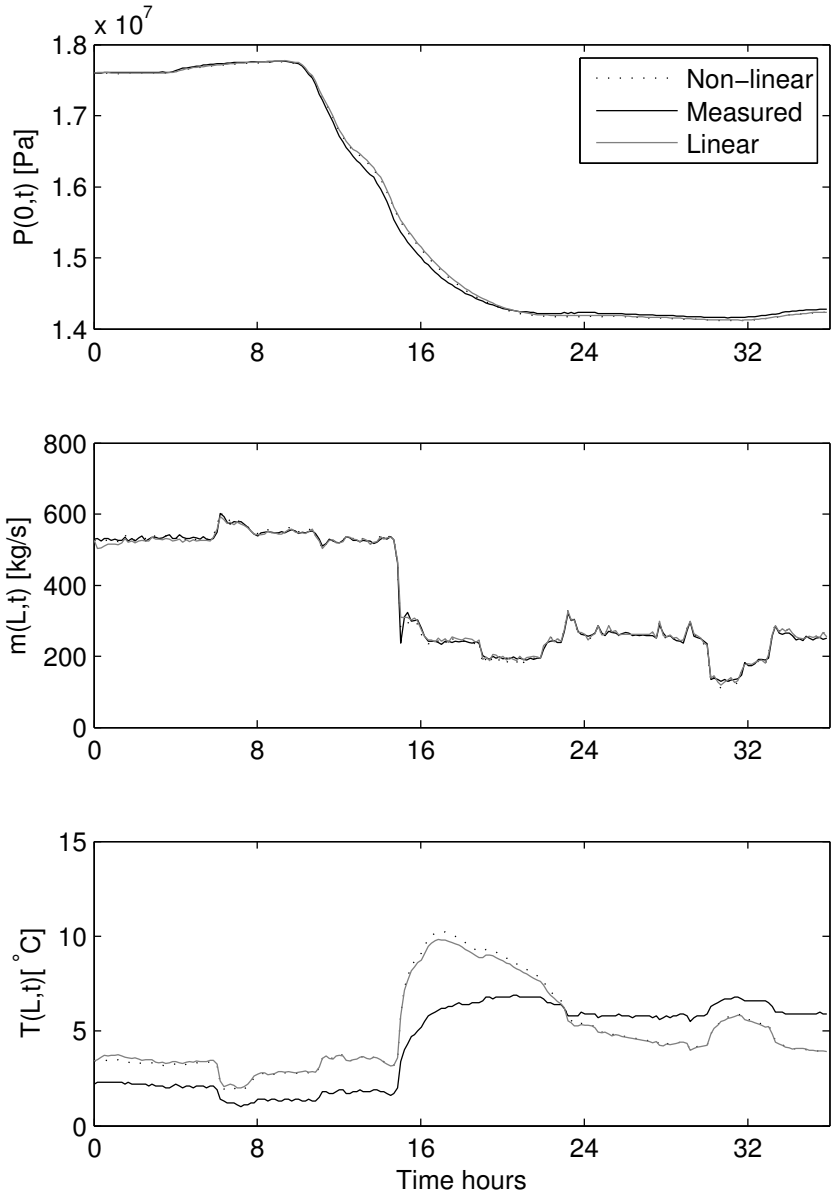

Figure 6: Simulated results validated against operational data for 650 km offshore pipeline using the linearized and non-linear implicit finite difference method. Top figure inlet pressure, middle outlet mass flow and bottom outlet temperature. The linearized method was approximately 100 times faster compared to the non-linear method.

article demonstrates how the governing equations can be linearized about the previous time step to get a linear system of equations. This greatly reduces the computation time for each time step. Results show that for large diameter high pressure transmission pipelines the linearized method gives almost the same result as the non-linear method. Validation against operational data from the industry confirm this. A linear implicit finite difference method should be used when simulating the flow of natural gas in long pipelines.

ACKNOWLEDGMENT

This work has been funded by the Norwegian gas operating company Gassco as part of a project to improve flow modeling of natural gas in offshore transmission pipelines.
The author would like to thank Professor Tor Ytrehus for his guidance and supervision.

REFERENCES

[1] Thorley, A.R.D.; Tiley, C.H.; Unsteady and transient flow of compressible fluids in pipelines - a review of theoretical and some experimental studies, *Heat and Fluid Flow* **8**(1):3-14, 1987.
[2] Wylie, E.B.; Stoner, M.A.; Streeter, V.L.; Unsteady-State Natural Gas Calculations in Complex Pipe Systems, *Society of Petroleum Engineering* **14**:35-43, 1974.
[3] Poloni, M.; Winterbone, D.E.; Nichols, J.R.; Comparison of Unsteady Flow Calculations in a pipe by the method of Characteristics and the two-step differential Lax-Wendroff method, *International Journal of Mechanical Sciences* **29**(5):367-378, 1987.
[4] Kiuchi, T.; An implicit method for transient gas flows in pipe networks, *International Journal of Heat and Fluid Flow* **15**(5):378-383, 1994.
[5] Abbaspour, M.; Chapman, K.S.; Nonisothermal Transient Flow in Natural Gas Pipeline, *Journal of Applied Mechanics* **75**(3):10-18, 2008.
[6] Osiadacz, A.J.; Chaczykowski, M.; Comparison of isothermal and non-isothermal pipeline gas flow models, *Chemical Engineering Journal* **81**:41-51, 2001.
[7] Luskin, M.; An Approximate Procedure for Nonsymmetric Nonlinear Hyperbolic Systems with Integral Boundary Conditions, *SIAM Journal on Numerical Analysis* **16**(1):145-164, 1979.
[8] Colebrook, C.F.; Turbulent flow in pipes, with particular reference to the transition region between the smooth and rough pipe laws, *J. Inst. Civil Eng.* **11**:133-156, 1939.
[9] Chaczykowski, M.; Transient flow in natural gas pipeline - The effect of pipeline thermal model, *Applied Mathematical Modelling* **34**:1051-1067, 2010.
[10] Liang, D.; Lin, B.; Falconer, R.A.; Simulation of rapidly varying flow using an efficient TVD-MacCormack scheme, *International Journal for Numerical Methods in Fluids* **53**:811-826, 2007.
[11] Gottlieb, S.; Shu, C-W.; Total variation diminishing Runge-Kutta schemes , *Mathematics of Computation* **67**:73-85, 1998.
[12] Chaczykowski, M.; Sensitivity of pipeline gas flow model to the selection of the equation of state, *Chemical Engineering Research and Design* **87**:1596-1603, 2009.

Article [b]

Coupling between Continuity/Momentum and Energy Equation in 1D Gas Flow

J.F. Helgaker and T. Ytrehus

Energy Procedia, Vol. 26, 2012, pages 82-89. In Proceedings of 2nd Trondheim Gas Technology Conference, Trondheim, 2011.

Available online at www.sciencedirect.com

SciVerse ScienceDirect

Energy Procedia 26 (2012) 82 – 89

Energy Procedia

2nd Trondheim Gas Technology Conference

Coupling between Continuity/Momentum and Energy Equation in 1D Gas Flow

Jan Fredrik Helgaker[a,b,*], Tor Ytrehus[b]

[a]Polytec R&D Institute, Sørhauggt 128, 5527 Haugesund, Norway
[b]Norwegian University of Science and Technology, Department of Energy and Process Engineering, Kolbjørn Hejes v 1B, 7491 Trondheim, Norway

Abstract

Transportation of natural gas through high pressure offshore transmission pipelines has been simulated by numerically solving the governing equations for one-dimensional compressible viscous heat conducting flow. For the implicit method the energy equation is solved one time step behind the continuity and momentum equation. Compared to solving all three equations simultaneously, this will decrease the computational time for each time step during the simulation. Under typical operating conditions for export pipelines in the North Sea this does not affect the results in any major way, indicating that the changes in temperature are sufficiently slow to allow the energy equation to be solved separately from the continuity and momentum equation.

Keywords: Natural gas pipelines, 1D unsteady flow, Simulations and models

1. Introduction

Natural gas is an important energy resource in Europe and the rest of the world. North Sea natural gas is transported from the continental shelf to processing terminals on the Norwegian mainland and then fed into long export pipelines to continental Europe and the UK. The offshore transportation system, which is operated by the Norwegian state owned company Gassco, consists of a network of 7800 km large diameter high pressure pipelines. An overview of the gas transport system is given in Fig.1. Measurements of the state of the gas, such as pressure, flow rate, composition and temperature are done only at the inlet and outlet of the pipelines. To know the state of the gas between these two points one has to rely on computer models. These models are used to monitor the gas, predicting the pipeline hydraulic capacity and providing estimated time of arrival for unwanted quality disturbances and pigs. Gassco uses one-dimensional simulator tools to model the flow of natural gas in their network. It is crucial that these models are as accurate as possible, but at the same time they are required to calculate the updated flow conditions in a fast and efficient way. Conditions in the pipelines are usually transient due to varying demands in supply or sudden shut down or failure of the operating system.

*Corresponding author. E-mail address: jan.fredrik.helgaker@polytec.no

1876-6102 © 2012 Published by Elsevier Ltd. Selection and/or peer-review under responsibility of the organizing committee of 2nd Trondheim Gas Technology Conference.
doi:10.1016/j.egypro.2012.06.013

Fig. 1. Overview of the Norwegian natural gas transport system in the North Sea which Gassco operates. Figure courtesy of Gassco.

Simulation of gas transmission involves the numerical solution of a system of initial valued partial differential equations for mass, momentum and energy conservation which are of a hyperbolic type. The governing equations and different numerical solution techniques can be found in base literature articles, for instance by Thorley and Tiley [1]. Different numerical techniques include the method of characteristics, finite difference and finite volume methods. Poloni et al. [2] compare the method of characteristics and the explicit finite difference method for unsteady pipe flow. An explicit finite difference method is fast and easy to implement, but the time step is restricted by the stability criterion. The implicit finite difference method is unconditionally stable with respect to the choice of time step and is therefore often used in one-dimensional unsteady flow simulation tools.

If the changes in temperature along the pipeline are small, an isothermal model can be applied. Only the continuity and momentum equations have to be solved for the flow. An isothermal model for transient flow using an implicit finite difference method is given in the paper by Kiuchi [3]. However, for large pipelines operating at high pressures the gas entering the pipeline usually has a temperature which is higher than the ambient temperature. Heat exchange with the surroundings and cooling due to expansion (Joule Thomson effect) will contribute to a significant temperature drop along the pipeline. One therefore has to, as shown by Osiadacz [4], solve the non-isothermal model. This was done, for instance by Abbaspour and Chapman [5] and Chacykowski [6]. In both these articles an implicit finite difference method is used to solve the continuity, momentum and energy equations for the flow. In the first case the Newton-Raphson technique is used to solve the resulting system of non-linear equations, while in the latter case the implicit multistep Gear's method was used.

Solving the implicit non-linear system of equations using the Newton-Raphson technique is very time consuming and becomes impractical when working with large pipeline networks. The CPU time can be greatly reduced by linearizing the non-linear terms about the previous time step and solving the implicit linear system of equations. The procedure is given in the article by Luskin [7]. Commercial software may

also solve the energy equation separately from the continuity and momentum equation in order to reduce the CPU time further. This decoupling of the energy and momentum budget makes the resulting system of equations easier to solve and reduces the CPU time for each time step. However, since the flow is considered compressible and viscous, decoupling the energy equation from the continuity and momentum equations will introduce an error in the solution, as the temperature is a function of pressure and density. In Gasscos case, even though one models also flows with large transients, the change in temperature in space and time is assumed to be sufficiently slow so that decoupling the energy equation from the continuity and momentum equations will not introduce a significant error. This will be investigated in the following. This article will present a transient model for one-dimensional pipeline flow, and two options for solution strategy will be considered; fully coupled or one-way coupled momentum-energy budget.

2. Governing equations

The governing equations describing one-dimensional compressible viscous heat conducting flow are

Continuity

$$\frac{\partial \rho}{\partial t} + \frac{\partial (\rho u)}{\partial x} = 0 \tag{1}$$

Momentum

$$\frac{\partial (\rho u)}{\partial t} + \frac{\partial (\rho u^2 + p)}{\partial x} = -\frac{f \rho u^2}{2D} - \rho g \sin\theta \tag{2}$$

Energy

$$\rho c_v \left(\frac{\partial T}{\partial t} + u \frac{\partial T}{\partial x} \right) + T \left(\frac{\partial p}{\partial T} \right)_\rho \frac{\partial u}{\partial x} = \frac{f \rho u^3}{2D} - \frac{4U}{D}(T - T_a) \tag{3}$$

The continuity and momentum equation are expressed in conservative form while the energy equation is in the non-conservative internal energy form. The density ρ can be exchanged for the pressure p by using a real gas equation of state

$$\frac{p}{\rho} = ZRT \tag{4}$$

where $Z = Z(p, T)$ is the compressibility factor. There exist several different types of equations of state. The sensitivity of the pipeline gas flow model to the selection of the equation of state was investigated by Chaczykowski [8]. In the following the Soave Redlich Kwong (SRK) [9] equation of state has been used to determine the Z factor. The Colebrook-White correlation [10] was used to determine the friction factor f

$$\frac{1}{\sqrt{f}} = -2 \log \left(\frac{\epsilon}{3.7D} + \frac{2.51}{Re\sqrt{f}} \right) \tag{5}$$

where ϵ is the surface roughness and Re the Reynolds number of the flow. The last term in the energy equation accounts for heat transfer between the gas and the medium surrounding the pipeline, where T_a is the ambient temperature and U the total heat transfer coefficient. By trading the density for the pressure and introducing the mass flow rate $\dot{m} = \rho u A$ (A being the constant pipeline cross-section) the governing equations become

$$\frac{\partial p}{\partial t} = \left[\frac{1}{T} + \frac{1}{Z} \left(\frac{\partial Z}{\partial T} \right)_p \right] \left[\frac{1}{p} - \frac{1}{Z} \left(\frac{\partial Z}{\partial p} \right)_T \right]^{-1} \frac{\partial T}{\partial t} - \frac{ZRT}{pA} \left[\frac{1}{p} - \frac{1}{Z} \left(\frac{\partial Z}{\partial p} \right)_T \right]^{-1} \frac{\partial \dot{m}}{\partial x} \tag{6}$$

$$\begin{aligned} \frac{\partial \dot{m}}{\partial t} = {} & \frac{\dot{m} ZRT}{pA} \left(-2 \frac{\partial \dot{m}}{\partial x} + \dot{m} \left[\frac{1}{p} - \frac{1}{Z} \left(\frac{\partial Z}{\partial p} \right)_T \right] \frac{\partial p}{\partial x} - \dot{m} \left[\frac{1}{T} + \frac{1}{Z} \left(\frac{\partial Z}{\partial T} \right)_p \right] \frac{\partial T}{\partial x} \right) \\ & - A \frac{\partial p}{\partial x} - \frac{f ZRT \dot{m} |\dot{m}|}{2DAp} - \frac{pA}{ZRT} g \sin\theta \end{aligned} \tag{7}$$

$$\begin{aligned}\frac{\partial T}{\partial t} &= -\frac{\dot{m}ZRT}{pA}\frac{\partial T}{\partial x} - \frac{\dot{m}(ZRT)^2}{pAc_v}T\left[\frac{1}{T}+\frac{1}{Z}\left(\frac{\partial Z}{\partial T}\right)_p\right] \\ &\times \left(\frac{1}{\dot{m}}\frac{\partial \dot{m}}{\partial x} - \left[\frac{1}{p}-\frac{1}{Z}\left(\frac{\partial Z}{\partial p}\right)_T\right]\frac{\partial p}{\partial x} + \left[\frac{1}{T}+\frac{1}{Z}\left(\frac{\partial Z}{\partial T}\right)_p\right]\frac{\partial T}{\partial x}\right) \\ &+ \frac{f}{2c_vD}\left(\frac{ZRT|\dot{m}|}{pA}\right)^3 - 4U\frac{ZRT}{pc_vD}(T-T_a) \end{aligned} \tag{8}$$

The procedure for deriving Eqs.6-8 is given in the article by Chaczykowski [6]. In this work the momentum equation (Eq.7) is derived from the conservative form (Eq.2), instead of the non-conservative substantial derivative form as used by Chaczykowski.

3. Numerical formulation

Equations 6 - 8 have to be solved numerically. If all terms are discretized in a fully implicit way, one has to simultaneously solve a system of non-linear equations. Abbaspour and Chapman [5] do this by using the Newton-Raphson technique, but this is very time consuming and impractical. The non-linear terms can be linearized about the previous time step as in the article by Luskin [7]. This gives an implicit linear system of equations which can be efficiently solved at each time step. After the equations are linearized they are discretized in time and space. The pipeline is divided into N sections and N+1 grid points. Section j is the section between point i and $i+1$. The flow variables are calculated at the grid points. The partial derivatives with respect to time at section j are approximated by

$$\frac{\partial Y}{\partial t} = \frac{Y_{i+1}^{n+1} + Y_i^{n+1} - Y_{i+1}^n - Y_i^n}{2\Delta t} \tag{9}$$

the partial derivatives with respect to x by

$$\frac{\partial Y}{\partial x} = \frac{Y_{i+1}^{n+1} - Y_i^{n+1}}{\Delta x} \tag{10}$$

and individual terms by

$$Y = \frac{Y_{i+1}^{n+1} + Y_i^{n+1}}{2} \tag{11}$$

where Y represents $\dot{m}$, p and T. This corresponds to the discretization used by Abbaspour and Chapman, which is second order correct in time and first order correct in space. Boundary values need to be assigned to each variable which is being computed. The mass flow and temperature were given at the inlet, while the pressure was given at the outlet. Two solution strategies will be considered, a fully coupled momentum-energy budget where Eqs.6-8 are solved simultaneously at each step, or a one-way coupled momentum-energy budget where the continuity and momentum equations are solved together using the temperature from the previous time step, before the energy equation is solved for the new temperature using the updated values for the pressure and mass flow.

4. Results

Two different setups will be considered. In Section 4.1 a simple test case with given boundary conditions is investigated. In Section 4.2 the model and solution strategies will be validated using operational data from an offshore transmission pipeline operated by Gassco.

4.1. Test case

A 650 km horizontal pipeline with diameter 1 meter was used as a test case for the two solution strategies. The outlet pressure and inlet temperature were kept constant at $10\ MPa$ and $25\ ^{\circ}C$ respectively. The inlet mass flow varied as in Fig.2. The ambient temperature was kept constant at $5\ ^{\circ}C$ and the heat transfer coefficient was set to $16\ W/(m^2K)$. The gas had a molecular weight of 17.95. The pipeline was divided into 101 grid points. A grid refinement confirmed this to be sufficient. In Fig.3 the local error scaling for pressure, mass flow and temperature as a function of grid points N is given. The time step Δt in the calculations was set to 60 seconds. The difference between the two solution strategies for the calculated inlet pressure, outlet mass flow and outlet temperature is very small and not visible in Fig.4. The difference can be seen in Fig.5-6 where the scaled inlet pressure and outlet mass flow found using the two different strategies are shown. The computational time was reduced by approximately 20% by solving the energy equation separately from the continuity and momentum equations.

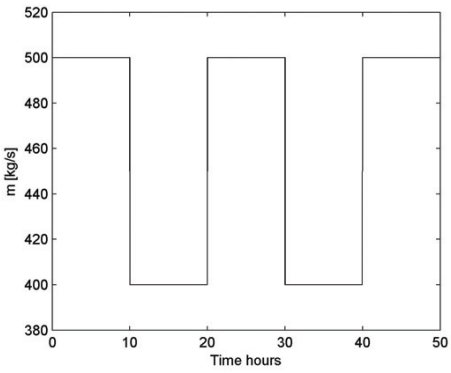

Fig. 2. Boundary condition for inlet mass flow used in the test case.

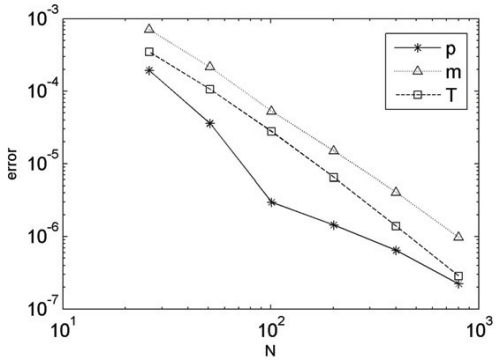

Fig. 3. Local error scaling for pressure, mass flow and temperature as a function of grid points N.

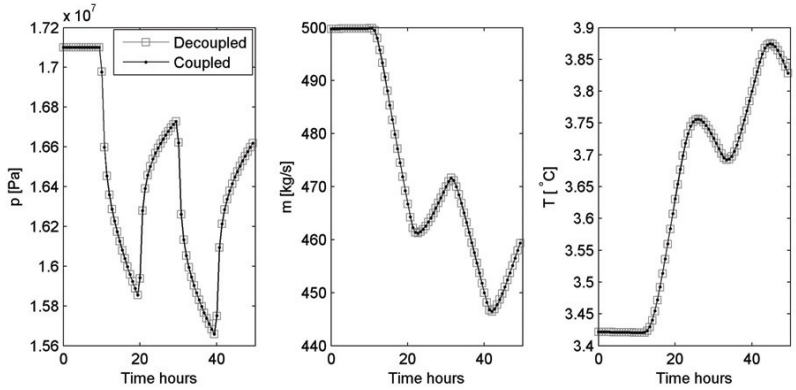

Fig. 4. Results for test case. Inlet pressure left, outlet mass flow middle and outlet temperature right. The difference between the two solution strategies is very small and not visible in the figure. The computational time was reduced by solving the energy equation separately from the continuity and momentum equations.

4.2. Model validation

The model was validated using operational data from a 650 km offshore pipeline operated by Gassco. The pipeline was divided into 98 grid points were values for $\dot{m}$, p and T were stored. The length of each

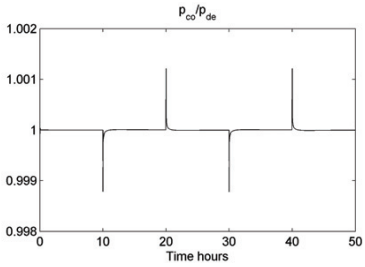

Fig. 5. Ratio of inlet pressure for the coupled and decoupled solution. There is a difference of 0.1% during transient conditions, while the difference in steady state is negligible.

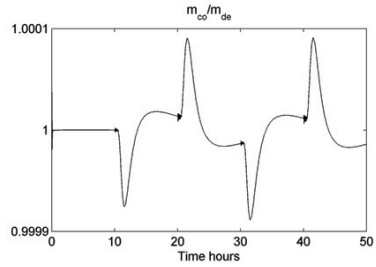

Fig. 6. Ratio of outlet mass flow for the coupled and decoupled solution. The ratio for the mass flow was found to be much less than for the pressure.

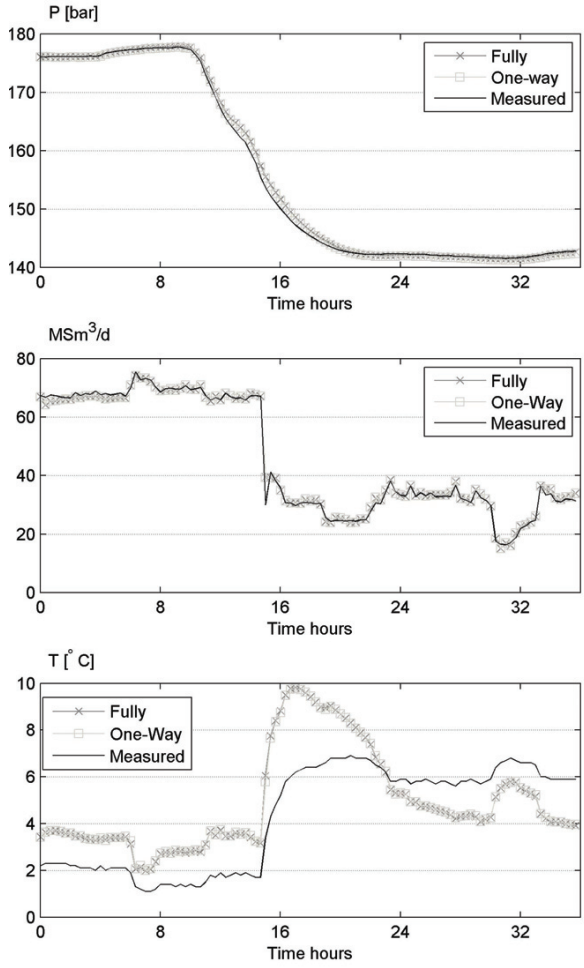

Fig. 7. Simulated results validated against operational data for 650 km pipeline. Top figure shows inlet pressure, middle outlet mass flow and bottom outlet temperature. Difference between fully coupled and one-way coupled solution is very small.

section varied, depending on the inclination angle θ. Steep inclination means short grid spacing, while little or no inclination leads to larger grid spacing. The results for both solution strategies are shown in Fig.7. The difference between them is very small and almost not visible. The modeled inlet pressure and outlet mass flow agree well with measured values. There is however a noticeable difference between modeled and measured outlet temperature. Two of the most important parameters in the model are the total heat transfer coefficient U and the ambient temperature T_a. Since the pipeline is an offshore pipeline one has to rely on oceanographic data for predicting the sea bottom temperature. In the model presented here there is some uncertainty in these parameters. To accurately predict the gas temperature one needs more accurate values for the heat transfer coefficient and the sea bottom temperature in the North Sea. Even if the modeled temperature can be improved by reducing the uncertainty in U and T_a, it is not likely that this would lead to any major differences between the two solution strategies presented here.

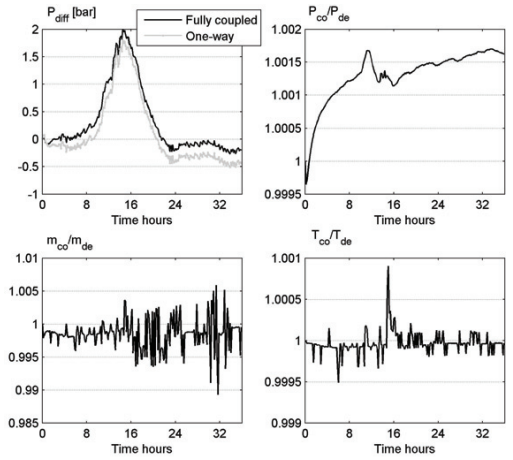

Fig. 8. Comparison of two different solution strategies. Top left shows difference between modeled and measured inlet pressure for the fully coupled and one way coupled momentum energy budget. Top right ratio of inlet pressure for the coupled and decoupled solutions. Bottom left the ratio of outlet mass transfer for the two strategies, bottom right the ratio of outlet temperature.

In Fig.8 the ratio between the fully coupled solution and the one-way coupled solution is shown for pressure (top right), mass flow (bottom left) and temperature (bottom right). There is approximately a 0.15% difference in pressure, $\pm$0.5% in mass flow and an even smaller difference in temperature. The difference between modeled and measured pressure at the outlet is shown in the top left corner of Fig.8. The difference between the two solution strategies is at most 0.5 bar. The computational time is reduced by solving the one-way momentum-energy budget compared to the fully coupled momentum-energy budget. When solving the system of linear equations at each time step the inverse of a square matrix has to be computed. For a pipeline consisting of $N + 1$ grid points the fully coupled momentum-energy budget requires finding the inverse of a $3N \times 3N$ non tridiagonal matrix. For the one-way momentum-energy budget the problem is reduced to finding the inverse of a $2N \times 2N$ and a $N \times N$ non tridiagonal matrix at each time step. This decreases the computational time for each time step.

5. Conclusions

Transportation of natural gas in high pressure transmission pipelines has been modeled using a 1D implicit finite difference method. The non-linear terms are linearized about the previous time step to give a linear model. For long pipelines operating at high pressures one has to solve the non-isothermal model, which means solving the three governing equations, continuity, momentum and energy at each point during each time step. The three governing equations are coupled and have in general to be solved simultaneously.

However, in long pipelines operating at high pressure the temperature changes in space and time are assumed to be sufficiently small so that the energy equation can be solved separately one time step behind the continuity and momentum equations. For typical long subsea export lines, it has been shown that solving the energy equation one time step behind the continuity and momentum equations does not change the results in any significant way. This has been demonstrated to reduce the computational time for each time step, and it may be implemented into commercial tools for modeling gas flow in large and complicated networks. For practical purposes a one-way coupled momentum-energy budget therefore gives just as good results as a fully coupled momentum-energy budget and reduces the computational time for simulating flow of natural gas in high pressure transmission pipelines.

6. Acknowledgment

This work has been funded by Gassco as part of a project to improve flow modeling of natural gas in high pressure offshore transmission pipelines. The authors would like to thank Sigmund Mongstad Hope (Polytec), Willy Postvoll and Leif Idar Langelandsvik (both Gassco) for their discussion and feedback.

Appendix A. Nomenclature

A - pipeline cross-section area $[m^2]$

c_v - heat capacity $[J/(kgK)]$

D - pipeline diameter $[m]$

f - friction factor

g - gravitational constant $[m/s^2]$

$\dot{m}$ - mass flow $[kg/s]$

p - pressure $[kg/(ms^2)]$

R - specific gas constant $[J/(kgK)]$

Re - Reynolds number

T - temperature $[K]$

T_a - ambient temperature $[K]$

t - time $[s]$

U - heat transfer coefficient $[W/(m^2K)]$

u - gas velocity $[m/s]$

x - spatial coordinate $[m]$

Z - compressibility factor

ϵ - pipe surface roughness $[m]$

ρ - density of the gas $[kg/m^3]$

θ - pipe inclination angle

References

[1] A. R. D. Thorley, C. H. Tiley, Unsteady and transient flow of compressible fluids in pipelines - a review of theoretical and some experimental studies, Heat and Fluid Flow 8 (1) (1987) 3–14.
[2] M. Poloni, D.E. Winterbone, J.R. Nichols, Comparison of Unsteady Flow Calculations in a Pipe by The Method of Characteristics and The Two-Step Differential Lax-Wendroff Method, International Journal of Mechanical Sciences 29 (5) (1987) 367–378.
[3] Tatsuhiko Kiuchi, An implicit method for transient gas flows in pipe networks, International Journal of Heat and Fluid Flow 15 (5) (1994) 378–383.
[4] A.J. Osiadacz, M. Chaczykowski, Comparison of isothermal and non-isothermal pipeline gas flow models, Chemical Engineering Journal 81 (2001) 41–51.
[5] M. Abbaspour, K.S. Chapman, Nonisothermal Transient Flow in Natural Gas Pipeline, Journal of Applied Mechanics 75 (2008) 031018–1–8.
[6] M. Chaczykowski, Transient flow in natural gas pipeline - The effect of pipeline thermal model, Applied Mathematical Modelling 34 (2009) 1051–1067.
[7] M. Luskin, An Approximation Procedure for Nonsymmetric Nonlinear Hyperbolic Systems with Integral Boundary Conditions, SIAM Journal on Numerical Analysis 16 (1) (1979) 145–164.
[8] M. Chaczykowski, Sensitivity of pipeline gas flow model to the selection of the equation of state, Chemical Engineering Research and Design 87 (2009) 1596–1603.
[9] G. Soave, Equilibrium constants from a modified Redlich-Kwong equation of state, Chemical Engineering Science 27 (1972) 1197–1203.
[10] C.F. Colebrook, Turbulent flow in pipes, with particular reference to the transition region between the smooth and rough pipe laws, J. Inst. Civil Eng 11 (1939) 133–156.

Article [c]

Energy Dissipation Effect in the One-Dimensional Limit of the Energy Equation in Turbulent Compressible Flow

T. Ytrehus and J.F. Helgaker

Journal of Fluids Engineering - Transactions of The ASME, Vol. 135(6), 2013.
doi:10.1115/1.4023656.

Is not included due to copyright

Article [d]

Transmission of Natural Gas through Offshore Pipelines - Effect of unsteady heat transfer model

J.F. Helgaker, A. Oosterkamp and T. Ytrehus

In B. Skallerud and H. Andersson, editors, MekIT'13: Seventh national conference on Computational Mechanics, pages 113-131, Akademika Publishing 2013.

Comment: Results in Figure 11 differ slightly from those in Figure 4.18 in the thesis (which is the same flow setup). Results in Figure 4.18 in the thesis agree better with measured values. The reason for this is that the composition used in Figure 11 was not correct. This was corrected for in the thesis. For results in Figure 11 an incorrect composition will not effect the difference between the two heat transfer models presented. Conclusions in the article are therefore the same.

Transmission of Natural Gas through Offshore Pipelines - Effect of unsteady heat transfer model

Jan Fredrik Helgaker[*1,2], **Antonie Oosterkamp**[1,2] **and Tor Ytrehus**[2]
[1]Polytec Research Institute, Haugesund, Norway

[2]Department of Energy and Process Engineering
The Norwegian University of Science and Technology, Trondheim, Norway
[*]e–mail: jan.fredrik.helgaker@ntnu.no

Summary Transportation of natural gas through large diameter high pressure pipelines is modeled by numerically solving the governing equations for one-dimensional compressible viscous heat conducting flow. The heat exchange between the gas and the pipeline surroundings is modeled using two different approaches. In the first case a steady state heat transfer model is investigated. This is compared to an unsteady heat transfer model which accounts for heat accumulation in the ground. Comparison of the two models show that the steady state heat transfer model over predicts the amplitude of temperature changes in the flow. Also, during large transients, a significant difference in modeled pressure and mass flow rate is observed between the two models. The models are validated using operational data from an offshore natural gas pipeline.

Introduction

Gassco is a state owned Norwegian company responsible for the operation of a network consisting of 8000 km of high pressure large diameter natural gas pipelines on the sea bed across the North Sea. Natural gas is transported from the continental shelf to processing terminals on the Norwegian mainland. After the gas has been processed and unwanted components are removed, it is fed into long export pipelines and transported to continental Europe and the UK. These pipelines on the seabed can be up to 1000 km in length. The state of the gas is only known at the inlet and outlet. Between these points one has to rely on computer models to predict the flow conditions in the pipeline. An overview of the North Sea natural gas transport system which Gassco operates is shown in Fig.1.

Gassco uses one-dimensional compressible flow models to simulate the flow of natural gas through their pipelines. These have several important applications which include designing, monitoring and operating natural gas pipelines. They are also used to predict the pipeline hydraulic capacity and are an important part of pipeline leak detection systems. Modeling the transmission of natural gas through high pressure pipelines involves finding the numerical solution to a system of initial valued partial differential equations representing continuity, momentum and energy conservation. These equations form a system of hyperbolic partial differential equations.

An overview of different numerical techniques commonly used to solve such a system of equations can be found in the base literature article by Thorley and Tiley [14]. These include the method of characteristics, finite difference, finite volume and finite element methods. Finite difference methods are the most commonly used methods to model unsteady flow in high pressure pipelines. Explicit finite difference methods are easy to implement, but allow only for small time steps due to the CFL stability criteria. Implicit finite difference methods are unconditionally stable and allow for large time steps. These are therefore often used in commercial tools. Implicit finite difference methods were used by Kiuchi [13], Abbaspour and Chapman [7] and Chaczykowski [9]. Kiuchi solves the isothermal model, which means solving the continuity and momentum equation to find the pressure and mass flow rate in the pipeline. For short

pipelines operating at low pressures it is admissible to assume an isothermal model. However, for large pipelines operating at high pressures one has to, as shown by Osiadacz [2], solve the non-isothermal model.

Figure 1: Overview of the Norwegian natural gas transport system in the North Sea which Gassco operates. Figure courtesy of Gassco.

Modeling the correct temperature in long subsea natural gas pipelines is of great importance when predicting the pipeline hydraulic capacity [5]. Calculating the correct temperature is quite complex as there are several different terms in the energy equation which have to be modeled in approximate ways. These include the change in internal energy, Joule-Thomson effect, dissipation term and the heat exchange with the surroundings. The temperature in the pipeline depends on several thermodynamic properties which are often calculated from a real gas equation of state. The sensitivity of the pipeline gas flow model to the selection of the equation of state was investigated by Chaczykowski [8]. Modeling the heat transfer between the gas and the pipeline surroundings for offshore pipelines has typically been done by using a total heat transfer coefficient [6]. The heat transfer coefficient is found from a combination of three steps and consists of heat transfer between the gas and the inner pipeline wall, transfer through the pipe wall and transfer between the surrounding and the outer pipe wall. This is a steady state process and does not allow for heat accumulation in the ground surrounding the pipeline. In the article by Chaczykowski [9] the effect of an unsteady heat transfer model, where heat accumulation in the ground is taken into account, is investigated. This model was compared to a traditional steady state heat transfer model. It was found that a steady state heat transfer model overestimates the amplitude of the temperature changes in transient flow. The unsteady heat transfer model was only investigated for on-shore pipelines buried under the ground. Also, the inlet pressure of the pipeline considered was 8.4 MPa, which is a lot lower compared to those operated by Gassco, which can have an inlet pressure of up to 20 MPa.

The purpose of this work is to investigate the effect of the unsteady heat transfer model as suggested by Chaczykowski [9] for an offshore natural gas pipeline operating at high pressure. This model will be compared to the steady state heat transfer model which has typically been

used for offshore pipelines. As the unsteady model is one-dimensional, the computed heat flux will be compared to that of a two-dimensional heat transfer model in order to verify the one-dimensional approximation. The models will be validated using operational data from one of Gasscos offshore natural gas pipelines.

Theory

Governing Equations

The governing equations for one-dimensional compressible viscous heat conducting flow are found by averaging the three dimensional versions over the pipe cross-section. The result is:

Continuity

$$\frac{\partial \rho}{\partial t} + \frac{\partial (\rho u)}{\partial x} = 0 \tag{1}$$

Momentum

$$\frac{\partial (\rho u)}{\partial t} + \frac{\partial (\rho u^2 + p)}{\partial x} = -\frac{f \rho u |u|}{2D} - \rho g \sin\theta \tag{2}$$

Energy

$$\rho c_v \left(\frac{\partial T}{\partial t} + u \frac{\partial T}{\partial x} \right) + T \left(\frac{\partial p}{\partial T} \right)_\rho \frac{\partial u}{\partial x} = \frac{f \rho u^3}{2D} - \frac{4U}{D}(T - T_a) \tag{3}$$

The continuity and momentum equations are expressed in the conservative form, while the energy equation is in the non-conservative internal energy form. In the energy equation the second term on the left hand side represents the Joule Thomson effect, which is cooling upon expansion. On the right hand side the first term is the dissipation term, which is the breakdown of mechanical energy to thermal energy. The last term is the heat exchange between the gas and the pipeline surroundings where the total heat transfer coefficient U has the usual definition

$$U = \frac{Q}{A(T - T_a)} \tag{4}$$

where Q is the heat flow, A the pipeline cross-section and T_a the ambient temperature. The density can be related to the pressure through a real gas equation of state

$$\frac{p}{\rho} = ZRT \tag{5}$$

where $Z = Z(p, T)$ is the compressibility factor. In this work the BWRS (Benedict-Webb-Rubin-Starling) [12] equation of state was used to determine the compressibility factor Z. The friction factor f can be determined from the Colebrook-White correlation [3]

$$\frac{1}{\sqrt{f}} = -2 \log \left(\frac{\epsilon}{3.7D} + \frac{2.51}{Re\sqrt{f}} \right) \tag{6}$$

where ϵ is the equivalent sand grain roughness, D the pipe inner wall diameter and Re the Reynolds number of the flow. Introducing the mass flow rate $\dot{m} = \rho u A$ and replacing the density ρ with the pressure p in Equations (1) - (3) the partial differential equations for p, $\dot{m}$ and T are developed into

$$\frac{\partial p}{\partial t} = \left[\frac{1}{p} - \frac{1}{Z} \left(\frac{\partial Z}{\partial p} \right)_T \right]^{-1} \left(\left[\frac{1}{T} + \frac{1}{Z} \left(\frac{\partial Z}{\partial T} \right)_p \right] \frac{\partial T}{\partial t} - \frac{ZRT}{pA} \frac{\partial \dot{m}}{\partial x} \right) \tag{7}$$

$$\begin{aligned}\frac{\partial \dot{m}}{\partial t} &= \frac{\dot{m}ZRT}{pA}\left(-2\frac{\partial \dot{m}}{\partial x}+\dot{m}\left[\frac{1}{p}-\frac{1}{Z}\left(\frac{\partial Z}{\partial p}\right)_T\right]\frac{\partial p}{\partial x}-\dot{m}\left[\frac{1}{T}+\frac{1}{Z}\left(\frac{\partial Z}{\partial T}\right)_p\right]\frac{\partial T}{\partial x}\right)\\ &- A\frac{\partial p}{\partial x}-\frac{fZRT\dot{m}|\dot{m}|}{2DAp}-\frac{pA}{ZRT}g\sin\theta \end{aligned} \tag{8}$$

$$\begin{aligned}\frac{\partial T}{\partial t} &= -\frac{\dot{m}ZRT}{pA}\frac{\partial T}{\partial x}-\frac{\dot{m}(ZRT)^2}{pAc_v}T\left[\frac{1}{T}+\frac{1}{Z}\left(\frac{\partial Z}{\partial T}\right)_\rho\right]\\ &\times \left(\frac{1}{\dot{m}}\frac{\partial \dot{m}}{\partial x}-\left[\frac{1}{p}-\frac{1}{Z}\left(\frac{\partial Z}{\partial p}\right)_T\right]\frac{\partial p}{\partial x}+\left[\frac{1}{T}+\frac{1}{Z}\left(\frac{\partial Z}{\partial T}\right)_p\right]\frac{\partial T}{\partial x}\right)\\ &+ \frac{f}{2c_vD}\left(\frac{ZRT|\dot{m}|}{pA}\right)^3-\frac{ZRT}{pc_v}\frac{4U}{D}(T-T_a)\end{aligned} \tag{9}$$

The procedure of deriving Equations (7)-(9) can be found in the article by Chaczykowski [9]. In the natural gas industry, measured quantities at the pipe inlet and outlet are often pressure p and mass flow rate $\dot{m}$. The rewrite of Equations (7)-(9) is beneficial as the measured flow values at the boundaries can be incorporated directly into the model, opposed to Equations (1)-(3) which require density ρ and velocity u as measured values at the boundaries.

Steady state heat transfer model

Gassco currently uses a steady state heat transfer model to predict the heat exchange between the gas and the pipeline surroundings [5]. For a buried pipeline, like that in Fig.2, the heat exchange between the gas and the pipeline surroundings is a combined mode of three different heat transfer processes.

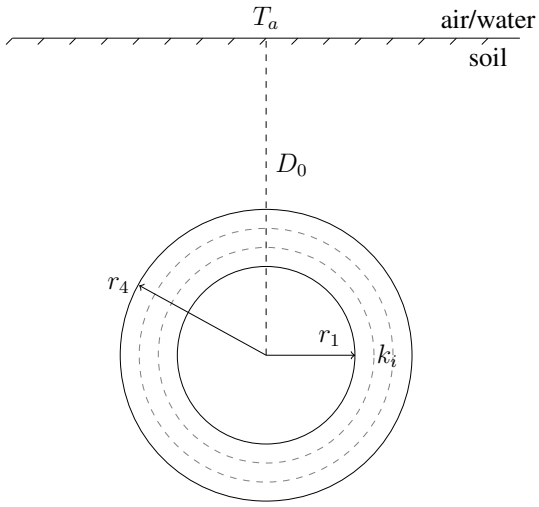

Figure 2: Cross-section of a buried pipeline consisting of three wall layers with inner radius r_1 and outer radius r_4. Each pipe layer has its specific thermal conductivity k_i. D_0 is the burial depth from ground level to the pipe centerline. T_a is the ambient temperature of either air or water.

The first process is the heat transfer between the gas and the inner wall, which is modeled using a film transfer coefficient determined from the Dittus-Boelter relation [4]

$$Nu = \frac{hL}{k} = 0.023 \cdot Re^{0.8} \cdot Pr^{n} \tag{10}$$

where Nu, Re and Pr are the Nusselt, Reynolds and Prandtl numbers respectively. h is the film transfer coefficient, L the characteristic length and k the thermal conductivity of the gas. When the gas is cooled by the ambient, $n = 0.4$, and in the reverse case $n = 0.3$. Heat transfer through the pipe wall is modeled as a conductive process. In Fig.2 the pipe wall consists of three different wall layers, each with a thermal conductivity k_i. The final process is the heat transfer between the outer wall and the surroundings which is modeled using an outer film coefficient determined from either a deep or shallow burial correlation, depending on the burial depth D_0. To compute the total heat transfer coefficient U, each heat transfer process is assigned a thermal resistance, and the total heat transfer coefficient is equal to the sum of all thermal resistances. The following expression can be derived for the pipeline in Fig.2 [1]

$$U = \left(\frac{1}{h_i} + r_1 \frac{\ln(r_2/r_1)}{k_1} + r_1 \frac{\ln(r_3/r_2)}{k_2} + r_1 \frac{\ln(r_4/r_3)}{k_3} + \frac{r_1}{r_3 h_o} \right)^{-1} \tag{11}$$

where h_i is the inner film coefficient, h_o the outer film coefficient and k the thermal conductivity of each layer.

Unsteady heat transfer model

While the steady state heat transfer model using the total heat transfer coefficient U allows for simple calculations of the heat exchange between the pipeline and the surroundings, it does not take into account time dependent heat accumulation in the ground and in the pipe wall. In the work by Chaczykowski [9] the heat transfer from the gas to the surroundings is considered as unsteady, so that the effect of heat accumulation is taken into account. Transient heat conduction in the solid surrounding the pipeline is now modeled by solving the one-dimensional radial heat conduction equation. Assuming azimuthal symmetry, the unsteady one-dimensional heat conduction equation takes the form

$$\rho c_p \frac{\partial T}{\partial t} = \frac{k}{r} \frac{\partial}{\partial r} \left(r \frac{\partial T}{\partial r} \right) \tag{12}$$

The model is axial symmetric where each thermal layer is represented by a coaxial cylindrical shell, which is now considered as a thermal capacitor, and not a thermal resistance as in the steady heat transfer model. Fig.3 shows the half plane of the cross-section of a buried pipeline with different thermal elements. Equation (12) is discretized using an implicit finite difference scheme

$$\rho_i c_{pi} \frac{T_i^{n+1} - T_i^n}{\Delta t} = \frac{(kr)_{i-1/2}}{r_i} \left(\frac{T_{i-1}^{n+1} - T_i^{n+1}}{\Delta r^2} \right) - \frac{(kr)_{i+1/2}}{r_i} \left(\frac{T_i^{n+1} - T_{i+1}^{n+1}}{\Delta r^2} \right) \tag{13}$$

where $r_{i+1/2}$ is the radial position located halfway between r_i and r_{i+1}. ρ_i and c_{pi} is the density and heat capacity of element i, while $k_{i+1/2}$ is the heat transfer coefficient between elements $i+1$ and i. In order to couple the one-dimensional radial heat equation with the one-dimensional flow model, the heat flow Q between the gas and the inner wall is defined as

$$Q = \frac{k_0 D}{4} (T - T_1) \tag{14}$$

where k_0 is the heat transfer coefficient between the the gas and the inner wall which, as in the steady heat transfer model, is determined by the film transfer coefficient in Equation (10). T_1 is the temperature of the first cylindrical shell in Fig.3. At the outer domain the ambient temperature T_a is set as the boundary condition. When solving the one-dimensional flow equations at a new time level, the heat flow Q from the previous time step is used in the energy equation to model the heat exchange between the gas and the surroundings. For an updated gas temperature, the radial heat equation (Equation (12)) is solved together with Equation (14) to update the temperature field around the pipeline and determine the heat flow Q between the gas and the surroundings.

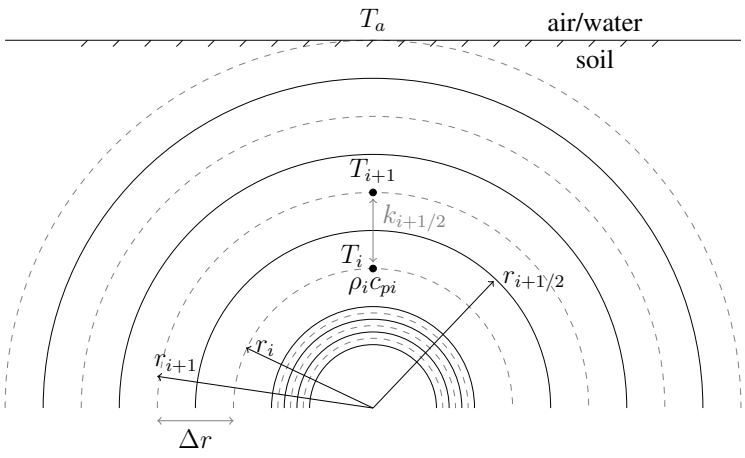

Figure 3: Half plane of the cross-section of a buried pipeline. Thermal elements are represented by coaxial cylindrical layers.

Numerical scheme

Equations (1)-(3) form a system of hyperbolic partial differential equations which have to be solved numerically. In this work an implicit finite difference scheme is used, which is preferred over an explicit scheme, as it is stable for any CFL number. Explicit methods are only stable for a CFL number less than 1. For transportation of natural gas through high pressure pipelines, the CFL number is $(u + c)\Delta t/\Delta x$, where c is the speed of sound, u the velocity of the gas and Δx and Δt the spatial and temporal step. The numerical value of $u + c$ is approximately 400 m/s. The spatial step between grid points Δx can vary, and depends on the inclination angle. For steep inclination a short Δx is required, while for little or no inclination a larger grid size may be used. In the case of an explicit method with a short grid space of $\Delta x = 100$ m, a time step of $\Delta t = 0.25$ s or less is required to ensure stability. During steady state periods one would typically use time steps much greater than this. When using an implicit method, the time step can be set to any reasonable value, regardless of what the spatial step is. This illustrates why it is advantageous to use an implicit method compared to an explicit method when modeling the flow of natural gas through long distance pipelines.

The numerical stencil is presented in Fig.4. The pipeline is divided into N grid points with Δx being the distance between points i and $i + 1$. Δt is the time step between time level $n + 1$ and n. Flow values are stored at the grid points, but are computed at the midpoint between two grid points.

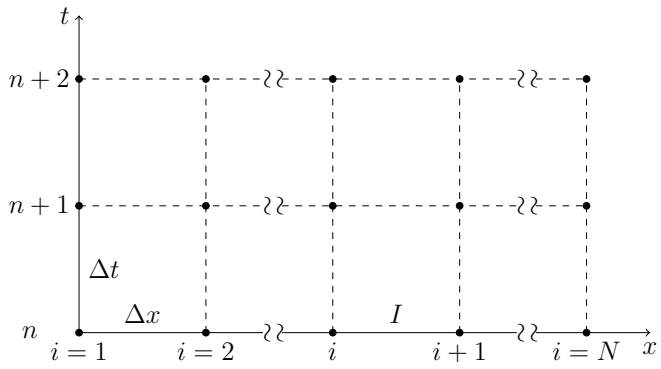

Figure 4: Stencil used in the finite difference method

For pipe section I, which is the section between points i and $i+1$, the partial derivative of a variable Y with respect to time is approximated by

$$\frac{\partial Y(x_I, t_{n+1})}{\partial t} = \frac{Y_{i+1}^{n+1} + Y_i^{n+1} - Y_{i+1}^n - Y_i^n}{2\Delta t} + \mathcal{O}(\Delta t) \tag{15}$$

the spatial derivative by

$$\frac{\partial Y(x_I, t_{n+1})}{\partial x} = \frac{Y_{i+1}^{n+1} - Y_i^{n+1}}{\Delta x} + \mathcal{O}(\Delta x^2) \tag{16}$$

and the individual term by

$$Y(x_I, t_{n+1}) = \frac{Y_{i+1}^{n+1} + Y_i^{n+1}}{2} + \mathcal{O}(\Delta x^2) \tag{17}$$

This method is first order correct in time and second order correct in space. When discretizing all terms in a fully implicit way, the governing equations form a system non-linear equations. Solving such a system can be computationally expensive, especially for long pipelines and complicated pipe networks. To simplify the computations the non-linear terms are linearized about the previous time step to give a system of linear equations. The procedure can be found in the article by Luskin [10]. The resulting system can be solved in an efficient way using simple linear algebra. This has been done in the following.

In the case where an unsteady heat transfer model is used, the radial heat equation is solved in the solid domain surrounding the pipeline at every grid point and time step. The number of thermal elements surrounding the pipeline depends on whether the pipeline is buried under ground or exposed to sea water. For the case where the pipeline is buried under ground each wall layer is assigned a thermal element, and the surrounding soil is divided into four layers. When exposed to sea water each wall layer is assigned a thermal element, while the heat transfer between the outer wall and the sea water is modeled using a film transfer coefficient, as there is no heat accumulation in the surrounding sea water.

Results

In the following a 650 km horizontal pipeline with an inner diameter of 1.016 m will be considered. Simulations will be run for both an on-shore and offshore pipeline. Offshore pipelines

are usually buried under the ground for the first and final lengths of the pipeline where the gas departs the processing terminal and arrives at the receiving terminal, as shown in Fig.5. This has been included in the offshore pipeline simulations.

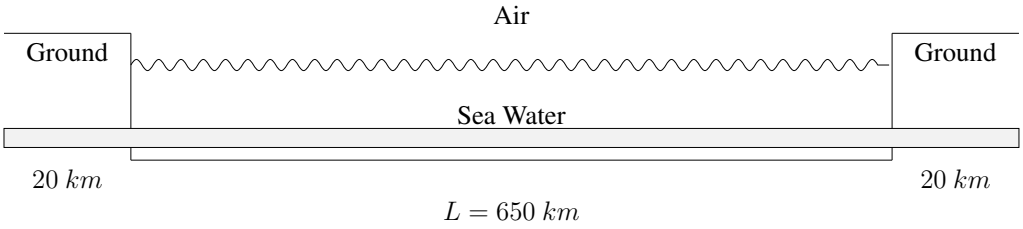

Figure 5: Offshore natural gas pipeline which is buried under ground for first and last 20 km. Pipeline is lying on seabed exposed to the sea water.

The following boundary conditions were used

$$\begin{aligned} p(L,t) &= 9\ MPa \\ T(0,t) &= 30\ ^{\circ}C \\ \dot{m}(0,t) &= f(t)\ kg/s \end{aligned} \tag{18}$$

where $f(t)$ is shown in Fig.6.

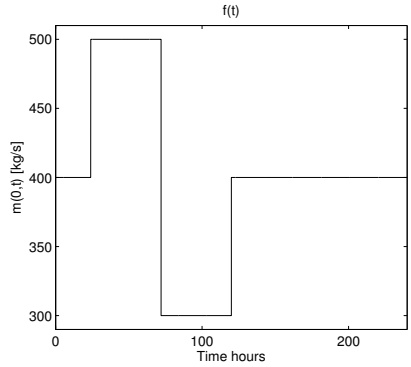

Figure 6: Inlet boundary condition for the mass flow rate.

The gas composition (in mol%) was set to: $CH_4 = 89.1704\%$, $C_2H_6 = 7.3513\%$, $C_3H_8 = 0.5104\%$, $iC_4H_{10} = 0.0251\%$, $nC_4H_{10} = 0.0311\%$, $N_2 = 0.6980\%$ and $CO_2 = 2.2209\%$. The pipe wall consists of a single steel layer with a thickness of 25 mm. The steel layer has a density of $\rho = 7850$ kg/m^3, heat capacity $c_p = 500$ J/(kg K) and thermal conductivity $k = 45$ W/(m K). For the buried pipeline the surrounding soil was assumed to have a density of $\rho = 2650$ kg/m^3, heat capacity of $c_p = 950$ J/(kg K) and thermal conductivity $k = 3$ W/(m K). All simulations were performed using both the steady and unsteady heat transfer model.

The pipeline was divided into 101 grid points with a grid spacing $\Delta x = 6.5$ km. A time step of $\Delta t = 60$ s was used. The convergence of the numerical scheme presented in the previous

section and the discretization errors were investigated, with the local error defined as

$$e = \frac{1}{N}\left(\sum_{i=1}^{N}\left(\frac{Y_i - Y_{i,hi}}{Y_{i,hi}}\right)^2\right)^{1/2} \tag{19}$$

where Y represents p, $\dot{m}$ and T at point i. The summation is done over all grid points N, where $Y_{i,hi}$ is the numerical solution computed using the finest grid and shortest time step (high resolution solution). Results are presented in Fig.7. The spatial discretization error as a function of grid points N is shown to the left. As the numerical method is second order correct in space, a line with slope -2 is indicated. Both the mass flow and temperature converge to order second order, while the pressure converges to an order of approximately 2.5. The temporal discretization errors as a function of time step Δt are shown to the right in Fig.7. The numerical method is first order correct in time. Both mass flow and temperature converge to first order, while the pressure converges to an order of approximately 1.5. The local errors for pressure, mass flow and temperature are small and results indicate that a grid consisting of 101 points and a time step of $\Delta t = 60$ s is sufficient to run simulations on long distance natural gas pipelines.

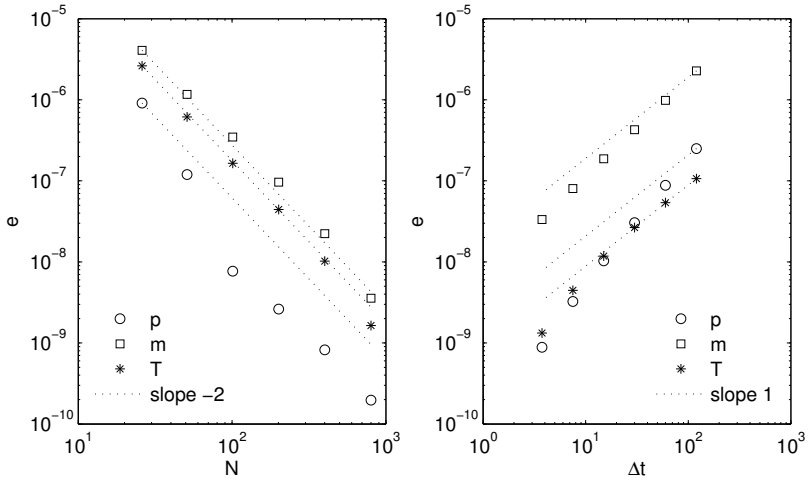

Figure 7: Local errors. Left: Local error for pressure, mass flow and temperature as a function of grid points N. Right: Local error for pressure, mass flow and temperature as a function of time step Δt.

On-shore pipeline

For the on-shore pipeline the distance from the ground surface to the pipe centerline was 2 m. The ambient air temperature was set to 5°C. Results for inlet pressure, outlet mass flow rate and outlet temperature using both the steady and unsteady heat transfer models are presented in Fig. 8. During steady state conditions there is no difference between the two solution strategies. However, when the flow conditions are transient a small difference in computed inlet pressure and outlet mass flow rate can be observed. But these differences are small compared to that of the outlet temperature which is shown at the bottom of Fig.8. During transient conditions a difference of up to 1°C was observed, with the steady state heat transfer model over predicting the amplitude of the temperature changes in the flow, which can clearly be seen in Fig. 8. At the final time step there is a small difference in outlet temperature between the two solution

strategies. The computed outlet temperatures will eventually converge to the same value, but because the thermal response of the unsteady heat transfer model is considerably slower than that of the steady heat transfer model, the time it takes for the temperature profiles in Fig. 8 to converge is longer than the simulation time.

Offshore pipeline

The offshore natural gas pipeline schematics is shown in Fig.5. For the first and final 20 km the pipeline is buried under ground, while for the remaining part it is lying on the seabed fully exposed to the sea water. The total length is the same as for the on-shore pipeline and the boundary conditions are unchanged. The ambient air temperature is 5°C while the ambient sea bottom temperature is 4°C. Because the sea water has a high heat capacity and currents on the sea bottom constantly move the water across the pipeline, it is assumed that there is no heat accumulation in the sea water. The heat transfer from the outer pipe wall to the surrounding sea water is modeled using a film coefficient which is computed from a Nusselt-number relation. The surrounding sea water is assumed to have a velocity of 0.5 m/s across the pipeline.

Results for inlet pressure and outlet mass flow rate are almost identical to those in Fig.8 for the on-shore case. Under the given operating conditions there was no significant difference in inlet pressure and outlet mass flow using the two different heat transfer models. There was however a small difference in outlet temperature which is presented in Fig.9.

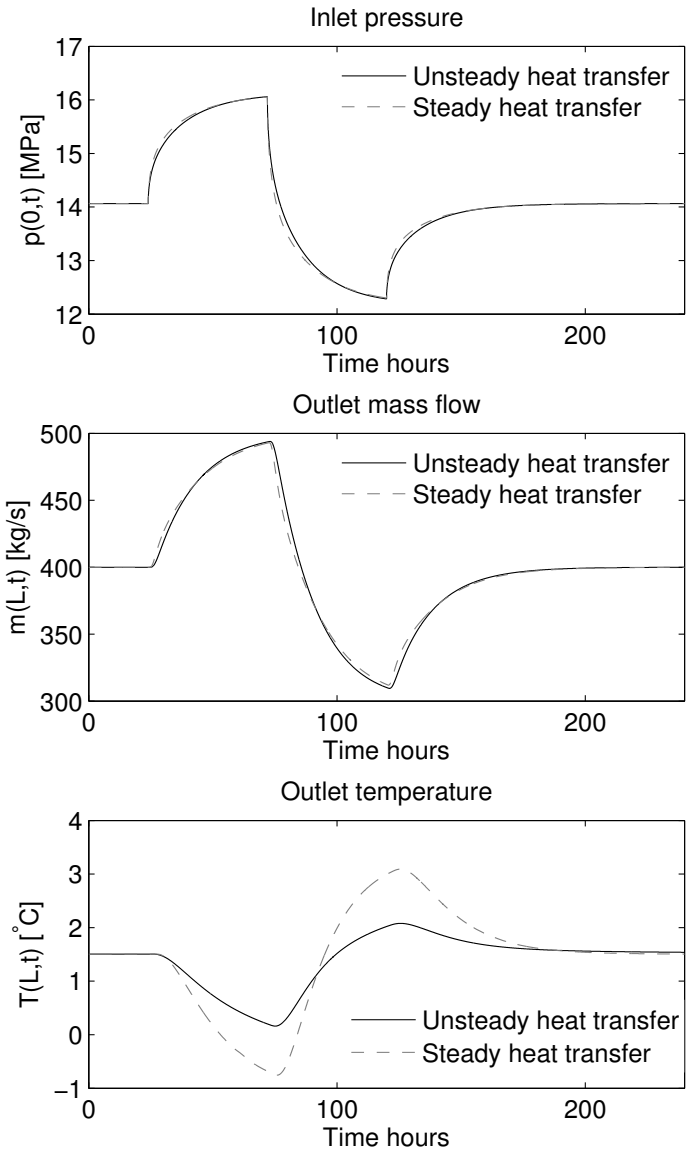

Figure 8: Results on-shore pipeline using the two different heat transfer models. Top inlet pressure, middle outlet mass flow rate and bottom outlet temperature. The steady heat transfer model over predicts the amplitude of temperature changes in the flow compared to the unsteady heat transfer model.

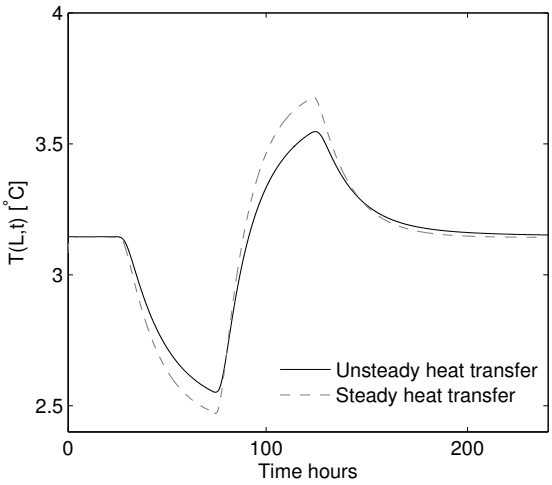

Figure 9: Outlet temperature for offshore pipeline using both unsteady and steady heat transfer model. Difference between the two temperature profiles is less than for the on-shore pipeline as there is no heat accumulation in the surrounding sea water.

Model validation

So far only a change in inlet mass flow rate has been considered, while the inlet temperature has been kept constant. In this section a change in both inlet mass flow rate and temperature will be considered. Boundary conditions are taken from operational data from a 650 km offshore pipeline operated by Gassco. The pipeline was buried under ground for the first and final 20 km. The effect of an unsteady heat transfer model on Gasscos pipelines will be investigated.

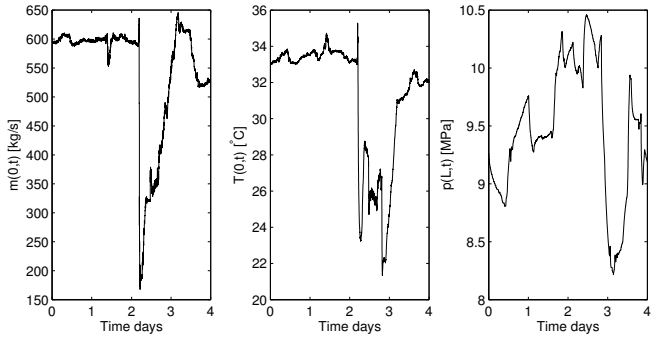

Figure 10: Boundary conditions for model validation. Left inlet mass flow, middle inlet temperature and right outlet pressure. Data courtesy of Gassco.

The pipeline diameter is approximately 1 m. The boundary conditions for outlet pressure, inlet mass flow rate and inlet temperature are given in Fig.10. After approximately 2 days a large transient occurs with a large reduction in inlet mass flow rate and temperature. The pipeline was discretized by 98 grid points with a varying Δx and $\Delta t = 60$ s. The data is from the winter season and the ambient temperature is approximately 6°C. Results are presented in Fig.11.

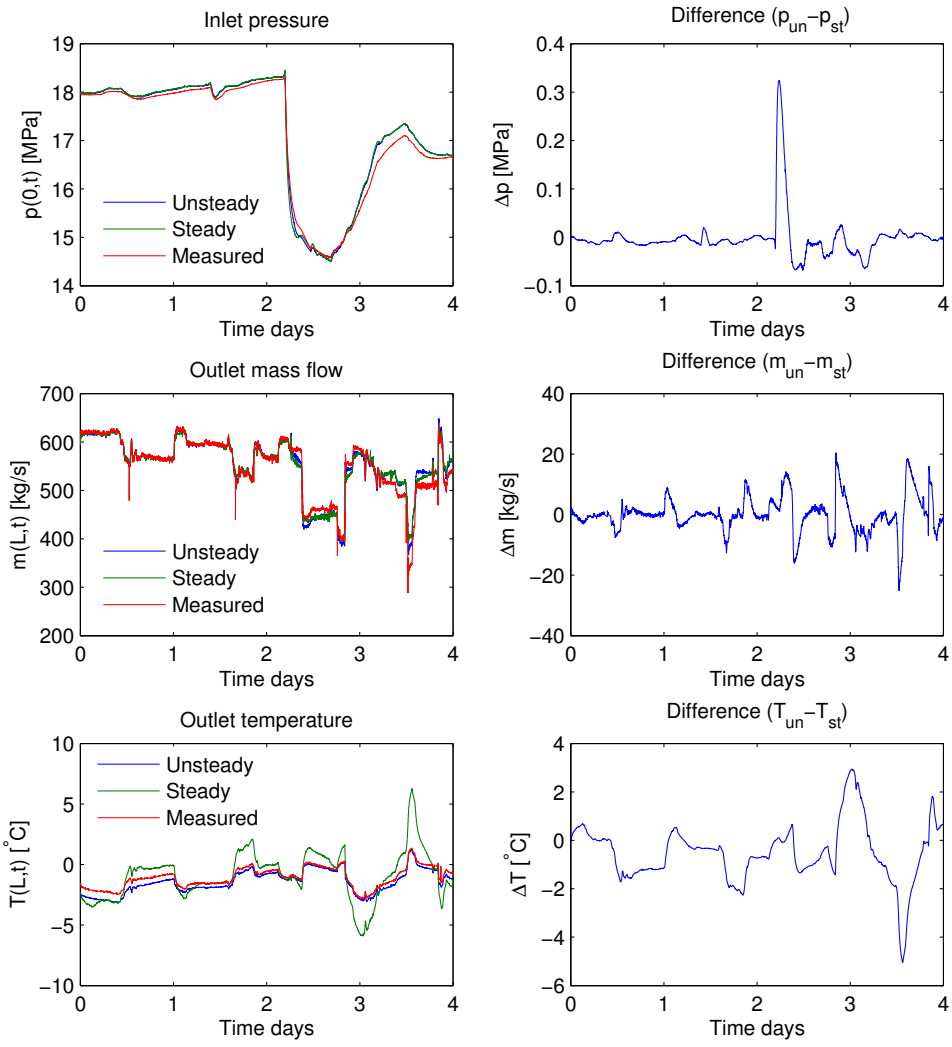

Figure 11: Results model validation. Top left: Computed inlet pressure found using unsteady and steady heat transfer model compared to measured inlet pressure. Top right: Difference inlet pressure between unsteady and steady heat transfer model. During transient a difference of 0.3 MPa can be observed. Middle left: Computed outlet mass flow using different heat transfer models compared to measured value. Middle right: Difference outlet mass flow between different heat transfer models. Bottom left: Outlet temperature using two different heat transfer models compared to measured outlet temperature. Steady heat transfer model over predicts temperature changes compared to unsteady. Bottom right: Difference outlet temperature using different heat transfer models.

Results for inlet pressure, outlet mass flow rate and outlet temperature in Fig.11 are compared to measured values from the offshore pipeline. For the inlet pressure (top Fig.11) a small difference during steady state conditions can be observed between the unsteady and steady heat transfer model. However, during transient conditions there is a considerable difference in inlet pressure. This difference is approximately 0.3 MPa and occurs at the beginning of the transient. For the outlet mass flow small differences are seen in Fig.11, although these small differences are present during both transient and steady state conditions. In agreement with Chaczykowski [9] the steady heat transfer model over predicts the amplitude of temperature changes in the flow. This is clearly visible in the outlet temperature (bottom Fig.11). Although Chaczykowski only investigated on-shore buried pipelines, results in Fig.11 demonstrate that a steady heat transfer model also over predicts the amplitude of temperature changes in the flow for offshore pipelines. Even though the pipeline investigated here was buried under the ground only for the first and final part of the pipe length, an unsteady heat transfer model for these short pipeline sections gives improved results for the computed outlet temperature.

Discussion

Unsteady heat transfer

The reason why there is such a considerable difference in inlet pressure between the two heat transfer models in Fig.11 during the transient can be interpreted as follows. In the steady state heat transfer model the heat exchange term between the gas and the pipeline surroundings in Equation (4) is proportional to the product of the total heat transfer coefficient U and the temperature difference $(T - T_a)$ between the gas and the ambient. As the ambient temperature in the model validation case was approximately $6°$C and the inlet temperature in Fig.10 is never less than $20°$C the temperature difference will always be positive. The total heat transfer coefficient U is also positive, implying that the heat exchange between the gas and the surroundings will always be modeled as a positive energy flux out of the pipeline. In the unsteady heat transfer model the temperature at each thermal layer is computed at every time step. After a steady state period the inner pipe wall is assumed to have the same temperature as the gas, while the outer pipe wall and soil layers further away have a lower temperature. When a transient occurs, and there is a large drop in inlet temperature like that in Fig.10, the gas temperature drops below the temperature of the inner wall. For a short period of time, before thermal equilibrium is reached, an energy flux will be transferred from the wall to the gas. By computing the temperature at each thermal layer the unsteady heat transfer model allows for energy to be transferred from the wall to the gas. This gives a higher gas temperature at points close to the inlet compared to a steady state heat transfer model, which in turn gives a higher inlet pressure during transients like the one observed in Fig.11.

The relation between heat conduction and heat storage can be determined by considering the Fourier number

$$Fo = \frac{\alpha t}{L^2} \tag{20}$$

where $\alpha = k/\rho c_v$ is the thermal diffusivity, t the characteristic time and L the characteristic length through which heat conduction occurs. For the on-shore pipeline the characteristic length is the burial depth, which is approximately 1.5 m. The time for the ramp up or ramp down to occur in Fig.8 is approximately 50 hours, and the thermal diffusivity of the soil is $1.2 \cdot 10^{-6}$ m^2/s, giving a Fourier number of 0.1. The physical meaning of this is that the heat conduction rate is an order of magnitude less than the heat storage rate, and the transient thermal response upon the change in the mass flow rate is predominantly dictated by the heat storage effect, even

on a two day time scale as is the case here. For shorter characteristic time scales, the larger the effect of heat storage compared to the effect of heat conduction. In this case, the value of the Fourier number underlines that the steady state approach for heat transfer is not valid. In such case it should be much larger then 1.

The Biot number gives the ratio of the heat transfer resistances inside of and at the surface of a body, and is defined as

$$Bi = \frac{hL}{k} \tag{21}$$

where h is the heat transfer film coefficient at the boundary of the body, L is the characteristic length and k is the thermal conductivity of the body. The Biot number determines whether or not the temperature inside a body will vary significantly in space when heated or cooled over time as a result of thermal gradients applied to its surface. For small Biot numbers (0.1 or less) the heat conduction inside the body is much faster than the heat convection at the surface, meaning that temperature gradients inside the body are negligible. For the on-shore pipeline the characteristic length L can be chosen as the volume of the body divided by the surface area. For the circular system of the pipeline buried under ground with ambient boundary condition there are two Biot numbers. At ground level, at a radius of 2 meters from the pipe centerline, the ambient temperature can be coupled with a heat transfer coefficient of 50 W/(mK). The characteristic length is $L = 4.5$ and the soil thermal conductivity $k = 3$ W/(m^{2}K). The Biot number is then 75. On the outer pipe wall we can consider the outer film coefficient as the heat transfer coefficient, or alternatively the combined wall resistance and inner wall film coefficient. This will also give a high Biot number. These high Biot numbers show that for a change of ambient temperature and heat transfer conditions at the pipe wall, the surrounding soil will react by developing time dependent temperature gradient. This further supports the need for an unsteady heat transfer model.

One-dimensional approximation

The unsteady heat transfer model is a simple and straightforward way to include heat accumulation in the ground. However, the model does have limitations. Because it is an axial-symmetric one-dimensional model, it has symmetric boundary conditions, implying that the ambient boundary condition which is set above the pipeline is automatically set for the entire circular domain surrounding the pipeline. This is not correct, as boundary conditions on each side and below generally differ from that of the ambient temperature boundary on top. This can only be set correctly using a two-dimensional model.

To verify the computed heat flux in the one-dimensional unsteady heat transfer model it is compared to the computed heat flux from a two-dimensional model, which was made in ANSYS Fluent. In this model, the soil and pipe are represented by a 2D finite volume grid, and the calculations incorporate solving the energy equation on the solid domain. The soil domain is 50 meters deep and extends 25 meters sideways in each direction from the pipe centerline, and consisted of approximately 35000 computational cells. Symmetric boundary conditions are employed at the left and right side of the soil domain. At the bottom of the soil domain a constant temperature boundary conditions is used which is set at 10 °C. At the top of the soil domain the ambient temperature is coupled through a heat transfer coefficient of 50 W/(m^{2}K). The gas temperature is connected to the inner wall of the pipe though the film transfer coefficient in Equation (10).

The following two cases were considered:

- 1) Gas temperature 30 °C, ambient temperature 5 °C
- 2) Gas temperature 1.5 °C, ambient temperature 5 °C

These two cases correspond to the conditions at the inlet and outlet of the on-shore pipeline during steady state conditions. The pipe setup and thermal data are the same as in the on-shore pipeline case. For case 1, the Reynolds and Prandtl number were $3.06 \cdot 10^7$ and 0.72 respectively. For case 2 these values were $3.69 \cdot 10^7$ and 0.71 respectively. The thermal conductivity of the gas was 0.0521 W/(m K) in the first case and 0.042 W/(m K) in the second. The calculated heat flux in W/m for both cases are presented in Table.1. The computed heat flux in the 1D model was approximately 50% more than the 2D model for both case 1 and 2. The temperature field around the pipeline for case 1 and 2 is shown in Fig.12 and 13 respectively. Results in Table.1 suggest that the 1D heat transfer model under the given operating conditions predicts too large values of the heat flux between the gas and the surroundings, owing to the one-dimensional axial-symmetric assumption.

	Case 1	Case 2
1D heat transfer model	353 W/m	-49 W/m
2D heat transfer model	230 W/m	-33 W/m

Table 1: Calculated heat flux in W/m using the 1D and 2D heat transfer model. The calculated heat flux in the 1D case was approximately 50% greater than in the 2D case.

The heat flux in the one-dimensional model can be adjusted to match that of the two-dimensional model by introducing the equivalent soil radius, as is done in other compressible flow models [11]. This should be investigated in more detail for the examples shown above.

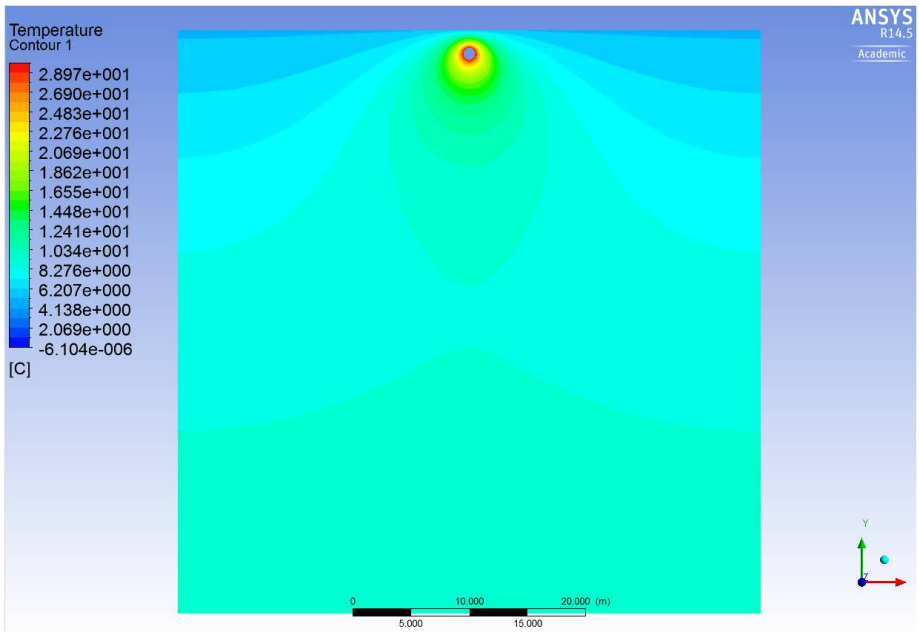

Figure 12: Contour lines for the temperature around the pipeline for case 1. The gas temperature is 30 °C and the ambient 5 °C.

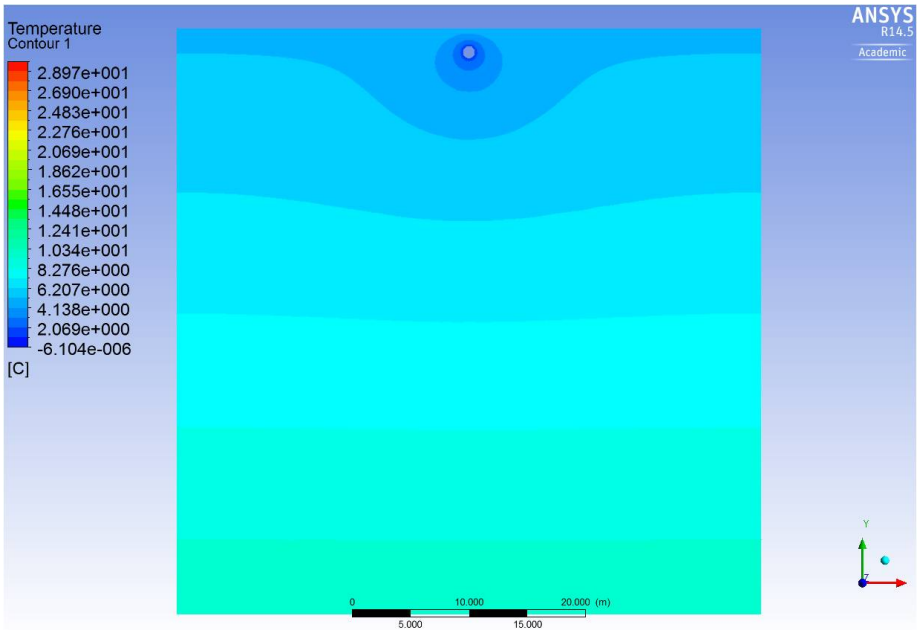

Figure 13: Contour lines for the temperature around the pipeline for case 2. The gas temperature is 1.5 °C and the ambient 5 °C.

Conclusion

An unsteady heat transfer model has been compared to a steady state heat transfer model for transmission of natural gas through high pressure large diameter pipelines. This model allows for heat accumulation in the pipe wall and ground surrounding the pipeline. Results for the on-shore buried pipeline demonstrate that the steady heat transfer model over predicts the amplitude of temperature changes in the flow. The same model was applied to an offshore natural gas pipeline. Even though heat accumulation is only present at beginning and end of the pipeline where it is buried under ground, and not along the main part which is exposed to sea water, the unsteady heat transfer model still has an effect on the flow conditions in the pipeline. For large transients considerable differences were observed between the two heat transfer models. As with the on-shore pipeline, the steady state heat transfer model for offshore pipelines over predicts the amplitude of temperature changes in the flow. Also, a significant difference in modeled inlet pressure was observed between the two models under transient conditions. The computed heat flux is compared to that of a two-dimensional heat transfer model. For the considered case the one-dimensional model over predicts the heat flux by 50% compared to the two-dimensional model. In order to investigate how this affects the flow, a detailed two-dimensional heat transfer model should be used at every grid point and be compared to the one-dimensional case. The presented models were validated using operational data from an offshore natural gas pipeline. Results suggest that an unsteady heat transfer model should be used for offshore natural gas pipelines.

Acknowledgment

This work has been financed by Gassco as part of a project to improve flow modeling in off-shore natural gas pipelines. The authors would like to thank Professor Bernhard Müller (NTNU)

and Principal Scientist Stein Tore Johansen (SINTEF Materials and Chemistry) for their guidance and feedback.

Nomenclature

c_p	heat capacity constant pressure [J/(kg·K)]
c_v	heat capacity constant volume [J/(kg·K)]
D	pipe inner wall diameter [m]
f	friction factor
g	gravitational acceleration [m/s^2]
h	film transfer coefficient [W/(m^2·K)]
k	heat transfer coefficient [W/(m·K)]
L	characteristic length [m]
$\dot{m}$	mass flow [kg/s]
Nu	Nusselt number
Pr	Prandtl number
p	pressure [Pa]
Q	heat flow [W]
T	temperature [K]
T_a	ambient temperature [K]
R	gas constant [J/(kg·K)]
r	pipe radius [m]
Re	Reynolds number
t	time [s]
U	total heat transfer coefficient [W/(m^2·K)]
u	gas velocity [m/s]
x	spatial coordinate [m]
Z	compressibility factor
α	thermal diffusivity [m^2/s]
ϵ	equivalent sand grain roughness [m]
ρ	density [kg/s]
θ	pipe inclination angle

References

[1] A.F. Mills *Heat and Mass Transfer* Irwin, 1995.

[2] A.J. Osiadacz, M. Chaczykowski Comparison of isothermal and non-isothermal pipeline gas flow models *Chemical Engineering Journal*, **vol.81**, 41–51, 2001.

[3] C.Colebrook Turbulent flow in pipes, with particular reference to the transition region between the smooth and rough pipe laws *J. Inst. Civil Eng.*, **vol.11**, 133–156, 1939.

[4] F.P. Incropera, D.P. DeWitt, T.L. Bergman, A.S. Lavine *Fundamentals of Heat and Mass Transfer* Wiley, 6 edition, 2007.

[5] J. Ramsen, S.E. Losnegård, L.I. Langelandsvik, A.J. Simonsen, W. Postvoll Important Aspect of Gas Temperature Modeling in Long Subsea Pipelines *Proceedings to 40th PSIG Annual Meeting in Galvestone Texas*, 2009.

[6] L.I. Langelandsvik *Modeling of natural gas transport pipeline and friction factor for large-scale pipelines* PhD thesis, NTNU, 2008.

[7] M. Abbaspour, K.S. Chapman Nonisothermal Transient Flow in Natural Gas Pipeline *Journal of Applied Mechanics*, **vol.75**, 031018–1–8, 2008.

[8] M. Chaczykowski Sensitivity of pipeline gas flow model to the selection of the equation of state *Chemical Engineering Research and Design*, **vol.87**, 1596–1603, 2009.

[9] M. Chaczykowski Transient flow in natural gas pipeline - The effect of pipeline thermal model *Applied Mathematical Modelling*, **vol.34**, 1051–1067, 2009.

[10] M. Luskin An approximate procedure for non-symmetric nonlinear hyperbolic systems with integral boundary conditions *SIAM Journal on Numerical Analysis*, **vol.16**(1), 145–164, 1979.

[11] SPT Group *OLGA 5 User Manual* Kjeller, Norway, 2010.

[12] K.Starling *Fluid Thermodynamic Properties for Light Petroleum Systems* Gulf Publishing Company, 1973.

[13] T. Kiuchi An implicit method for transient gas flows in pipe networks *International Journal of Heat and Fluid Flow*, **vol.15**(5), 378–383, 1994.

[14] A.Thorley and C.Tiley Unsteady and transient flow of compressible fluid in pipelines - a review of theoretical and some experimental studies *International Journal of Heat and Fluid Flow*, **vol.8**(1), 3–15, 1987.

Article [e]

Transient Flow in Natural Gas Pipelines using Implicit Finite Difference Schemes

J.F. Helgaker, B. Müller and T. Ytrehus

Submitted to ASME Journal of Fluids Engineering, June 2013.

Is not included due to copyright

Article [f]

Validation of 1D Flow Model for Transmission of Natural Gas through Offshore Pipelines

J.F. Helgaker, A. Oosterkamp , L.I. Langelandsvik and T. Ytrehus

Submitted to Journal of Natural Gas Science and Engineering, June 2013.

Validation of 1D Flow Model for High Pressure Offshore Natural Gas Pipelines

Jan Fredrik Helgaker[a,b,*], Antonie Oosterkamp[a,b], Leif Idar Langelandsvik[c], Tor Ytrehus[b]

[a] *Polytec Research Institute, 5527 Haugesund, Norway*
[b] *Norwegian University of Science and Technology, Department of Energy and Process Engineering, 7491 Trondheim, Norway*
[c] *Gassco AS, 4250 Koppervik, Norway*

Abstract

Transportation of natural gas through high pressure large diameter offshore pipelines is modeled by numerically solving the governing equations for one-dimensional compressible pipe flow using an implicit finite difference method. The pipelines considered have a diameter of 1 m and length of approximately 650 km. The influence of different physical parameters which enter into the model are investigated in detail. These include the friction factor, equation of state and heat transfer model. For high pressure pipelines it is shown that the selection of the equation of state can have a considerable effect on the simulated flow results, with the recently developed GERG 2004 being compared to the more traditional SRK, Peng-Robinson and BWRS equations of state. Also, including heat accumulation in the ground is important in order to model the correct temperature at the outlet of the pipeline. The flow model is validated by comparing computed results to measured values for an offshore natural gas pipeline.

Keywords: Transportation, Offshore pipelines, Compressible flow, Friction factor, Equation of state, Heat transfer model,

*Corresponding author
Email address: jan.fredrik.helgaker@polytec.no ()

Nomenclature

A	pipe cross section [m^2]
c_p	heat capacity at constant pressure [J/(kg·K)]
c_v	heat capacity at constant volume [J/(kg·K)]
D	pipe diameter [m]
Fo	Fourier number
f	friction factor
g	gravitational constant [m/s^2]
h	film transfer coefficient [$W/(m^2 \cdot K)$]
k	thermal conductivity [W/(m·K)]
$\dot{m}$	mass flow rate [kg/s]
p	pressure [Pa]
p_c	critical pressure [Pa]
p_r	reduced pressure
Q	heat flow [W]
R	gas constant [J/(kg·K)]
Re	Reynolds number
r	pipe radius [m]
T	Temperature [K]
T_a	Ambient temperature [K]
T_c	critical temperature [K]
T_r	reduced temperature
t	time [s]
U	total heat transfer coefficient [$W/(m^2 \cdot K)$]
u	gas velocity [m/s]
x	spatial coordinate [m]
Z	compressibility factor
ϵ	equivalent sand grain roughness [m]
ρ	density [kg/m^3]
ρ_m	molar density [$kg \cdot mol/m^3$]
θ	pipe inclination angle

1. Introduction

Natural gas may be transported over long distances through high pressure transmission pipelines. An overview of the Norwegian natural gas transport

system lying in the North Sea is shown in Fig. 1. The network is operated by the Norwegian state owned company Gassco. After the gas has been processed and unwanted components are removed it is fed into long export pipelines and transported from Norway to continental Europe and the UK. The pipelines have a diameter of approximately 1 and can be between $600 - 800$ km in length. Measurements of the state of the gas such as pressure, mass flow, temperature and composition are available only at the inlet and outlet. To know the state of the gas between these two points one has to rely on computer models.

Transmission of natural gas through high pressure pipelines can be modeled by numerically solving the governing equations for one-dimensional compressible viscous heat conducting flow. Such mathematical models have several important applications in the gas industry. These include designing, operating and monitoring natural gas pipelines and predicting the pipeline hydraulic capacity. High accuracy in transport capacity is important to ensure optimal utilization of the network, as failure to deliver the forecasted capacity can result in penalties and a poor reputation as a gas network operator (Langelandsvik et al. (2009)). They also play an integral part in software based leak detection systems. It is therefore crucial that these models are as accurate as possible, but at the same time fast and efficient as conditions in the pipeline are usually transient.

An overview of different numerical techniques used to solve the governing flow equations can be found in base literature articles (Thorley and Tiley (1987)). These include the method of characteristics, finite difference, finite volume and finite element methods. Finite difference methods have commonly been used to model the flow of natural gas through pipelines (Abbaspour and Chapman (2008), Chaczykowski (2010), Kiuchi (1994)), with implicit methods being preferred to explicit, as these are stable for any choice of time and spatial step.

In order to accurately model the flow through high pressure pipelines one has to solve the full non-isothermal model (Osiadacz and Chaczykowski (2001)), which implies solving the continuity, momentum and energy conservation equations for the flow. As well as solving the governing flow equations, several physical processes have to be modeled in appropriate ways. These include the friction factor, equation of state and heat exchanges between the gas and the surrounding environment. Previous research has looked into the sensitivity of the pipeline gas flow model to the selection of the equation of state (Chaczykowski (2009)) and the effect of the pipeline thermal

Figure 1: Overview of the Norwegian natural gas transport system in the North Sea. Figure courtesy of Gassco.

model (Chaczykowski (2010)). However, in both these cases the investigated pipeline had an inlet pressure of 8.4 MPa, which is typical that of an onshore distribution network. Offshore pipeline like those in Fig. 1 can have an inlet pressure of up to 20 MPa, well above that typically considered in the literature.

The objective of this study is to validate the one-dimensional flow model for high pressure offshore natural gas pipelines. An implicit finite difference method is used to solve the governing flow equations. The model is validated by running simulations on an offshore natural gas pipeline and comparing numerical results to measured values. Different physical processes which enter into the one-dimensional flow model will be investigated and discussed in detail. These include the friction factor, equation of state and heat transfer between the gas and the surrounding environment. For the equation of state the recently developed GERG 2004 will be compared to the more traditional SRK, Peng-Robinson and BWRS equations of state currently used today. The heat exchange between the gas and the surroundings will be modeled using both a steady and unsteady external heat transfer model. The main difference between these two approaches is that the unsteady heat transfer

model takes into account heat accumulation in the ground surrounding the pipeline.

2. Theory

2.1. Governing Equations

The governing equations for one-dimensional compressible viscous heat conducting flow are found by averaging the three-dimensional versions across the pipe cross section. The result is:

Continuity

$$\frac{\partial \rho}{\partial t} + \frac{\partial (\rho u)}{\partial x} = 0 \tag{1}$$

Momentum

$$\frac{\partial (\rho u)}{\partial t} + \frac{\partial (\rho u^2 + p)}{\partial x} = -\frac{f \rho u |u|}{2D} - \rho g \sin\theta \tag{2}$$

Energy

$$\rho c_v \left(\frac{\partial T}{\partial t} + u \frac{\partial T}{\partial x} \right) + T \left(\frac{\partial p}{\partial T} \right)_\rho \frac{\partial u}{\partial x} = \frac{f \rho u^3}{2D} - \frac{4U}{D}(T - T_a) \tag{3}$$

In the momentum equation the first term on the right hand side is the friction term, where f is the friction factor. The final term is the gravity term where θ is the pipe inclination angle. In the energy equation the second term on the left hand side represents the Joule-Thomson effect, which is cooling upon expansion. On the right hand side the first term is the dissipation term, which is breakdown of mechanical energy to thermal energy. The final term represents the heat exchange between the gas and the surroundings.

The density can be related to pressure and temperature by using a real gas equation of state

$$\frac{p}{\rho} = ZRT \tag{4}$$

where $Z = Z(p, T)$ is the compressibility factor. When working with natural gas pipelines, one is often interested in knowing the pressure and mass flow at the inlet and outlet. By replacing the density with pressure and introducing the mass flow rate $\dot{m} = \rho u A$, where A is the pipeline cross section, Equations

(1)-(3) can be developed into partial differential equations for p, $\dot{m}$ and T (Chaczykowski (2010)). The result is:

$$\begin{aligned}
\frac{\partial p}{\partial t} &= \left[\frac{1}{T}+\frac{1}{Z}\left(\frac{\partial Z}{\partial T}\right)_p\right]\left[\frac{1}{p}-\frac{1}{Z}\left(\frac{\partial Z}{\partial p}\right)_T\right]^{-1}\frac{\partial T}{\partial t} \\
&- \frac{ZRT}{pA}\left[\frac{1}{p}-\frac{1}{Z}\left(\frac{\partial Z}{\partial p}\right)_T\right]^{-1}\frac{\partial \dot{m}}{\partial x} \qquad (5) \\
\frac{\partial \dot{m}}{\partial t} &= \frac{\dot{m}ZRT}{pA}\Bigg(-2\frac{\partial \dot{m}}{\partial x}+\dot{m}\left[\frac{1}{p}-\frac{1}{Z}\left(\frac{\partial Z}{\partial p}\right)_T\right]\frac{\partial p}{\partial x}-\dot{m}\left[\frac{1}{T}+\frac{1}{Z}\left(\frac{\partial Z}{\partial T}\right)_p\right]\frac{\partial T}{\partial x}\Bigg) \\
&- A\frac{\partial p}{\partial x}-\frac{fZRT\dot{m}|\dot{m}|}{2DAp}-\frac{pA}{ZRT}g\sin\theta \qquad (6) \\
\frac{\partial T}{\partial t} &= -\frac{\dot{m}ZRT}{pA}\frac{\partial T}{\partial x}-\frac{\dot{m}(ZRT)^2}{pAc_v}T\left[\frac{1}{T}+\frac{1}{Z}\left(\frac{\partial Z}{\partial T}\right)_\rho\right] \\
&\times \left(\frac{1}{\dot{m}}\frac{\partial \dot{m}}{\partial x}-\left[\frac{1}{p}-\frac{1}{Z}\left(\frac{\partial Z}{\partial p}\right)_T\right]\frac{\partial p}{\partial x}+\left[\frac{1}{T}+\frac{1}{Z}\left(\frac{\partial Z}{\partial T}\right)_p\right]\frac{\partial T}{\partial x}\right) \\
&+ \frac{f}{2c_vD}\left(\frac{ZRT|\dot{m}|}{pA}\right)^3-\frac{ZRT}{pc_v}\frac{4U}{D}(T-T_a) \qquad (7)
\end{aligned}$$

2.2. Friction factor

The friction factor accounts for the frictional force between the fluid and the pipe wall. The friction factor f for a pipe, commonly denoted the Darcy-Weisbach friction factor, is defined as

$$f=\frac{-dp/dx}{\frac{1}{2}\rho u^2}D \qquad (8)$$

This is a semi-empirical parameter, meaning that no analytical description of these forces has been developed. For pipeline flow with high turbulence intensity (described by the Reynolds number), it is also impossible to fully calculate this parameter by computational simulations.

Today the Colebrook-White formula is the most widespread relation for determining f, which combines the two main regions for the friction factor. For low Reynolds numbers the friction factor is solely dependent on Reynolds number (smooth turbulent flow), whereas for higher Reynolds numbers the friction factor becomes independent of Reynolds number and only depends on

the internal roughness (rough turbulent flow). Colebrook-White is a mathematical combination of these two expressions that was developed in the 1930s (Colebrook (1939))

$$\frac{1}{\sqrt{f}} = -2\log\left(\frac{\epsilon}{3.7D} + \frac{2.51}{Re\sqrt{f}}\right) \tag{9}$$

where ϵ is the equivalent sand grain roughness, D the diameter of the pipe and Re the Reynolds number of the flow. Later, several modifications to the smooth turbulent law have been suggested (McKeon et al. (2005)), while how to determine the roughness elements on the inner wall by means of measurement has been discussed based on recent experiments (Langelandsvik et al. (2008), Shockling et al. (2006)). For transportation of natural gas through offshore pipelines, the Reynolds number is typically of the order 10^7, meaning the friction factor lies in the region between smooth and fully rough turbulent flow. Based on operational data from natural gas pipelines, it is stated that the friction factor in the transition region in the Colebrook-White correlation bears significant uncertainty (Langelandsvik et al. (2005)). A modified friction factor formula was proposed by the European Gas Research Group (GERG) (Gersten et al. (2000))

$$\frac{1}{\sqrt{f}} = -\frac{2}{n}\log\left[\left(\frac{1.499}{dr\,Re\sqrt{f}}\right)^{0.942\cdot n\cdot dr} + \left(\frac{\epsilon}{3.7D}\right)^{n}\right] \tag{10}$$

where dr is the draught factor which accounts for other pressure losses such as curvature and pipe joints, and n is used to control the shape of the transition. $n = 1$ corresponds to a smooth Colebrook-White transition while $n = 10$ a more abrupt transition.

In Fig. 2 the friction factor f computed using the Colebrook-White and GERG friction factor formulas for an equivalent sand grain roughness of 3 μm is shown. For $dr = 1.01$ and $n = 3$ the GERG friction factor formula gives a more abrupt transition from smooth to fully rough turbulent flow compared to Colebrook-White. However, limited information is available as to what values of dr and n should be used. It is therefore difficult to conclude whether the GERG friction factor formula is any significant improvement of the traditional Colebrook-White correlation. Hence, the GERG friction factor formula has limited capability to predict frictional pressure drop in new pipelines.

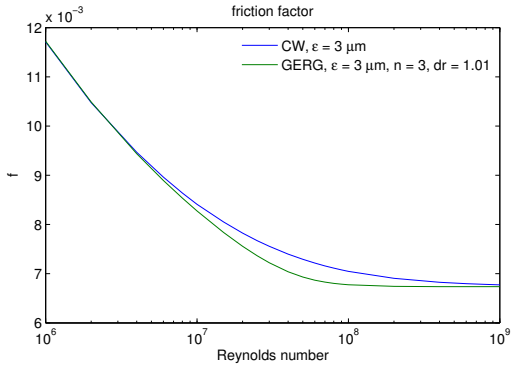

Figure 2: Friction factor f computed using the Colebrook-White (CW) and GERG friction factor correlation. The GERG friction factor formula predicts a more abrupt transition from smooth to fully rough turbulent flow compared to Colebrook-White.

2.3. Equation of state

The equation of state is the relationship between state variables. Several different equations of state, including SRK, Peng-Robinson, BWRS, AGA-8, GERG 88 and GERG 2004, are applied in the industry today. The sensitivity of the gas pipeline flow model to the selection of the equation of state has been investigated previously (Chaczykowski (2009)) for the SRK, BWR, AGA-8 and GERG 88 equations of state. These did not influence the computed flow parameters and line-pack values in any significant way. However, the inlet pressure in the considered pipeline was only 8.4 MPa, which is typical that of an on-shore distribution network. Offshore natural gas pipelines can have inlet pressures in the range 18 - 20 MPa. The sensitivity of the selection of the equation of state for high pressure pipelines will therefore be investigated in the following. The equations of state considered are SRK, Peng-Robinson, BWRS, GERG 88 and GERG 2004.

SRK

The Soave-Redlich-Kwong (SRK) is a modification of the Redlich Kwong equation of state and was first published in 1972 (Soave (1972)). It is a cubic equation of state, and in the original article by Soave it is validated up to 12 MPa. It can conveniently be expressed as

$$Z^3 - Z^2 + Z(A - B - B^2) - AB = 0 \tag{11}$$

where A and B are constants which depend on reduced pressure and temperature

$$A = 0.427\frac{\alpha p_r}{T_r} \tag{12}$$

$$B = 0.08664\frac{p_r}{T_r} \tag{13}$$

where the subscript r denotes reduced state variables ($p_r = p/p_c$, $T_r = T/T_c$, p_c and T_c being critical pressure and temperature). The parameter α is a function which depends on the reduced temperature and the accentric factor. Mixing rules are applied to gas mixtures.

Peng-Robinson

Peng-Robinson is also a cubic equation of state and is structurally similar to SRK. It was first published in 1976 and is claimed to predict the liquid phase densities more accurately compared to SRK (Peng and Robinson (1976)). On polynomial form it can be expressed as

$$Z^3 - (1-B)Z^2 + (A - 3B^2 - 2B)Z - (AB - B^2 - B^3) = 0 \tag{14}$$

where

$$A = 0.45724\frac{\alpha p_r}{T_r} \tag{15}$$

$$B = 0.07780\frac{p_r}{T_r} \tag{16}$$

As with SRK α is a function of reduced temperature and accentric factor. Owing to their simple mathematical structure, cubic equations of state such as SRK and Peng-Robinson along with their modifications are still frequently used in the industry today. However, they have proven to be inaccurate, especially for pressures above 12 MPa (Modisette (2000)).

BWRS

The Benedict-Webb-Rubin-Starling (BWRS) equation of state is based on a virial expansion in density. It was published in 1973 and is a modification of the BWR equation of state (Starling (1973)). The BWRS equation of state is formulated as

$$\begin{aligned} p &= \rho_n RT + \left(B_0 RT - A_0 - \frac{C_0}{T^2} + \frac{D_0}{T^3} - \frac{E_0}{T^4}\right)\rho_n^2 + \left(bRT - a - \frac{d}{T}\right)\rho_n^3 \\ &+ \alpha\left(a + \frac{d}{T}\right)\rho_n^6 + \frac{c\rho_n^3}{T^2}(1+\gamma\rho_n)\exp(-\gamma\rho_n^2) \end{aligned} \tag{17}$$

In total it contains 11 coefficients. Values and mixing rules can be found in the literature. Because of its ability to cover both liquid and gases the BWRS is widely used for simulations of pipelines with high density hydrocarbons (Modisette (2000)). For the offshore network in Fig. 1, the operator Gassco currently uses a BWRS equation of state with coefficients which are especially tuned for hydrocarbons, which will be denoted as BWRS* in the following.

GERG88

The European Gas Research Group (GERG) has performed an extensive research into compressibility factor measurements. The GERG 88 virial equation of state was developed to accurately predict the compressibility factor of natural gas mixtures (Jaeschke et al. (1991)). It takes the form

$$Z = 1 + B_M(T)\rho_m + C_M(T)\rho_m^2 \tag{18}$$

$$B_M(T) = \sum_{i=1}^{n}\sum_{j=1}^{n} x_i x_j B_{ij}(T) \tag{19}$$

$$C_M(T) = \sum_{i=1}^{n}\sum_{j=1}^{n}\sum_{k=1}^{n} x_i x_j x_k C_{ijk}(T) \tag{20}$$

where $B_M(T)$ and $C_M(T)$ are the second and third virial coefficients which depend on temperature and gas composition. x_i, x_j and x_k represent the mole fractions of the ith, jth and kth component. For compressibility factor calculations GERG 88 is claimed to have an uncertainty of less than 0.1% for pressures up to 12 MPa and temperatures in the range $265 - 335$ K.

GERG 2004

GERG has since published the GERG 2004 equation of state which accurately predicts compressibility factors for pressures and temperatures up to 30 MPa and 365 K respectively (Kunz (2007)). The GERG 2004 is explicit in Helmholtz free energy a with density and temperature as independent variables. As a function of reduced density δ and temperature τ the compressibility factor is determined from

$$\frac{p(\delta,\tau)}{\rho RT} = 1 + \delta\alpha_\delta^r \tag{21}$$

where α_δ^r is the dimensionless Helmholtz free energy. The GERG 2004 equation of state can also conveniently be used to predict other thermodynamical properties such as enthalpy, internal energy, heat capacity and Joule-Thomson coefficients to mention a few.

The compressibility factor as a function of pressure and temperature for a typical North Sea natural gas mixture was calculated using all the equations of state mentioned above. The composition of the gas in mol% was set to the following: $CH_4 - 89.16\%$, $C_2H_6 - 7.35\%$, $C_3H_8 - 0.51\%$, $nC_4H_{10} - 0.03\%$, $iC_4H_{10} - 0.03\%$, $nC_5H_{12} - 0.002\%$, $iC_5H_{12} - 0.001\%$, $N_2 - 0.70\%$, $CO_2 - 2.22\%$. In the 1D flow model (Equations (5) - (7)) the partial derivatives of Z with respect to temperature and pressure are required. These are found by taking the derivative of the expression for Z with respect to p and T. In Fig.3 the compressibility factor Z as a function of pressure at different temperatures is presented. Up to 10 MPa the different equations of state predict almost the same value of the Z factor. Above 10 MPa a more noticeable difference is observed. Partial derivatives of Z with respect to temperature and pressure are presented in Fig.4 - 6. In Fig.4 and Fig.5 the computed values agree well with each other over the entire pressure range. In Fig. 6 some deviations above 20 MPa are observed.

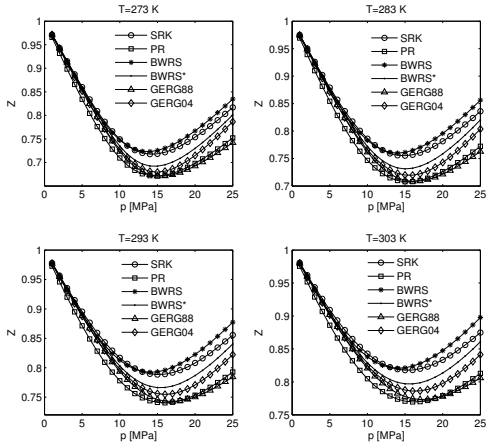

Figure 3: Compressibility factor Z as a function of pressure at different temperatures. For pressures below 10 MPa only small differences between the different equations of state are observed. For pressures above 10 MPa a considerable difference can be seen.

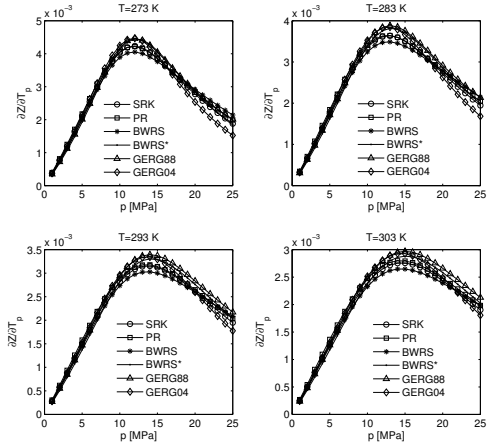

Figure 4: Partial derivative of Z with respect to temperature at constant pressure $(\partial Z/\partial T_p)$.

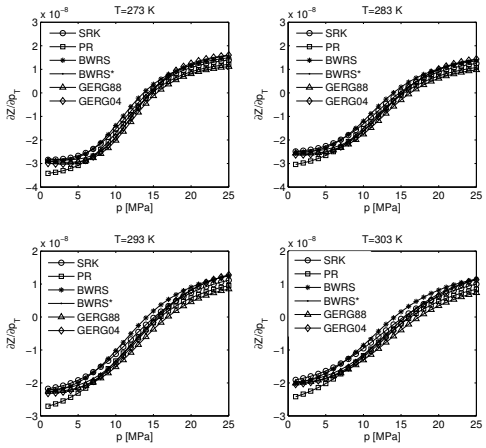

Figure 5: Partial derivative of Z with respect to pressure at constant temperature $(\partial Z/\partial p_T)$.

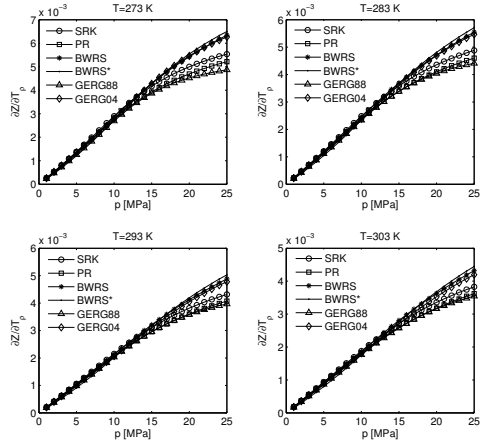

Figure 6: Partial derivative of Z with respect to temperature at constant density ($\partial Z/\partial T_\rho$).

2.4. Heat transfer model

The final term in the energy equation (Equation (7)) represents the heat exchange between the gas and the surrounding environment. This term is currently modeled by Gassco using a total heat transfer coefficient U (Ramsen et al. (2009)). The heat transfer coefficient for a pipeline consisting of multiple wall layers is

$$U = \left[\frac{r_o}{r_i} \frac{1}{h_i} + \sum_{n=2}^{N} \left(\frac{r_o}{k_n} \ln \left(\frac{r_n}{r_{n-1}} \right) \right) + \frac{1}{h_o} \right]^{-1} \tag{22}$$

where r_o is the outer radius of the pipe, r_i the inner radius, r_n outer radius of wall n, k_n the thermal conductivity of wall n, h_i the inner wall film heat transfer coefficient and h_o the outer film heat transfer coefficient. This is a steady state approach which does not allow for heat accumulation in the ground. To include heat accumulation in the ground one has to solve the unsteady heat transfer model (Chaczykowski (2010)). In the unsteady heat transfer model the one-dimensional radial heat equation is solved in the domain surrounding the pipeline.

$$\rho c_p \frac{\partial T}{\partial t} = \frac{k}{r} \frac{\partial}{\partial r} \left(r \frac{\partial T}{\partial r} \right) \tag{23}$$

The radial heat equation can be expressed on dimensionless form as

$$\frac{\partial T^*}{\partial t^*} = \frac{Fo}{r^*}\frac{\partial}{\partial r^*}\left(r^*\frac{\partial T^*}{\partial r^*}\right) \tag{24}$$

where * represents a dimensionless variable. Fo is the Fourier number which is defined as

$$Fo = \frac{\alpha t}{L^2} \tag{25}$$

where $\alpha = k/\rho c_p$ is the thermal diffusivity, t the characteristic time and L the characteristic length through which heat conduction occurs. The Fourier number is the ratio of the heat conduction rate to the heat storage rate. For small Fourier numbers (much less than 1) the heat storage rate is greater than the heat conduction rate, underlining that heat accumulation should be included in the model. The radial heat conduction equation is solved on the domain shown in Fig.7. The model is axial symmetric, where each thermal layer is represented by a coaxial cylindrical shell. Equation (23) is discretized using finite differences

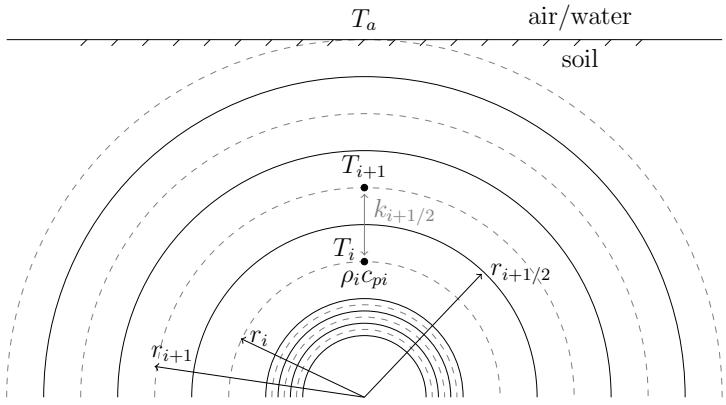

Figure 7: Half plane of the cross-section of a buried pipeline. Thermal elements are represented by coaxial cylindrical layers, with each element assigned a temperature T_i, heat capacity c_{pi} and density ρ_i. $k_{i+1/2}$ is the heat transfer coefficient between elements i and $i+1$.

In order to couple the one-dimensional radial heat equation with the one-dimensional flow model, the heat flow Q between the gas and the inner wall

is defined as

$$Q = h_i A(T - T_1) \tag{26}$$

where h_i is the inner wall film coefficient, A the area through which heat transfer takes place, T the gas temperature and T_1 the temperature of the first thermal element. For an updated gas temperature the radial heat equation is solved in the domain surrounding the pipeline to determine the updated temperature field. For an updated temperature field the heat flow Q between the gas and the surroundings is computed. This value is then used to model the heat exchange between the gas and surroundings at the next time step.

3. Numerical Scheme

Transportation of natural gas through high pressure natural gas pipelines is modeled by numerically solving the governing equations for one-dimensional compressible flow. Equations (5)-(7) form a system of hyperbolic partial differential equations which are solved using finite differences, with the discretization being implicit in time. The numerical stencil is presented in Fig.8.

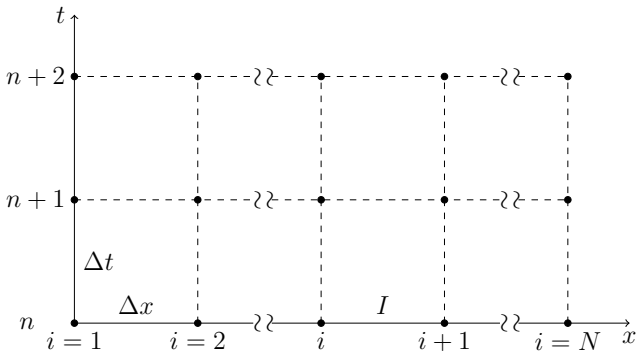

Figure 8: Stencil used in the finite difference method

A pipeline is divided into N grid points. The distance between point i and $i + 1$ is the discretization length Δx, while the time step between time level $n + 1$ and n is Δt. Flow values are stored at grid points, but are computed at the midpoints between two grid points. For pipe section I, being the pipe section between points i and $i + 1$, the partial derivative of a flow variable Y

with respect to time is approximated by

$$\frac{\partial Y(x_I, t_{n+1})}{\partial t} = \frac{Y_{i+1}^{n+1} + Y_i^{n+1} - Y_{i+1}^n - Y_i^n}{2\Delta t} + \mathcal{O}(\Delta t) \tag{27}$$

the spatial derivative by

$$\frac{\partial Y(x_I, t_{n+1})}{\partial x} = \frac{Y_{i+1}^{n+1} - Y_i^{n+1}}{\Delta x} + \mathcal{O}(\Delta x^2) \tag{28}$$

and the individual terms by

$$Y(x_I, t_{n+1}) = \frac{Y_{i+1}^{n+1} + Y_i^{n+1}}{2} + \mathcal{O}(\Delta x^2) \tag{29}$$

This is method is first order correct in time and second order correct in space, and is the same method as in the work by Kiuchi (Kiuchi (1994)) and Abbaspour and Chapman (Abbaspour and Chapman (2008)). When discretizing all terms in a fully implicit way, the governing equations form a system on non-linear equations. Kiuchi and Abbaspour and Chapman solve the system of non-linear equations using the Newton-Raphson method. This can however be time consuming, especially for long pipelines and complicated networks, and would not be feasible for real time applications. To simplify the computations the non-linear terms are linearized about the previous time step to give a system of linear equations. This system can be solved in an efficient way using simple linear algebra, which is done in the following.

4. Results

The influence of the friction factor, equation of state and heat transfer model on the transmission of natural gas through offshore pipelines is investigated. In Sections 4.1 - 4.4 a simple 650 km constructed pipeline is considered, with the setup shown in Fig.9. For the first and final 25 km the pipeline is buried under ground and is lying on-shore. For the 600 km between this it is an offshore pipeline lying at a depth of 100 m. The pipeline is lying on the seabed and is completely exposed to the seawater.

The composition of the gas was kept constant and was set to: $CH_4 - 89.16\%$, $C_2H_6 - 7.35\%$, $C_3H_8 - 0.51\%$, $nC_4H_{10} - 0.03\%$, $iC_4H_{10} - 0.03\%$, $nC_5H_{12} - 0.002\%$, $iC_5H_{12} - 0.001\%$, $N_2 - 0.70\%$, $CO_2 - 2.22\%$. Inlet mass flow, inlet temperature and outlet pressure were given as boundary conditions. The inlet mass flow is depicted in Fig.10. The outlet pressure was kept constant at 9 MPa and the inlet temperature at 30°C.

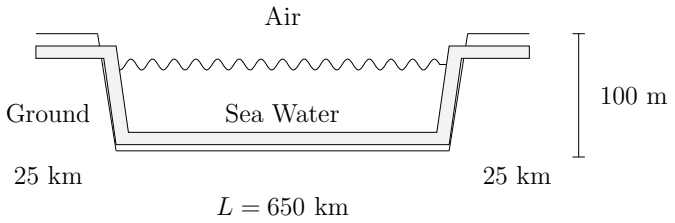

Figure 9: Offshore natural gas pipeline which is buried under ground for the first and final 25 km. The total length is 650 km.

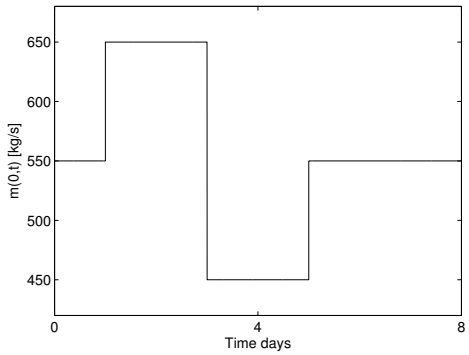

Figure 10: Boundary condition inlet mass flow.

4.1. Discretization errors

When using finite differences the governing equations are transformed into algebraic expressions in discrete time and space. Such a process introduces discretization errors in the solution. As the numerical method presented in Section 3 is first order correct in time and second order correct in space, the discretization errors will be proportional to Δt and Δx^2 respectively. In order to investigate the discretization errors in the model, the local error is defined as

$$e = \frac{1}{N}\left(\sum_{i=1}^{N}\left(\frac{Y_i - Y_{i,hi}}{Y_{i,hi}}\right)^2\right)^{1/2} \tag{30}$$

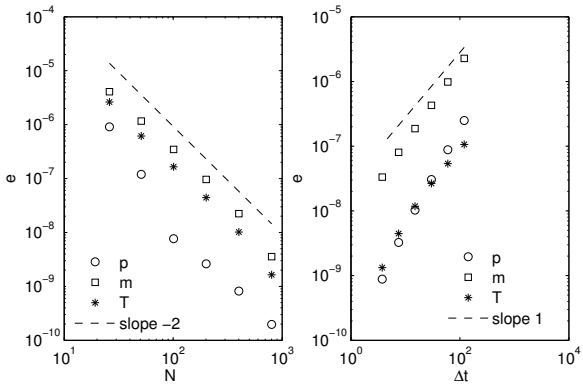

Figure 11: Local discretization errors for pressure p, mass flow $\dot{m}$ and temperature T. Left: Spatial discretization error as a function of grid points N. Right: Temporal discretization error as a function of time step Δt.

where Y represents p, $\dot{m}$ and T at point i. The summation is done over all grid points N, where $Y_{i,hi}$ is the numerical solution computed using the finest grid and the shortest time step (high resolution solution). Results for the local error are presented in Fig.11.

To the left in Fig.11 the spatial discretization error as a function of grid points N is presented, while the temporal discretization error as a function of time step Δt is presented to the right. As the numerical method is first order correct in time and second order correct in space, the 1 and -2 slopes are included. The numerical method converges to the expected order. The local discretization errors are small and are not considered to effect the flow field solution in any way. When modeling the flow of gas through long distance pipelines, discrepancies between computed results and measured values are thought to be because of physical approximation errors, and not numerical errors. Some of the modeled physical processes which enter into the flow model will be discussed in the next sections.

4.2. Influence of friction factor

The two different friction factor formulas presented in Section 2.2 were investigated for the flow. The equivalent sand grain roughness was set to 3 μm. For the GERG formula the draught factor and transition shape factor

were set to $dr = 1.01$ and $n = 3$ (Piggott et al. (2002)). A change in the friction factor is most noticeable in the modeled inlet pressure. In Fig. 12 the modeled inlet pressure using both the Colebrook-White and the GERG friction factor formulas is shown. The Colebrook-White formula predicts an inlet pressure which is approximately 0.3 MPa higher than the GERG formula.

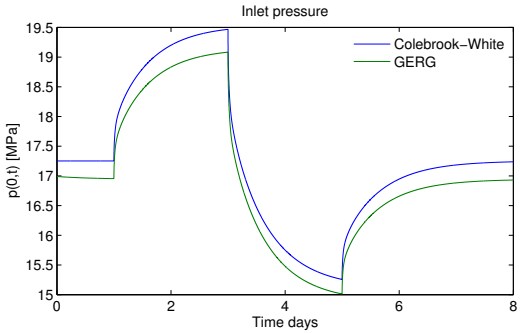

Figure 12: Modeled inlet pressure using both the Colebrook-White and the GERG friction factor formulas for an equivalent sand grain roughness of 3 μm.

4.3. Influence of Equation of State

The influence of the equation of state on the flow model was investigated by running simulations with SRK, Peng-Robinson, BWRS, GERG 88 and the GERG 2004 equation of state. Results for inlet pressure, outlet mass flow and outlet temperature are presented in Fig.13. Gassco currently uses the BWRS equation of state with coefficients especially tuned for hydrocarbons, denoted as BWRS*.

The most noticeable difference between the different equations of state was observed in the inlet pressure. Results for computed inlet pressure is in the range $17-19.5$ MPa. For such high pressures the GERG 2004 equation of state is believed to be the most accurate. Compared to GERG 88 the GERG 2004 predicts an inlet pressure which is approximately 0.1 MPa higher, while compared to BWRS* it is approximately 0.1 MPa lower. The influence of the selection of the equation of state on outlet mass flow and temperature is not that significant as with the inlet pressure. The outlet mass flow computed using the GERG 2004 equation of state lies between computed mass flow

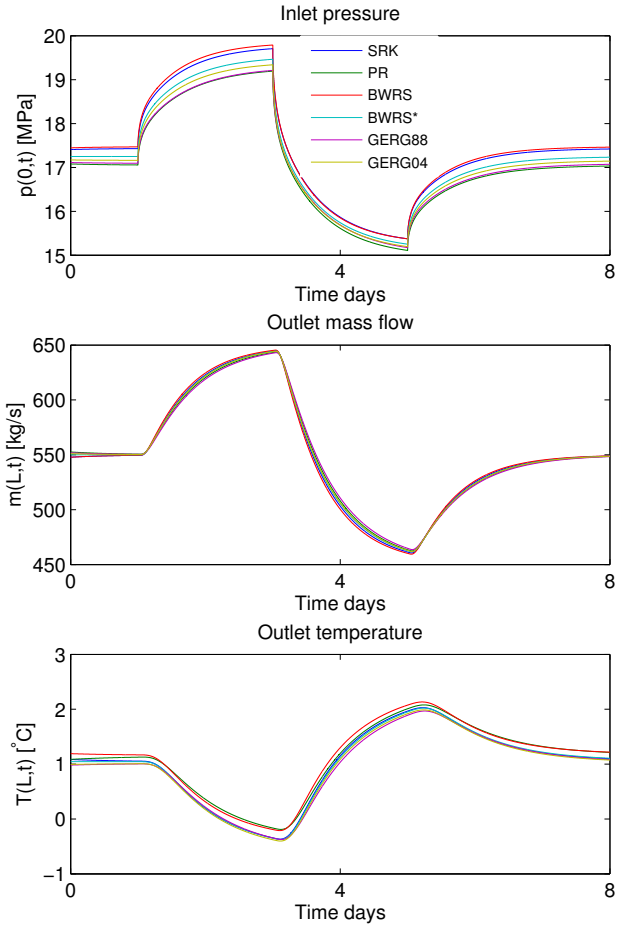

Figure 13: Influence of the equation of state on the flow model. Top inlet pressure, middle outlet mass flow and bottom outlet temperature. Results found using the SRK, Peng-Robinson, BWRS, BWRS*, GERG 88 and GERG 04 equations of state.

values using the other equations of state. For modeled outlet temperature GERG 2004 generally predicts a slightly lower outlet temperatures compared to the other equations of state. However, this difference is small and not noticeable in Fig.13.

4.4. Heat transfer model

Using the same boundary conditions, the model was run using both the steady and unsteady external heat transfer models. Results for outlet temperature are presented in Fig.14. The steady heat transfer model over predicts the amplitude of temperature changes in the flow compared to the unsteady heat transfer model which takes into account heat accumulation in the ground.

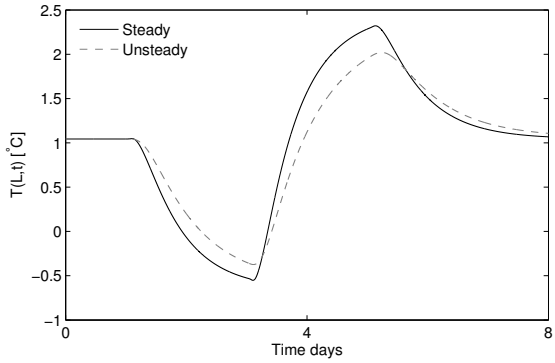

Figure 14: Results outlet temperature using both the unsteady and steady heat transfer model. The steady heat transfer model over predicts the amplitude of temperature changes in the flow compared to the unsteady heat transfer model.

4.5. Model Validation

The one-dimensional flow model was validated by running simulations on one of Gasscos offshore pipelines, with simulated results being compared to measured values. Operational data was used as boundary conditions, with the pipe setup being similar to that in Fig.9. Results for inlet pressure, outlet mass flow and outlet temperature are presented in Fig.15.

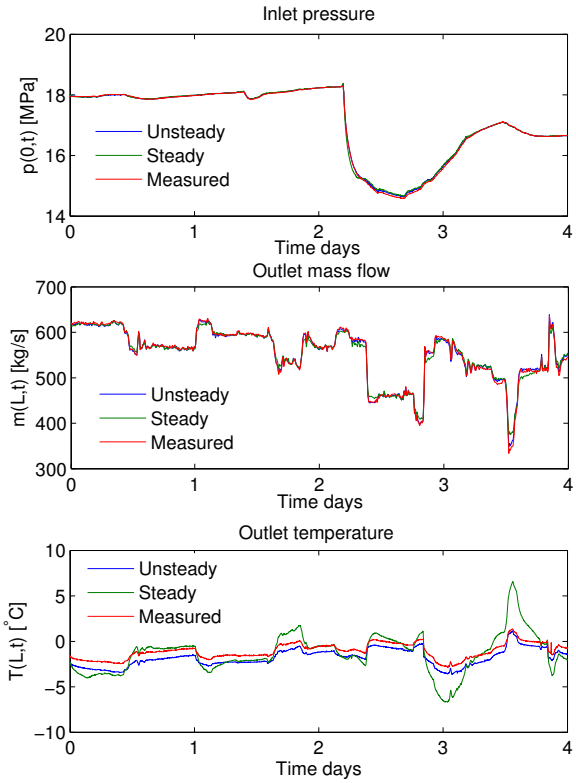

Figure 15: Simulated results compared to measured values using both the steady and unsteady external heat transfer models. Top inlet pressure, middle outlet mass flow, bottom outlet temperature.

The tuned BWRS equation of state was used to determine the compressibility factor, while the friction factor was computed from the Colebrook-White correlation. Simulations were run with both the steady and unsteady external heat transfer model. For the outlet temperature the steady heat transfer model over predicts the amplitude of temperature changes in the

flow. When using the unsteady heat transfer model, the amplitude of the temperature changes agree well with measured values. There is also a observable difference in computed outlet mass flow between the two heat transfer models. After abrupt changes in outlet mass flow, the unsteady heat transfer model agrees better with measured values compared to the steady heat transfer model.

5. Discussion

For most of the computations in this work the Colebrook-White friction factor formula was used to determine the frictional force between the fluid and the pipe wall. The Colebrook-White formula was compared to the more recently developed GERG friction factor formula, which is stated to give a more abrupt transition from smooth to fully rough turbulent flow. For a Reynolds number of approximately 10^7, the difference in computed inlet pressure between the two relations was quite significant, with the GERG formula predicting a considerably lower inlet pressure than Colebrook-White. However, the GERG formula contains two new factors which are not well documented in the literature, and there is little information as to what values these parameters should have for given flow conditions. The Colebrook-White frictional factor formula is therefore still the preferred choice when predicting the frictional pressure drop in the pipeline.

For the different equations of states considered in Section 4.3, the biggest influence was observed in the modeled inlet pressure. As the inlet pressure lies in the region $16 - 19$ MPa, this is also the region where the different equations of state differ most from each other, as was observed in Fig.3. As the GERG 2004 is the only equation of state which is explicitly stated to be valid for such high pressures, it is also believed to be the best reference. At the outlet the difference in computed outlet mass flow and temperature is small. As the outlet pressure was set constant at 9 MPa, the different equations of state agree well with each other in this pressure region in Fig.3. Therefore, the difference in computed flow variables at the outlet is not that significant.

Together with the GERG 88 equation of state the tuned BWRS equation of state currently used by Gassco matches the results of the GERG 2004 quite well. Owing to the fact that it is validated for pressured up to 30 MPa and temperatures up to 365 K, and that it can conveniently be used to determine physical properties such as heat capacity, enthalpy, entropy and

internal energy, GERG 2004 would be the preferred equation of state when modeling the flow through high pressure natural gas pipelines. However, compared to all other equations of states considered here, GERG 2004 is the most computationally demanding. For the examples considered above, the computational time for the entire simulation using GERG 2004 was found to be approximately 10 times greater compared to other equations of state. This significant increase in computational time is likely due to all coefficients which are required in the case of GERG 2004. Because of this great increase in computational time, the tuned BWRS equation of state is still the preferred choice for real time applications. The difference in computed inlet pressure between GERG 2004 and the tuned BWRS was approximately 0.1 MPa. This pressure difference can be compensated for by tuning the equivalent sand grain roughness when using the BWRS equation of state in order to match the GERG 2004 results.

It is shown by example how the heat exchange between the gas and the surroundings should be modeled using an unsteady heat transfer model which accounts for heat accumulation in the ground. Results in Fig.15 for the outlet temperature illustrate how a steady heat transfer model over predicts the amplitude of temperature changes in the flow, while the unsteady heat transfer model shows a better agreement with measured values. Heat accumulation in the ground is only considered important where the pipeline is buried under ground, and not where it exposed to sea water. In the examples above, the pipeline was only buried under ground at the beginning and end of the pipeline where the gas leaves the processing terminal and arrives at the receiving terminal. Both of these lengths are approximately 25 km. Even for such a short section of pipeline, an unsteady heat transfer model should be used. In the example in Section 4.3, the relation between heat conduction and heat storage can be determined by considering the Fourier number. The thermal diffusivity of the soil is approximately $1.2 \cdot 10^{-6}$. The characteristic length, in this case the burial depth, is 1.5 m, while the characteristic time is the time for the ramp up and ramp down to occur in Fig.13. With this being approximately 50 hours, the Fourier number is determined to be 0.1. The physical meaning of this is that the heat conduction rate is an order of magnitude less than the heat storage rate, and the transient thermal response upon the change in the mass flow rate is predominantly dictated by the heat storage effect, even on a two day time scale as is the case here. For shorter characteristic time scales, the larger the effect of heat storage compared to the effect of heat conduction. This underlines that the steady state

approach for heat transfer is not valid, and that an unsteady heat transfer model should be used.

For the model validation case in Section 4.5, the computed inlet pressure and mass flow agree well with measured values. For the outlet temperature, an unsteady heat transfer model gives better results for the amplitude of temperature changes in the flow compared to a steady heat transfer model. However, the modeled temperature lies slightly below the measured temperature. The reason for this deviation between measured and modeled temperature arises either because of an incorrect ambient temperature or that the assumed burial depth is not correct. As it is an offshore pipeline, the ambient sea bottom temperature along the pipeline is determined from oceanographic models. In order to accurately model the flow, it is important to know the correct ambient temperature along the whole pipeline.

6. Conclusion

The flow of natural gas through high pressure offshore pipelines is modeled by numerically solving the governing equations for unsteady one-dimensional compressible viscous heat conducting flow. The numerical discretization errors are shown to be small, and discrepancies between modeled and measured flow values is most likely due to physical approximation errors, and not numerical errors. The selection of the equation of state for high pressure pipelines is studied in detail. The different equations of state gave different results for inlet pressure, with the recently developed GERG 2004 believed to be the best reference. However, as it is computationally demanding to solve, the BWRS equation of state is still used for compressibility factor calculations in offshore pipelines. The difference in computed inlet pressure between GERG 2004 and the tuned BWRS was approximately 0.1 MPa. This difference can be compensated for by tuning the equivalent sand grain roughness in order to match the modeled inlet pressure when using the BWRS and GERG 2004 equations of state. It is shown by example how an unsteady heat transfer model which takes into account heat accumulation in the ground greatly improves the modeled outlet temperature compared to a steady heat transfer model which has traditionally been used when modeling the flow through offshore pipelines. Some discrepancies between the modeled and measured outlet temperature are still present, which most likely are due to an incorrect ambient temperature.

Acknowledgment

This work has been funded by the Norwegian gas operating company Gassco as part of a project to improve flow modeling in offshore natural gas pipelines. The contributions of Willy Postvoll (Gassco) are greatly acknowledged.

References

Abbaspour, M., Chapman, K.S., 2008. Nonisothermal Transient Flow in Natural Gas Pipeline. Journal of Applied Mechanics 75, 031018.

Chaczykowski, M., 2009. Sensitivity of pipeline gas flow model to the selection of the equation of state. Chemical Engineering Research and Design 87, 1596-1603.

Chaczykowski, M., 2010. Transient flow in natural gas pipeline - The effect of pipeline thermal model. Applied Mathematical Modelling 34, 1051-1067.

Colebrook, C., 1939. Turbulent flows in pipes, with particular reference to the transition region between the smooth and rough pipe laws. J. Inst. Civil Eng. 81, 133-156.

Gersten, K., Papenfuss, H.D., Kurschat, T.H., Genillon, P.H., Fernandes Perez, F., Revell, N., 2000. New transmission-factor formula proposed for gas pipelines. Oil and Gas Journal Feb 2000, 58-62.

Jaeschke, M., Audlbert, S., Caneghem, P.v., Humphreys, A.E., Rosmalen, R.J., Pellel, Q., Schouten, J.A., Michels, J.P.J., 1991. Accurate Prediction of Compressibility Factors by the GERG Virial Equation. Society of Petroleum Engineers Aug 1991, 343-349.

Kiuchi, T., 1994. An implicit method for transient gas flows in pipe networks. International Journal of Heat and Fluid Flow 15, 378-383

Kunz, O., Klimeck, R., Wagner, W., Jaeschke, M., 2007. The GERG-2004 Wide-Range Equation of State for Natural Gases and Other Mixtures. GERG Technichal Monograph.

Langelandsvik, L.I., Postvoll, W., Svendsen, P., Øverli, J.M., Ytrehus, T., 2005. Evaluation of the friction factor formula based on operational data. In Proceedings of the 37th PSIG Annual Meeting, San Antonio Texas 2005.

Langelandsvik, L.I., Kunkel, G.J., Smits, A.J., 2006. Flow in a commercial steel pipe. Journal of Fluid Mechanics 595, 323-339.

Langelandsvik, L.I., Postvoll, W., Aarhus, B., Kaste, K.K., 2009. Accurate calculations of pipeline transport capacity. Proceedings to 24th World Gas Conference, Buenos Aires Argentina.

McKeon, B.J., Zagarola, M.V., Smits, A.J., 2005. A new friction factor relationship for fully developed pipe flow. Journal of Fluid Mechanics 538, 429-433.

Modisette, J.L., 2000. Equation of state tutorial. In Proceedings of the 32nd PSIG Annual Meeting, Savannah Georgia 2000

Osiadacz, A.J., Chaczykowski, M., 2001. Comparison of isothermal and non-isothermal pipeline gas flow model. Chemical Engineering Journal 81, 41-51.

Peng, D.Y., Robinson, D.B., 1976. A New Two-Constant Equation of State. Ind. Eng. Chem., Fundam 15, 59-64.

Piggott, J., Revell, N., Kurschat, T., 2002. Taking the Rough with the Smooth - a new look at transmission factor formulae. Proceedings to 34th PSIG Annual meeting Portland Oregon.

Ramsen, J., Losnegård, S.E., Langelandsvik, L.I., Simonsen, A.J., Postvoll, W., 2009. Important Aspects of Gas Temperature Modeling in Long Subsea Pipelines. Proceedings to 40th PSIG Annual meeting Galvestone Texas.

Shockling, M.A., Allen, J.J., Smits, A.J., 2006. Roughness effects in turbulent pipe flow. Journal of Fluid Mechanics 564, 267-285.

Soave, G., 1972. Equilibrium constants from a modified Redlich-Kwong equation of state. Chemical Engineering Science 27, 1197-1203.

Starling, K.E., 1973. Fluid Thermodynamic Properties for Light Petroleum Systems. Gulf Publishing Company 1973.

Thorley, A.R.D., Tiley, C.H., 1987. Unsteady and transient flow of compressible fluids in pipelines - a review of theoretical and some experimental studies. International Journal of Heat and Fluid Flow 8, 3-15.